# Mathematical Study on Enzyme Catalysed Reaction for HIV-1 Replication: Insight into the Antiviral Drug Treatment

Thesis submitted
in partial fulfillment of the requirements
for the award of the degree of
DOCTOR OF PHILOSOPHY (SCIENCE)

By


## Srijita Mondal


under the supervision of


## Prof.(Dr.)Ashis Kumar Sarkar

Professor, Department of Mathematics
Jadavpur University, Kolkata - 700032




Department of Mathematics
Jadavpur University
Kolkata - 700032, India


January, 2025

যাদবপুর বিশ্ববিদ্যালয়

FACULTY OF SCIENCE
DEPARTMENT OF MATHEMATICS

JADAVPUR UNIVERSITY
Kolkata - 700 032, India
Telephone : 91 (33) 2457 2269

## CERTIFICATE FROM THE SUPERVISOR

This is to certify that the thesis entitled "**Mathematical Study on Enzyme Catalysed Reaction for HIV-1 Replication: Insight into the Antiviral Drug Treatment**" is submitted by **Mrs. Srijita Mondal** whose name was registered vide INDEX NO. 10/18/Maths./25 dated **31.01.2018** for the award of Doctor of Philosophy (Science) degree of Jadavpur University, Kolkata 700032. This thesis is absolutely based upon her own work under my supervision and is worthy of consideration for the award of Ph.D.(Sc.) degree. Neither this thesis nor any part of this work has been submitted to any other University or Institute for the award of any degree/diploma or any other academic award anywhere before.

30/01/2025

(Signature of the Supervisor with date and official seal)

Professor
DEPARTMENT OF MATHEMATICS
Jadavpur University
Kolkata - 700 032, West Bengal

*Dedicated to my beloved parents.*

# Acknowledgement

*This thesis marks the culmination of my journey toward earning my Ph.D. I am deeply grateful to the many individuals who have provided guidance, advice, support, and encouragement throughout this program. As I conclude this thesis, I take great pleasure in expressing my heartfelt appreciation to everyone who played a role in helping me successfully complete this study, making it a transformative experience in my life.*

*I would like to take this opportunity to express my heartfelt gratitude to my advisor, Prof. Ashis Kumar Sarkar. His guidance, support, and encouragement have been invaluable throughout my journey. I am truly thankful to him for choosing me as his student during a pivotal moment in my Ph.D. I sincerely appreciate his insightful advice, constructive criticism, and the in-depth discussions we've had about my work. His unwavering courage and conviction continue to inspire me.*

*I would like to sincerely thank the "Innovation in Science Pursuit for Inspired Research" (INSPIRE) program, under the Department of Science & Technology (DST), Government of India, for their generous financial support through a research fellowship. This assistance greatly facilitated my work and allowed me to carry out my research with ease.*

*I want to extend my sincere gratitude to the Department of Mathematics at Jadavpur University for their invaluable support. I am truly thankful to the members of the Doctoral Committee for their insightful guidance and feedback during my research journey. Furthermore, I am deeply appreciative of all the staff in my department for their help in my academic endeavors, which made this experience genuinely enjoyable.*

*I have had the pleasure of collaborating with several esteemed individuals, including Prof. James F. Peters from the Computational Intelligence Laboratory at the University of Manitoba, Canada; Dr. Koyel Chakravarty from the Department of Mathematics at the School of Engineering and Applied Sciences, SRM University, Andhra Pradesh; Dr. Sourav Kumar Sasmal from the Department of Applied Mathematics and Scientific Computing at IIT Roorkee; and Ms. Tanushree Murmu from the Department of Mathematics at Rammohan College, Kolkata, India. This work would not have been possible without their enthusiastic support and invaluable contributions. I would like to extend my heartfelt gratitude to Dr. Priyanka Ghosh and Dr. Dibyendu Biswas for their unwavering cooperation in my publications. Additionally, I am grateful to Dr. Md Sadikur Rahman from the Department of Mathematics at Khalisani Mahavidyalaya, Hooghly, West Bengal, for his insightful advice.*

*I want to sincerely thank Prof. Priti Kumar Roy from the Department of Mathematics at Jadavpur University for his tremendous support and contributions to my research publications.*

*I would like to express my heartfelt gratitude to my co-researchers for creating a stimulating and enriching environment that made my time here truly enjoyable. A special thanks goes to Dr. Arunabha Sengupta, Dr. Sudipta Sarkar, Dr. Jahangir Chowdhury, Dr. Sudip Chakraborty, and Mr. Somnath Mondal for their friendly support in helping me complete my research.*

*Finally, I want to express my deepest gratitude to my parents, Salil Mondal and Pampa Mondal, whose unwavering support and love have been my foundation. Their sacrifices, moral encouragement, and blessings have been instrumental in shaping this thesis. I am truly indebted to them. I also want to extend my heartfelt thanks to my husband, Pratik Das, for his invaluable assistance during this journey. Words cannot fully convey my appreciation, but I am filled with admiration for both of them.*

*In addition, many individuals have contributed to the successful completion of this project, both knowingly and unknowingly. I want to extend my sincere gratitude to each of them for their unwavering support, and I apologize for not being able to acknowledge everyone individually.*

Place: Jadavpur University
Date:

(SRIJITA MONDAL)

# Abstract

The thesis, **Mathematical Study on Enzyme Catalysed Reaction for HIV-1 Replication: Insight into the Antiviral Drug Treatment**, concentrates on modelling the "within-infected-cell" replication of Human Immunodeficiency Virus Type 1 (HIV-1) infection and conducting an in-depth study of the antiviral drug treatment.

In this thesis, we develope a set of nonlinear differential equations that describe the enzymatic activity of Cytochrome P3A4 (CYP3A4) in HIV-1 infected patients who consume alcohol. We conduct an analytical comparison of the metabolism of protease inhibitors (PIs) between alcoholic and non-alcoholic HIV-1 infected individuals. Additionally, the study examines the role of alcohol consumption in increasing viral load, thereby accelerating the progression of the infection.

Next, we consider a mathematical model comprising a system of nonlinear differential equations that describe the biochemical reactions catalysed by HIV-1 reverse transcriptase (RT) and integrase (IN), based on Michaelis–Menten enzyme kinetics. This model incorporates a dual inhibitor for HIV-1 RT/IN, which functions as both a non-nucleoside reverse transcriptase inhibitor and an integrase inhibitor. To assess the effectiveness of this dual inhibitor against HIV-1 infection, a one-dimensional impulsive differential equation model is developed, leading to the numerical determination of an optimal dosing regimen. The results of the analytical and numerical analyses provide essential insights into identifying the minimum effective dose for the administration of HIV-1 RT/IN dual inhibitors in preventing HIV-1 infection.

Furthermore, we investigate the affect of Tat inhibitor on the suppression of HIV-1 transcription through a mathematical model based on nonlinear differential equations. It frames the analysis as an optimal control problem, assessing the potential of the Tat inhibitor as a therapeutic approach for HIV-1 infection. A one-dimensional impulsive differential equation model is developed to evaluate the maximum concentration of the elongating complex ($P_2$) and determine the optimal timing for successive dosages. The present findings indicate that impulsive dosing is more effective than continuous dosing in inhibiting HIV-1 transcription. Next, an enzyme kinetic model is formulated to observe the impact of viral proteins Tat and Rev on HIV-1 replication, and the efficacy of combined drug therapy (administering Tat and Rev inhibitor) is examined using an optimal control framework. Applying the Pontryagin maximum principle, the study aims to minimize therapy costs while optimizing its effects on Tat-Rev regulation of HIV-1 replication, supported by numerical simulations with varying system parameters.

**Keywords:** HIV-1, AIDS, CYP3A4 enzyme, Alcohol, Tat, Rev, Protease inhibitor, Dual Inhibitor, Integrase, Reverse Transcriptase, Impulsive Differential Equation, Optimal Control.

# Contents

# Chapter 1

# Introduction

## 1.1 Background

### 1.1.1 Biochemistry

The field of biochemistry has had a profound impact on various areas of human activity and will continue to do so in the future. It is a captivating and aesthetically pleasing body of knowledge that plays a significant role in medicine and beyond. Progress in biochemistry is empowering researchers to address some of the most intriguing questions in biology and medicine (Giordano et al., 2020; Kendrew et al., 1958; Lander et al., 2001; Watson and Crick, 1953).

Biochemistry, also known as biological chemistry, is the examination of chemical reactions in living organisms. It focuses on comprehending the chemical foundation that enables biological molecules to generate intracellular and intercellular processes. These processes are closely connected to the examination and comprehension of tissues, organs, organisms, as well as their structures and functions (Karp, 2009). Biochemical methodology and research play a significant role in advancing and encompassing nearly all areas of life sciences (Miller, 2012). Most of the biochemical research revolves around studying the structures, functions, and interactions of biological macromolecules, including proteins, nucleic acids, carbohydrates, and lipids.

This research provides valuable insights into the cellular structure and the execution of vital life functions (Copeland, 2004; Slabaugh, 2004). The findings of biochemical research play a vital role in medicine, nutrition, and agriculture, with a particular significance in medicine for comprehending disease origins and treatments (Finkel, 2009; Marshall, 2014). Biochemistry can be categorized into enzymology, structural biology, and metabolism (Boyer, 2002). Throughout the latter part of the 20th century, biochemistry has significantly advanced the understanding of biological processes through these three areas of study (Centennial, 2006).

#### 1.1.1.1 Enzymology

Biochemistry, with its primary fields such as enzymology, holds a key role in both the physical and biological sciences (Garcia, 2019). Enzymology serves as a bridge between these two disciplines, offering a shared foundation for the practice of the above-mentioned two divisions of natural science (Meister, 2009). For biochemists, enzymes are just one component of a broader field that encompasses all biological processes (Price and Frey, 2001). In a way, biochemistry can be seen as a comprehensive study of enzymes, as most biochemical processes rely on enzymes for catalysis or on other proteins with enzyme-like properties (Jencks, 1987).

Enzymes, known as biological catalysts, accelerate the speed of a reaction without undergoing any changes themselves (Cornish-Bowden, 2013), and are crucial for speeding up slow biological reactions. They are highly specific, typically catalyzing the reaction of only a single specific substrate or closely related substrates. Moreover, enzymes are generally regulated through different positive and negative feedback systems, enabling precise supervision over the rate of reaction. Therefore, In the field of biology, studying both the catalytic mechanisms of enzymes and the rates of the reactions at which they catalyze is important. The assessment of the speed at which an enzyme functions is referred to as enzyme kinetics. The speed at which a reaction occurs is referred to as the reaction rate, which indicates how quickly products are formed or how fast substrates are disappeared. In the case of enzyme-catalyzed reactions, the rate of product formation ($v$) can be defined by the equation $v = k[ES]$, where $k$ represents the rate constant for a specific reaction and $[ES]$ denotes the concentra-

tion of the enzyme-substrate complex. The reaction is therefore first order in relation to the concentration of complex ($[ES]$). However, the directly measurable substrate ($S$) concentration does not have a first-order effect on the reaction rate. Instead, under steady state conditions where $[ES]$ remains effectively constant, the velocity ($v$) of the enzyme-catalyzed reaction follows a hyperbolic function of $[S]$, represented by $v = \frac{V_{max}[S]}{K_M+[S]}$. This equation is known as the Michaelis-Menten equation and includes two parameters: $V_{max}$ (the maximum rate of reaction) and $K_M$ (the Michaelis constant). $V_{max} = k_{cat}[E]_{total}$ is determined by the total enzyme concentration ($[E]_{total}$) and the catalytic rate constant ($k_{cat}$) of the enzyme for the reaction. The rate of reaction reaches its maximum, $V_{max}$, when the enzyme is fully saturated with substrate, while $K_M$ represents the substrate concentration at which the enzyme achieves half of the maximum rate $V_{max}$. The relationship between the rate of reaction ($v$) and the concentration of substrate ($S$) is determined by the enzyme's affinity for its substrate. The affinity of enzyme is inversely proportional to the value of $K_M$, i.e., as the value of $K_M$ decreases, the affinity of enzyme increases. Therefore, an enzyme with a high $K_M$ value needs a higher concentration of substrate to attain $V_{max}$. The values of $K_M$ and $V_{max}$ are found by conducting an enzyme incubation process with different amounts of substrate, and the outcomes can be depicted through a rate of reaction ($v$) versus substrate concentration ($[S]$) graph, which usually exhibits a hyperbolic shape. It can be challenging to accurately fit the best hyperbola through the experimental data points, and difficult to establish $V_{max}$ precisely at infinite substrate concentration. One straightforward approach to determine $V_{max}$ and $K_M$ from a data set of velocity versus substrate information is to utilize the double reciprocal (Lineweaver-Burk) plot, which is a linear transformation of the Michaelis-Menten equation. By rearranging the Michaelis-Menten equation, the Lineweaver-Burk double reciprocal plot is expressed as: $\frac{1}{v} = \frac{1}{V_{max}} + \frac{K_M}{V_{max}} * \frac{1}{[S]}$. This rearrangement enables the establishment of a linear relationship, facilitating a more accurate fitting to the experimental data and estimation of $K_M$ and $V_{max}$ values.

However, enzyme activity can be influenced by various molecules. Molecules that interact with enzymes and reduce the rate of an enzyme-catalysed reaction are called inhibitors, whereas activators are molecules that increase enzyme activity (Lopina, 2017).

Since enzymes are highly desirable as drug targets due to their crucial catalytic activity and their inherent susceptibility to inhibition by small, drug-like molecules, many drugs act as enzyme inhibitors (Balbaa and EI Ashry, 2012; Copeland and Harpel, 2007). The effectiveness of a medicinal enzyme inhibitor is typically evaluated based on its specificity, or its ability to bind to other proteins, as well as its potency, which is measured by the inhibitor's dissociation constant and indicates the concentration required to inhibit the enzyme. A high level of specificity and potency guarantees that the drug (medicinal enzyme inhibitor) will have minimal side effects and low toxicity. There are two types of enzyme inhibitors: (a) Reversible Inhibitors and (b) Irreversible Inhibitors. Reversible inhibitors can further be classified into three categories: (i) Competitive Inhibitors, (ii) Noncompetitive Inhibitors, and (iii) Uncompetitive Inhibitors. Competitive Inhibitors bind non-covalently to the active site of the enzyme and compete with the substrate. This competition prevents the formation of enzyme-substrate complexes, resulting in a decrease in the reaction rate. The extent of inhibition is determined by the concentrations of both the substrate and the inhibitor. Competitive inhibition results in an increase in $K_M$ without affecting $V_{max}$. Non-competitive inhibitors bind to both the free enzyme and to the enzyme-substrate complex ($ES$) or subsequent species. They bind to an allosteric site rather than the active site of the enzyme. This binding causes a change in the enzyme's structure, slowing down the formation of the enzyme-substrate complex ($ES$), which results in fewer product formations. Unlike competitive inhibitors, noncompetitive inhibitors are not influenced by substrate concentration. In noncompetitive inhibition, $V_{max}$ is reduced, but $K_M$ remains unaltered. Uncompetitive inhibitors bind exclusively to the enzyme-substrate complex ($ES$) or subsequent species in the reaction pathway. Certain enzyme inhibitors form a covalent bond with the active site of the enzyme, completely inhibiting its overall activity. These inhibitors are referred to as enzyme poisons and their effect is irreversible or permanent.

Enzyme inhibitors have a crucial role in cells as they are typically specific to one enzyme and regulate its activity. They are responsible for controlling the production of unnecessary molecules in metabolic pathways by inhibiting enzymes later in the pathway. This negative feedback mechanism is essential for maintaining cellular bal-

ance. Enzyme inhibitors also play a role in controlling vital enzymes like proteases or nucleases, preventing them from causing damage to cells. Additionally, many poisons produced by animals or plants act as enzyme inhibitors, blocking the activity of important enzymes in prey or predators. Therefore, the exploration and improvement of enzyme inhibitors remains a vibrant field of study in the realms of biochemistry and pharmacology.

#### 1.1.1.2 Clinical enzymology

Clinical enzymology can be described as a branch of biochemistry that focuses on studying and measuring enzyme activities for diagnosis and treatment of diseases (BARMAN, 2011; DANCIS, 1972; Srivastava and Chosdol, 2008). Enzyme inhibitors have become a crucial aspect of drug discovery in the pharmaceutical industry and at drug research centers (Bhagavan and HA CE, 2015; Copeland and Harpel, 2007; Galluzzi, 2020; Pirmohamed et al., 1998). Currently, over a hundred enzyme inhibitors are being marketed as drugs, with twice as many in various stages of development (Kalman, 1981). These inhibitors demonstrate their specific effects within bacterial cells, viruses, and the human body (Strelow et al., 2012). They can be utilized to treat a variety of disorders and illnesses, such as bacterial diseases (Liu et al., 2018), methanol poisoning (Pohanka, 2019), asthma (Page, 2015), chronic obstructive pulmonary disease, cardiovascular diseases (Lopez-Sendon et al., 2004), erectile dysfunction (Huang and Lie, 2013), gastrointestinal disorders (Ianiro et al., 2016), hepatitis $B$ virus infection (Dawood et al., 2017), hepatitis $C$ virus infection, herpes virus infections, human immunodeficiency virus (HIV)/acquired immune deficiency syndrome (AIDS) (Santos et al., 2015; Sierra, 2012), as well as rheumatoid arthritis and associated inflammatory diseases. Antimetabolites, the key pharmaceutical agents, are effective due to their ability to competitively inhibit enzymes (Thomson, 1959; Woolley, 1952). These compounds have a slightly different structure than the natural substrate and fall into the category of competitive enzyme inhibitors. By competing with the unwanted substrate for the enzyme's active site, antimetabolites prevent the formation of undesirable products by forming an enzyme-inhibitor complex. Most of the antibacterial, antiviral and antitumor drugs belong in the same group following the enzyme inhibition property.

The administration of those drugs to the patients exhibits limited toxicity due to the presence of only a few crucial metabolic pathways that are specific to tumors, viruses, or bacteria. Consequently, drugs that eliminate these organisms often result in the death of host cells.

Highly active antiretroviral therapy (HAART) is the most comprehensive treatment method for individuals with acute HIV infection. Currently, there are approximately 26 FDA-approved drugs for AIDS that target various stages of the HIV life cycle (Das and Arnold, 2013). These drugs can be categorized into four classes: (i) Entry/Fusion Inhibitors (ii) Reverse Transcriptase Inhibitors (including Nucleoside/Nucleotide Reverse Transcriptase Inhibitors, i.e., NRTIs and Non-Nucleoside Reverse Transcriptase Inhibitors, i.e., NNRTIs) (iii) Integrase Inhibitors and (iv) Protease Inhibitors, i.e., PI. NRTIs act as competitive inhibitors, leading to chain termination, while NNRTIs allosterically inhibit DNA polymerization. NRTIs not only disrupt viral DNA and RNA replication but also affect normal cell DNA replication due to their poor selectivity (Gu et al., 2016). NNRTIs target the allosteric site of viral reverse transcriptase, altering the enzyme's conformation and interfering with the binding between the enzyme and substrate (Gu et al., 2016). Recently approved integrase inhibitors (*raltegravir* and *elvitegravir*) attach to the active site of HIV-1 integrase within a pre-integration complex, preventing the integration of viral DNA into host cell chromosomes. The antiretroviral protease inhibitors also work as competitive inhibitors by binding to the catalytic site of the HIV protease, thereby preventing the process of breaking down viral polyprotein precursors into mature, essential proteins needed for viral replication. The antiretroviral combination therapy (HAART) usually involves (i) two NRTIs + one NNRTI or protease inhibitor (PI) and (ii) combination of an integrase or entry inhibitor with RTIs and PIs (Das and Arnold, 2013). Antibacterial medications are also a significant application of enzyme inhibition in the clinical field (Rahal et al., 1968; Waisbren, 1957). These drugs work by inhibiting enzymes necessary for the survival of pathogens. Bacteria possess a robust cell wall composed of a net-like polymer known as peptidoglycan. Antibiotics like *Penicillin* and *Vancomycin* hinder the enzymes required for bacterial cell proliferation during cell wall synthesis. Consequently, these medications cause the strands of the peptidoglycan polymer to cross-link, resulting in

a weakened cell wall and the bursting of bacteria (Kapoor et al., 2017; Soares, 2012). The design of antibiotic drugs is facilitated when an enzyme crucial to the survival of a pathogen is either absent or significantly different in humans (Haag et al., 2012). This allows for the development of inhibitors that target processes like peptidoglycan synthesis, which humans do not produce, resulting in selective toxicity towards bacteria. Selective toxicity can also be achieved by targeting differences in bacterial ribosome structure or fatty acid synthesis. Various studies have highlighted the importance of enzyme inhibitors in the pharmaceutical industry (Balbaa and EI Ashry, 2012; Copeland and Harpel, 2007; Walpole and Wrigglesworth, 1989). To address the wide range of applications of enzymes in medicine, the field of clinical enzymology has evolved.

### 1.1.2 Computational biochemistry

The field of computational biochemistry combines mathematical reasoning and numerical simulation to effectively complement the biochemical field (Érdi and Tóth, 1989). This approach has been extensively utilized to gain insights into biochemical mechanisms. To fully comprehend the workings and regulation of all biological processes, a deep understanding of biochemical mechanisms from multiple perspectives is necessary. Isolation, purification, and characterization of proteins and other cellular components have significantly contributed to our understanding of the biochemical basis of biological processes (Glenner et al., 1971). These approaches have also provided insights into the regulation of cellular functions. Although understanding biochemical mechanisms necessitates various approaches, many of these approaches have predominantly relied on experimental methods over the last fifty years. As the complexity of systems increases, relying solely on experimental approaches becomes inadequate for understanding their functioning. While intuitive reasoning and experiments may suffice for systems with few components, quantitative methods are necessary for comprehending systems with many components and interactions (Chen et al., 2010). Mathematical analysis and numerical simulation, based on empirical experimental observations, are highly valuable for drawing mechanistic inferences about the organization, functioning,

and regulation of biochemical systems (Yang et al., 2013).

Enzyme kinetics, a well-established field in computational biochemistry, has offered a detailed understanding of how proteins and enzymes function. Through mathematical reasoning and computational analysis closely linked with experimental data, the mechanism behind various enzyme reactions, including cooperativity (Qian, 2008) and allosteric regulation (Jeltsch, 2006), has been developed. By the mid-seventies, the mathematical foundation for enzyme kinetics had advanced enough to produce textbooks like the one written by Segel (Segel, 1975). Currently, computational enzymology, a swiftly evolving field of biochemistry, is exploring catalysis theories, questioning traditional mechanisms, and discovering new catalytic processes. This area holds promising practical applications such as interpretation of experimental data, designing catalysts, and developing to drugs (Kumar and Kumar, 2011). Several effective techniques have been developed to advance the understanding of enzymes and their mechanisms. One particularly productive approach has been the utilization of computational chemistry tools to study enzyme catalysis (Lewars, 2011). The results obtained from computer simulations can help interpret experimental results and predict the behavior of natural and modified enzyme systems, saving time and resources needed for conducting small-scale experiments (Knowlton and Graham, 2010; van GUNSTEREN and Mark, 1992; Walters and Holling, 1990). This integration of theory and practice has made enzymology a prime example of mutual benefit between the two disciplines.

#### 1.1.2.1 Modeling approach

The use of modelling techniques to understand enzyme-catalysed reaction mechanisms is becoming increasingly significant in the field of biochemistry. Through molecular simulation and modelling, we can acquire a thorough comprehension of the atomic-level processes involved in biological catalysts. This modelling approach is directly aiding experimental studies on enzyme-catalysed reactions. Computational models in systems biology enable us to investigate the development of intricate diseases, enhance our comprehension of underlying molecular mechanisms, and facilitate the optimization of treatment strategies and discovery of new drugs. By utilizing multi-omics data for in-depth analysis and predictions, systems biology has the potential to shed light on

the mechanisms behind complex diseases. Utilizing computational or mathematical models to study biological systems at various levels is a valuable method for identifying novel drugs. These models can elucidate how cells control signaling and metabolic pathways in response to external stimuli or drug interventions at the intracellular level (Ji et al., 2014). The advancement of high-throughput experimental techniques, including gene microarray, RNA-seq, mass spectrometry, and metabolic profiling, has enabled researchers to gain a deeper understanding of complex cellular systems through computational and mathematical modeling of biological processes (Wang et al., 2012). Scientists have developed multiple computational models to understand the intricate behaviors of cancer, including tumor growth, resistance to drugs, and immune evasion. These models can help answer important questions in enzyme reactions and may lead to advancements in drug development for a range of illnesses and conditions.

It is well known that bioinformatics relies on data, while systems biology is driven by hypotheses (Leggett et al., 2013; Schmid and Blank, 2010; Schmidt et al., 2015). We often create testable hypotheses based on small-scale experiments and then develop systemic models to gain insights into mechanisms. Various modeling approaches, such as Ordinary Differential Equations ($ODEs$) (Coddington and Levinson, 1955), Boolean Networks (Shmulevich et al., 2002), Petri Nets (Murata, 1989), Linear Programming ($LP$) models (Fishbone and Abilock, 1981; Gass, 2003), Agent-based models, and genetic variation-based systems biology models, can simulate the dynamic changes in regulatory networks, tumor growth, and micro environments. In this study, we focus on the $ODE$ based model to meet our research needs.

**ODE Based Modeling:** Due to the rapid advancement in computer performance, ordinary differential equation ($ODE$) based techniques have become prevalent for continuous dynamic modeling in complex biological systems (Eisenhammer et al., 1991). These methods capture the interactions among various biological molecules, such as protein kinases or metabolites, and reflect the time-dependent effects of biological processes. Depending on the specific biological hypotheses or experimental data, current $ODE$ based methods can be classified into three types: the Law of Mass Action (Koh and Lee, 2011; Peng et al., 2014), Hill Function (Shao et al., 2013), and Michaelis-

Menten Kinetics (Sun et al., 2013). The selection of a particular method relies on biological inquiries or available experimental data. In this article, we demonstrate the application of these kinetic approaches in describing biochemical reactions.

***Law of Mass Action:*** The law of mass states that the rate of a chemical reaction is directly related to the probability of reactants colliding. This probability is also proportional to the concentration of reactants raised to the power of their molecularity and the number of reactants involved in the specific reaction (Oliveira et al., 2000). For instance, a reaction involving $X$, $Y$, and $Z$ can be expressed as shown below:

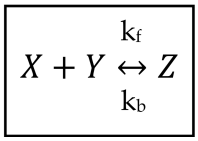


Figure 1.1: The schematic diagram of a reaction following the Law of Mass Action.

Here, $k_f$ and $k_b$ are the forward and backward rates of reaction, respectively.
Now, following the Law of Mass Action, the concentration changes over the time of the reactants ($X$ and $Y$) and product ($Z$) are described by the $ODEs$ as below:

$$\begin{aligned} \frac{d[X]}{dt} &= -k_f[X][Y] + k_b[Z], \\ \frac{d[Y]}{dt} &= -k_f[X][Y] + k_b[Z], \\ \frac{d[Z]}{dt} &= k_f[X][Y] - k_b[Z], \end{aligned} \tag{1.1.1}$$

with satisfying the initial conditions of the reaction.

***Hill Function:*** Hill functions are commonly utilized in $ODE$ models of signaling pathways to depict a protein's activation or inhibition resulting from its upstream parental nodes. In biochemistry, cooperative binding refers to the enhancement of ligand binding to a large molecule when another ligand is also bound to it. An example of positive cooperativity is the binding of oxygen to hemoglobin. Hemoglobin has four oxygen binding sites and when an oxygen atom attaches to one binding site on hemoglobin, the remaining three binding sites experience an increase in their affinity for oxygen, allowing the other oxygen molecules to bind more easily. The expression dynamics of each protein in the signaling pathways can be represented using Hill func-

tions, as demonstrated in the formula below:

$$\frac{dy}{dt} = \sum_{i=1}^{m} f_+(x_i) + \sum_{j=1}^{n} f_-(x_j) - y * d_y, \tag{1.1.2}$$

where, $y$ is the concentration of activated protein, $x_i$ $(i = 1, 2, ..., m)$ is the $ith$ protein which activates protein $y$, and $x_j$ $(j = 1, 2, ..., n)$ represents the $jth$ protein, which inhibits protein $y$. In the above formula, $f_+(x)$ and $f_-(x)$ are the activating profile $(+)$ and inhibiting profile $(-)$ induced by protein $x$, respectively. Here, $d_y$ is the degradation rate of protein $y$. The expression of $f_\pm(x)$ is like below,

$$f_\pm(x) = k_{xy} \frac{x^{\pm n_x}}{{H_x}^{\pm n_x} + x^{\pm n_x}}, \tag{1.1.3}$$

where, $k_{xy}$ represents activating rate (+) or inhibiting rate (-), $H_x$ is the microscopic dissociation constant and $n_x$ is the Hill coefficient.

***Michaelis-Menten Kinetics:*** The Michaelis-Menten kinetics can be employed to explain the relationship substrate and enzyme concentrations and the reaction rate of a specific reaction when an enzyme catalyses a signaling reaction. In this scenario, the enzyme may create a transient complex with the substrate involved in the reaction. For such reaction, the Michaelis-Menten kinetics can describe the reaction rate assuming the quasi-steady-state approximation ($QSSA$), and it is expressed as follows:

$$v = \frac{V_{max}[S]}{K_M + [S]}, \tag{1.1.4}$$

where, $v$ is the reaction rate, $V_{max}$ indicates the maximum rate of reaction. Here, the Michaelis constant is denoted as $K_M$, and $[S]$ represents the substrate concentration. A comprehensive explanation of Michaelis-Menten kinetics can be found in *Section (1.1.1.1)*, along with the illustration of enzymology.

$ODE$ based methods have been utilized to study the complex mechanisms of diseases at both intracellular and intercellular levels. Peng et al. developed a set of $ODE$ based techniques using the *Law of Mass Action* to effectively model intracellular pathways and make significant biological findings (Peng et al., 2011, 2012, 2014). Shao and colleagues introduced a model using $ODE$s with *Hill Functions* to analyze the signaling network patterns, considering both therapeutic and side effects. This model was

utilized to evaluate the optimal treatment concentration of *27* kinase inhibitors (Shao et al., 2013). Sun et al. developed an $ODE$ based model incorporating Michaelis-Menten kinetics to study antiapoptotic pathways in prostate cancer, shedding light on the molecular mechanisms of stress signaling in therapy-resistant cancer (Sun et al., 2013). Additionally, $ODE$s were effectively employed to depict the dynamic alterations of metabolites in small-scale metabolic reaction systems (Finn et al., 2011).

Collectively, the afore-mentioned works suggest that $ODE$ based models are appropriate for representing the ongoing kinetics in small-scale intracellular or intercellular networks (Arisi et al., 2006; Papin et al., 2005).

#### 1.1.2.2 Analytical Tools for model systems

Over the past few decades, significant resources have been dedicated to the development of a variety of tools and techniques aimed at understanding the intricate mechanisms of biological and biochemical systems. Some key tools commonly employed to elucidate these mechanisms include:

***Optimal Control Theory***: The optimal control therapeutic strategy plays a significant role in managing kinetic reactions. By applying this theorem, optimal control measures can be established to enhance product outcomes in enzymatic systems. The fundamental equation of optimal control theory can be formulated through various methods, including the *Pontryagin Minimum Principle* (Bonnans and Hermant, 2009; Pontryagin, 1987). This tool has numerous applications for accurately analysing a wide range of biological and biochemical systems (Grigorieva et al., 2014; Shen et al., 2021; Swan, 1981). Depending on the specific problem at hand, either the Pontryagin Minimum or Pontryagin Maximum Principle can be utilized as needed.

***Variational Iteration Method***: The Variational Iteration Method ($VIM$) is a successful technique for solving a variety of non-linear problems, developed by J. H. He (He, 1999). This method does not rely on the presence of small parameters in the differential equation, and instead provides the solution (or an approximation to it) through a sequence of iterations. It does not require the non-linearities to

be differentiable with respect to the dependent variable and its derivatives. This technique has gained popularity in recent years for its flexibility and adaptability in approximating analytical solutions (Omidiniya and Alipour, 2019; Wazwaz et al., 2016; Yildirim et al., 2012).

***Delay Differential Equations***: There exists a time delay in the conversion process of enzyme - substrate complex to enzyme - product complex before releasing the product for a biochemical reaction. Introducing a time delay during this conformational change stage can help to investigate the impact of other participating reactants in the specific biochemical reaction. The variational iteration method cannot address this time lag; hence, delay differential equations ($DDEs$) serve as an appropriate mathematical tool for studying chemical systems in this context. From a mathematical perspective, the introduction of time delay is crucial for realistic simulation of biochemical and biological processes. Numerous studies have been conducted and are ongoing using this viable mathematical tool (Albornoz and Parravano, 2007; Cai and Wang, 2007; Culshaw and Ruan, 2000; Tian and Liu, 2009).

***Fractional Order Differential Equations***: Fractional calculus, a highly effective method in Mathematical Sciences, was first introduced by *Leibnitz* in a letter written in 1695 (Ross, 1977). Fractional order differential equations ($FODEs$) serve as generalizations of integer order systems, helping to study mathematical models and minimize errors by considering neglected parameters. Recently, some authors have applied $FODEs$ in biochemical reactions to enhance their research (Abdullah, 2011; Alawneh, 2013).

***Impulsive Differential Equations***: Most enzymatic reactions in living systems involve the input of substrates and the removal of products. However, this process does not always occur simultaneously when drugs enter the body. Various systems, such as mechanical systems with impacts, biological systems like heartbeats and blood flow, population dynamics, chemical technology, metallurgy, ecology, biotechnology processes, and chemistry, do not operate continuously but instead

experience sudden changes or perturbations. Additionally, it is not always feasible to constantly add reactants in real-life situations. Therefore, there is a need to account for the impulse to add reactant concentrations based on the actual situation. Systems that experience sudden perturbations are described by Impulsive Differential Equations ($IDEs$), which have been extensively studied in the literature (Baınov and Simeonov, 1993; Lakshmikantham and Lakshmikantham, 1989; Miron and Smith, 2014; Sun et al., 2008; Wang and Chen, 2009). $IDEs$, or differential equations with impulse effects, are a common way to describe the evolution of real-world problems. Impulsive perturbations can make systems more difficult to solve, but in some cases, the models can be simplified into discrete-time mappings or difference equations when the continuous models can be explicitly solved. This is why most research on impulsive systems focuses on the basic theory of impulsive equations, which is rarely used to study enzyme kinetics. Different diseases in the human body often require varying doses of medication throughout the day and can develop resistance to drugs. Drug metabolism involves the interaction between drugs and enzymes in the liver, making impulsive differential equations valuable for modeling this process *in vivo*. Impulsive differential equations are currently utilized for modeling drug dynamics and examining the behavioral characteristics of non-linear models, including the impulsive effects of drugs (Smith and Wahl, 2004, 2005). This approach is also suitable for studying biochemical processes that are affected by short-term perturbations acting in the form of instantaneous impulses. In recent years, impulsive differential equations have become a valuable tool for depicting such biochemical systems.

**Fundamentals of IDEs:** In recent decades, significant advancements have been made in the theory of impulsive differential equations (IDEs) (Baınov and Simeonov, 2017). An IDE consists of three key components: a continuous-time differential equation that describes the system's state between impulses; an impulse equation that represents an impulsive jump, characterized by a jump function at the moment an impulse takes place; and a jump criterion that specifies a set of events where the impulse equation is applicable (Bainov and Simeonov, 1995). The mathematical formulation of

this theory is as follows:

$$\begin{aligned} \frac{dX(t)}{dt} &= f(t, X(t)) \qquad t = t_k, \\ \Delta X(t_k) &= I_k(X(t_k)) \qquad k = 1, 2, 3, ..., n. \end{aligned} \tag{1.1.5}$$

Let's consider the parameterized problem of impulsive differential equations, which can be expressed as follows:

$$\begin{aligned} \frac{dX(t)}{dt} &= f(t, X(t)) \qquad t \neq t_k, \\ X({t_k}^-) &= \alpha X({t_k}^+) + \beta \qquad t = t_k, \end{aligned} \tag{1.1.6}$$

with $X(0) = X_0$ and where, $k = 1, 2, 3, ..., n$; $\alpha, \beta \in \Re$; $\alpha \neq 0$.
In this context, $t_k$ refers to instants or moments of impulse, while $I_k$ denotes the change in state at each $t_k$, $X({t_k}^+) = \lim_{h \to 0+} X(t_k + h)$ and, $X({t_k}^-) = \lim_{h \to 0-} X(t_k + h)$ represent the right and left limits, respectively, of the state at $t = t_k$.

In recent years, impulsive differential equations have gained popularity as a method for analyzing real-life problems through modeling (Jose et al., 2022; Rattanakul and Chaiya, 2024; Wijaya et al., 2021). $IDEs$ are a modern approach to creating mathematical models of drug dynamics, making a significant impact on biochemistry for quantitative measurement. We have utilized this tool extensively to realistically simulate the biochemical processes involved in our study.

By the conclusion of Section *Section (1.1.2)*, it is apparent that advancements have resulted in an increased acknowledgment that computations and simulations are expected to complement experiments in regulatory biochemistry.

## 1.2 Scope and objective

There are multiple studies that demonstrate the impact of alcohol consumption on HIV-1 infected patients undergoing antiretroviral treatment. These studies have discussed the involvement of cytochrome P450 3A4 (CYP3A4) enzyme in metabolizing

anti-HIV drugs, such as Protease Inhibitors (PI) and non-nucleoside reverse transcriptase inhibitors (NNRTI) (Kumar and Kumar, 2011; Kumar et al., 2012). While there is a wealth of data on experimental studies examining how ethanol affects PIs, it is crucial to develop mathematical models for better understanding the afore-mentioned mechanisms. In our studies, we have addressed this issue by formulating a mathematical model that describes how CYP3A4 enzyme interacts with ethanol to alter drug metabolism. In conducting analytical and numerical studies, we effectively address the above unexplored issue in mathematical biochemistry and achieve satisfactory results.

On the other hand, numerous mathematical models have been developed to unravel the complex dynamics of viral replication in HIV-1 infection (Covert and Kirschner, 2000; Nowak and May, 2000; Perelson, 2002). These models have been enhanced with a variety of treatment approaches, including the impacts of different drug therapies (Nowak and May, 2000; Perelson, 2002; Wahl and Nowak, 2000). The effect of perfect adherence to antiretroviral therapy has been examined through the use of impulsive differential equations (Lou and Smith, 2011; Smith, 2006). Using the method mentioned above, the dosing period and the threshold values of dosage can be precisely estimated. When treating HIV-1 infection, there persist issues related to side effects and drug resistance, necessitating the exploration of new drugs that can target several distinct steps in the HIV-1 life cycle.

In this context, several analytical studies have been conducted on the development of dual inhibitors for HIV-1 reverse transcriptase (RT) and integrase (IN) in AIDS treatment, and the theoretical efficacy of these inhibitors in combating HIV-1 infection has also been discussed (De and Camarasa, 2018; Gu et al., 2016). A dual inhibitor of HIV-1 RT/IN is a single chemical entity that simultaneously inhibits both the viral enzymes reverse transcriptase (RT) and integrase (IN). Recent findings on the dual inhibitors of HIV-1 RT/IN indicate that these inhibitors are less prone to developing drug resistance from the virus due to their ability to target multiple facets of the virus and their cost-effectiveness. In addition, a handful theoretical studies have confirmed information about how the Tat and Rev inhibitors suppress HIV-1 transcription and decrease viral replication (Cecchetti et al., 2000; Mousseau et al., 2012, 2015; Wan and Chen, 2014). Despite several clinical studies on new drug development to better con-

trol HIV-1 infection, there is a noticeable lack of mathematical models addressing this topic. While there has been extensive research on HIV-1 infection in clinical settings, there remains a need to systematically monitor therapeutic treatment and determine an effective dosing regimen for applying the afore-mentioned inhibitors using a mathematical approach. The cost-effectiveness of the treatment in relation to mathematics is an important but overlooked area in this matter. It needs to be addressed, especially because it disproportionately affects low-income communities. In our research, we have tackled the mentioned concerns individually, utilizing impulsive differential equations and optimal control methods.

We have obtained the closed form solution of the impulsive differential equation model by using the Lambert W function. Also, we formulate an enzyme kinetics model on Tat-mediated HIV-1 transcription with the incorporation of Tat inhibitor to examine its impact on the reduction of HIV-1 transcription by employing an optimal control problem. Here, we also utilize the theory of impulsive differential equations to model the periodic drug dosing effectively. In one of our research studies, we formulate a mathematical model for combination drug therapy involving Tat and Rev inhibitors to demonstrate strategies for overcoming drug resistance. The goal is to minimize the cost of therapy while simultaneously optimizing the effect of this combination therapy on Tat-Rev regulation of HIV-1 replication.

In addition, by tackling the two main challenges mentioned above, we have incorporated impulsive differential equations ($IDEs$) and optimal control theory into the chemical reaction, a rare occurrence in the field of biochemistry.

## 1.3 Highlights of the thesis

This thesis consists of six chapters aimed at providing a comprehensive understanding of various mathematical models related to within-infected-cells replication of HIV-1. Below is a brief overview of each chapter, offering a general insight into the topics addressed throughout the thesis.

***Chapter 1:*** This chapter provides a concise overview of the biochemical mechanisms and highlights the significance of biochemistry in the clinical domain, along with the role of mathematical modeling in enhancing this study. Additionally, it outlines the scope and objectives of the thesis.

***Chapter 2:*** In this chapter, we have studied a mathematical model based on the enzymatic activity of cytochrome $P3A4$ ($CYP3A4$) for the alcoholic HIV infected patients. Alcohol consumption is prevalent in HIV/AIDS infected patients. It possesses serious effects on protease inhibitors ($PIs$), which are used as antiviral drug. While taking $PIs$, the secretion of Cytochrome $P3A4$ ($CYP3A4$) enzymes occurs from liver and it metabolises the drug to $CYP3A4 - PI$ complex. Alcohol consumption increases the rate of metabolism of $PIs$. In this chapter, we have analytically compared the dynamics of $PIs$ metabolism between alcoholic and non-alcoholic HIV infected patients and also investigated how infection is being accelerated by enhancing viral load due to alcohol consumption. Our analytical results are verified by numerical findings.

***Chapter 3:*** Reverse transcriptase (RT) and integrase (IN) are two pivotal enzymes in HIV-1 replication. RT converts the single-stranded viral RNA genome into double-stranded DNA and IN catalyzes the integration of viral double-stranded DNA into host DNA. In this chapter, we develop a mathematical model comprising a system of non-linear differential equations describing HIV-1 RT/IN catalysed biochemical reactions based on Michaelis-Menten enzyme kinetic reaction. In the formulated model we incorporate HIV-1 RT/IN dual inhibitor which simultaneously works as a non-nucleoside RT inhibitor and IN inhibitor. To examine the efficacy of HIV-1 RT/IN dual inhibitor in the treatment of HIV-1 infection we have introduced a one dimensional impulsive differential equation model and determined an effective dosing regimen for applying the inhibitor numerically. Furthermore, the exact closed form solution of the impulsive differential equation model is carried out by using the Lambert W function and the local stability of the periodic solution is also obtained analytically. The results obtained from analytical as well as numerical studies provide

a basic idea to investigate the minimum dose with the highest efficacy for administering HIV-1 RT/IN dual inhibitors to prevent HIV-1 infection.

***Chapter 4:*** In this chapter, we have constructed an enzyme kinetic model consisting of a system of non-linear differential equations representing the biochemical reactions associated with the HIV-1 transcription process. The investigation of the impact of a Tat inhibitor on the suppression of the transcriptional activity of HIV-1 is the aim of this inquiry. The perspective of an optimal control problem is assumed for this investigation. Additionally, it evaluates the effectiveness of the Tat inhibitor as a potential treatment for HIV-1 infection. To facilitate this assessment, we have utilized a one-dimensional impulsive differential equation model, which calculates the mathematically derived maximum concentration of the elongating complex ($P_2$). The crucial aspect of this investigation is the consideration of the optimal timing between successive dosages. A comparative analysis is conducted to evaluate the distinct effects of continuous dosing versus impulse dosing of the Tat inhibitor. Numerical analysis is employed to contrast the outcomes of these dosing strategies. The present findings highlight that impulsive dosing demonstrates superior effectiveness compared to continuous dosing in the inhibition of HIV-1 transcription. Ultimately, the model's parameter sensitivities are visualized through graphical representations. These visualizations serve to enhance the understanding of the underlying physiological and biochemical processes within this intricate system.

***Chapter 5:*** In this chapter, we have formulated another enzyme kinetic model in order to observe the effect of both the viral proteins: Tat and Rev on HIV-1 replication. We have examined the impact and effectiveness of a combined drug therapy (administering Tat and Rev inhibitor) by employing an optimal control problem. By using the Pontryagin maximum principle, the optimal control problem of minimizing the cost of therapy while simultaneously optimizing the effect of this therapy on Tat-Rev regulation of HIV-1 replication has been studied. To comprehend the qualitative study, numerical simulations are conducted using different values of the system parameters.

***Chapter 6:*** Chapter 6 presents the conclusion, summarizing the theoretical and numerical results from all the chapters of the thesis. Additionally, this chapter outlines the potential future directions for the research.

# Chapter 2

# Effect of alcohol consumption during antiretroviral therapy on HIV-1 replication: role of cytochrome P3A4 enzyme

## 2.1 Introduction

HIV-1 infection is a global problem with 36.9 million people affected in the world at the end of 2017. The African region remains most severely affected with accounting for nearly two-thirds of the people living with HIV worldwide (Kumar et al., 2012). There were approximately 1.8 million people becoming newly infected in 2017 globally. People with HIV infection have to take a combination of anti-AIDS drugs on a daily basis to stay healthy.

There are about 26 FDA approved anti-AIDS drugs currently available acting on different stages of the HIV life-cycle (Das and Arnold, 2013); most fall into 4 classes: (i) Entry/Fusion Inhibitors (ii) Reverse Transcriptase Inhibitors (Nucleoside/Nucleotide Reverse Transcriptase Inhibitors, i.e., NRTI and Non-Nucleoside Reverse Transcriptase

inhibitors, i.e., NNRTI) (iii) Integrase Inhibitors and (iv) Protease Inhibitors, i.e., PI. The most extensive treatment approach for acutely infected HIV patients is highly active antiretroviral therapy (HAART), which typically includes 2 NRTIs along with 1NNRTI and PI.

The prevalence of alcohol abuse is approximately three times higher in HIV-infected individuals than in the general population and is associated with adverse health effects (Chander, 2011; Gonzalez et al., 2011; Kumar et al., 2012; Purohit et al., 2011). Heavy alcohol consumption and alcoholism can cause liver and pancreatic damage. Also, alcohol increases the progress rate of AIDS and neuroAIDS (Chander et al., 2009; Norman and Kumar, 2006). Although HIV-infected patients should avoid alcohol especially while on HAART treatment, patient compliance is limited (Hirsch et al., 2008; Miguez et al., 2003). Chronic alcohol consumption during HAART decreases patient adherence to HAART as well as increases neuronal toxicity (Chander et al., 2006; Ferrari and Levine, 2010; Hendershot et al., 2009; Hirsch et al., 2008; Witteveen and Ameijden, 2002). The enzyme Cytochrome P450 3A4 (CYP3A4) plays an important role in interactions between antiretrovirals (ART) and alcohol.

Cytochrome P450 3A4 (CYP3A4) is the major metabolic enzyme in the human liver, which is responsible to metabolize about 50% of the therapeutic drugs including non-nucleoside reverse transcriptase inhibitors (NNRTIs) and protease inhibitors (PIs) (Kumar and Kumar, 2011; Midde et al., 2016). Inhibition or inactivation of CYP3A4 can cause mild to severe drug-drug interactions resulting in unanticipated adverse reactions or therapeutic failures (Kumar and Kumar, 2011; Pal and Mitra, 2006; Walubo, 2007). NNRTIs and PIs act as either inducers or inhibitors of CYP3A4 while all PIs are inhibitors of CYP3A4 (Kumar et al., 2012). Ritonavir, a protease inhibitor which is an extremely potent inhibitor of CYP3A4 is present in most of the HAART regimens. It is generally used as a booster to increase the plasma concentrations and the half-life of other ARTs because of its strong binding affinity to CYP3A4 and inhibition of CYP3A4 (Kumar and Kumar, 2011). Thus, ritonavir increases the bioavailability of NNRTIs and PIs by decreasing their metabolism by CYP3A4 (Acosta, 2002; Kumar et al., 2012; Xu and Desai, 2009). But in this case, alcohol consumption may alter the rate of metabolism of PIs by changing CYP3A4-PIs interactions.

Alcohol interacts with PIs, through CYP3A4 induction leading to altered drug metabolism and toxicity in the liver (Flexner et al., 2001; Kumar et al., 2012). Since Ethanol has greater binding affinity to enzyme CYP3A4 than PIs, it first binds with the enzyme forming CYP3A4-Ethanol complex. Thus Ethanol alters the inhibition of CYP3A4 by PIs which may lead to relatively faster metabolism of PIs. For this, the effectiveness of the PIs, as well as, NNRTIs decreases. Thus, individuals who consume ethanol and take PI drugs are at high risk of deleterious ethanol PIs interaction.

There are ample mathematical models available in literature considering HIV/AIDS transmission those are being implemented either in cellular or in social population level. In 2015, (Roy et al., 2015) determined the media impact on the HIV outbreak and suggested that infection level reduces the effective contacts between human and media. Also, it has been shown the impact of an awareness campaign to combat Leishmaniasis (Biswas et al., 2016), and the methodology of satellite data utilization in Multi-Modeling Approach for socio-ecological risks (Kostyuchenko, 2018). A handful of mathematical models have examined various treatment strategies and the effects of different drug therapies. The effect of perfect adherence to antiretroviral therapy has been studied using impulsive differential equations (Lou and Smith, 2011; Smith and Wahl, 2004, 2005; Smith?, 2008; Song et al., 2011). Several mathematical models have been developed to describe the interaction of the human immune system with HIV, the decline in CD4+ T cell count and the effects of different drug therapies (Chatterjee and Roy, 2012). Recently, (Chowdhury and Roy, 2016) examined the effect of combination therapy on viral dynamics using Enfuvirtide and PIs. Also, several studies have shown the alcohol consumption effects for HIV-infected patients while they are on HAART. They also describe the role of CYP450 enzymes in the metabolism of drugs used in HAART (i.e., Protease Inhibitors (PI) and non-nucleoside reverse transcriptase inhibitors (NNRTI)) (Kumar and Kumar, 2011; Kumar et al., 2012). Even Ghosh et al. has done some mathematical works by formulating enzyme kinetics models on alcoholism (Ghosh and Roy, 2018; Ghosh et al., 2018). Although there is a lot of information on experimental works involving the effects of ethanol on PIs, there is a need to establish mathematical models to improve our understanding of these processes. Thus, in this research work, we have formulated a mathematical

model describing the CYP3A4-ethanol interactions involved in order to alter drug metabolism. We start by making schematic themes where we show how consumption of alcohol inhibits CYP3A4-PI interaction. The model is studied both analytically and numerically based on the biological and chemical interactions of CYP3A4-PI-Ethanol complexes.

The research article has been arranged as follows: Section (2) describes the model formulation followed by the analytical part in section (3). Section (4) deals with the numerical experimentation and section (5) contains the conclusion.

## 2.2 Formulation of mathematical model

For the HIV infected patients, Protease Inhibitors ($I$) are metabolized into the CYP3A4-PI complex ($EI$) by the liver secreted cytochrome P3A4 (CYP3A4) enzymes ($E$) and little portion of the complex ($EI$) reverts. For this reaction, the forward and the backward rate constants are $k_1$ and $k_{-1}$ respectively. Since, alcohol ($S$) has higher affinity towards the P3A4 (CYP3A4) enzymes ($E$) than PIs ($I$), alcohol binds with the single active sited enzyme ($E$) for an alcoholic HIV infected patient and forms enzyme-alcohol complex ($ES$). A little portion of this complex ($ES$) reverts and remaining portion of it breaks down into the alcohol ($S'$) and the enzyme ($E_s$) again, slight changing their internal properties. The released enzyme ($E_s$) becomes more strong than previous one, which actually helps to bind and metabolize the PIs ($I$) more effectively. For this, the utilization of the drug PIs ($I$) decreases and metabolism of it increases, which is harmful for a HIV infected patient. However, the enzyme ($E_s$) and PIs ($I$) reacting with each other form intermediate complex ($E_sI$), a little portion of which reverts and remaining portion is transformed into another complex ($E_sIS'$) binding with the changed alcohol ($S'$). Finally, the last complex ($E_sIS'$) breaks down into a product ($P$) with unrecognised property and the enzyme ($E_s$) as well as slight portion of it ($E_sIS'$) reverts. The forward and the backward rate constants for this alcohol induced PIs metabolism system are $k_2, k_3, k_4, k_5, k_6$ and $k_{-2}, k_{-4}, k_{-5}$ respectively. The above facts are represented in the schematic diagram as in Figure (2.1).

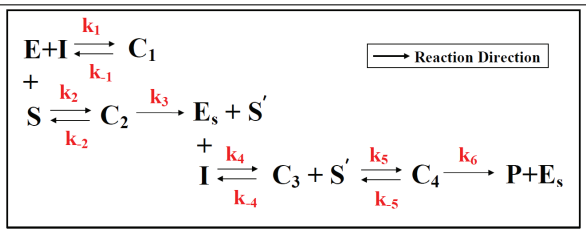


Figure 2.1: The schematic diagram of competitive inhibition reaction.

To simplify the above system and avoid the complexity of the analytical as well as numerical studies we can imagine a zoom out image of the whole system.

We skip the further break down of $C_2$ and therefore the concentrations of $E_s$ and $S'$ are automatically omitted from the second horizontal line of the reaction chain. Carrying the consequence of the second row, $C_4$ is also deleted with $S'$ from the third row as $C_4$ is nothing other than a complex from $S'$ and $C_3$ reaction. Hence, here we neglect two further steps of reaction in two different horizontal lines. In fact, if we think more realistically those steps are truly negligible for the rapidity of the reaction. Except those ignored parts, the schematic diagram is same as above and the notations carry their usual meaning. Furthermore, there are some other notations seen in the inland mathematical model. For instance, $\lambda$ is the secretion rate of enzyme $E$ and $\mu_1, \mu_2, \mu_3, \mu_4$ are the natural dissociation or clearance rates of $E, I, S, P$ respectively. In addition, $\bar{I}$ and $\bar{S}$ are the rates of required concentration for $I$ and $S$, those absorb in the mentioned enzymatic reaction. Now, the modified schematic diagram is as follows:

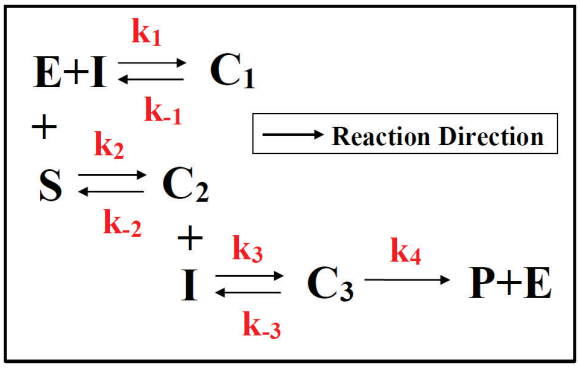


Figure 2.2: The modified schematic diagram of competitive inhibition reaction.

Following the Law of Mass Action, the set of nonlinear differential equations for the above enzymatic reaction is as follows:

$$\begin{aligned}
\frac{dE}{dt} &= \lambda - k_1EI + k_{-1}C_1 - k_2ES + k_{-2}C_2 + k_4C_3 - \mu_1E,\\
\frac{dI}{dt} &= \bar{I} - k_1EI + k_{-1}C_1 - k_3C_2I + k_{-3}C_3 - \mu_2I,\\
\frac{dC_1}{dt} &= k_1EI - k_{-1}C_1,\\
\frac{dS}{dt} &= \bar{S} - k_2ES + k_{-2}C_2 - \mu_3S,\\
\frac{dC_2}{dt} &= k_2ES - k_{-2}C_2 - k_3C_2I + k_{-3}C_3,\\
\frac{dC_3}{dt} &= k_3C_2I - k_{-3}C_3 - k_4C_3,\\
\frac{dP}{dt} &= k_4C_3 - \mu_4P,
\end{aligned} \tag{2.2.1}$$

with the initial conditions $E(0) = E_0, I(0) = I_0, C_1(0) = C_{10}, S(0) = S_0, C_2 = 0, C_3 = 0$, and $P(0) = 0$.

## 2.3 Model Property

### 2.3.1 Non-negativity

In this section, we want to show the non-negativity of the solutions of the system (2.2.1) using the following theorem.

**Theorem 2.3.1** *Each solution of the system (2.2.1) with initial conditions, remains non-negative for all* $t \geqslant 0$.

**Proof.** From the first equation of system (2.2.1), we can write,

$$\begin{aligned}
\frac{dE}{dt} &= \lambda - k_1EI + k_{-1}C_1 - k_2ES + k_{-2}C_2 + k_4C_3 - \mu_1E\\
&> -k_1EI - k_2ES - \mu_1E \quad \forall \quad t \in [0, t_1].
\end{aligned} \tag{2.3.1}$$

Hence,

$$E(t) > E(0)e^{-\int_0^t (k_1I(T) + k_2S(T) + \mu_1)dT}, \tag{2.3.2}$$

as $t \in [0, t_1]$ and as long as

$$\int_0^t I(T)dT < +\infty \quad and \quad \int_0^t S(T)dT < +\infty. \tag{2.3.3}$$

Again from the second equation, we have

$$\begin{aligned} \frac{dE}{dt} &= \bar{I} - k_1 EI + k_{-1}C_1 - k_3 C_2 I + k_{-3}C_3 - \mu_2 I \\ &> -k_1 EI - k_3 C_2 I - \mu_2 I \quad \forall \quad t \in [0, t_1]. \end{aligned} \tag{2.3.4}$$

Which implies,

$$I(t) > I(0)e^{-\int_0^t (k_1 E(T) + k_3 C_2(T) + \mu_2)dT}, \tag{2.3.5}$$

as $t \in [0, t_1]$ and as long as

$$\int_0^t E(T)dT < +\infty \quad and \quad \int_0^t C_2(T)dT < +\infty. \tag{2.3.6}$$

In a similar way, we can show the non-negativity of $S$ and $C_1$ in $[0, t_1]$.
Now, we prove the non-negativity of $C_2, C_3$, and $P$.
Here,

$$\begin{aligned} \frac{dC_2}{dt} &= k_2 ES - k_{-2}C_2 - k_3 C_2 I + k_{-3}C_3 \\ &> -k_{-2}C_2 - k_3 C_2 I. \end{aligned} \tag{2.3.7}$$

But the initial value of $C_2$ is zero. So, we can write,

$$\frac{dC_2}{dt} \geqslant 0, \tag{2.3.8}$$

implies,

$$C_2 \geqslant 0. \tag{2.3.9}$$

In similar manner we can also show the non-negativity of $C_3$ and $P$.

Thus, we prove the non-negativity of the solutions of the system (2.2.1) with the initial conditions.

### 2.3.2 Boundedness

In this section, it is shown that the solutions of the system (2.2.1) are bounded, using the following theorem.

**Theorem 2.3.2** *Every solution of the system (2.2.1) with initial conditions, starts in $R_+^7$, is uniformly bounded.*

**Proof.** $\lambda, \bar{I}$ and $\bar{S}$ are the entering rate of $E, I$ and $S$ respectively for the proposed enzymatic reaction. It is obvious that the concentration of $E, I$ and $S$ always lie within their entering concentration. Therefore, we can write $E \leq \lambda, I \leq \bar{I}$ and $S \leq \bar{S}$ for any time $t$.

Now, from the third equation of the system (2.2.1), we can write

$$\begin{aligned} \frac{dC_1}{dt} &= k_1 EI - k_{-1} C_1 \\ &\leq k_1 \lambda \bar{I} - k_{-1} C_1. \end{aligned} \tag{2.3.10}$$

Solving the above inequality, we get

$$C_1 \leq \frac{k_1 \lambda \bar{I}}{k_{-1}} + C_1(0) e^{-} k_{-1} t, \tag{2.3.11}$$

for long time interval, we obtain

$$C_1(t) \leq \frac{k_1 \lambda \bar{I}}{k_{-1}}, \text{the maximum value of CYP3A4-PI.} \tag{2.3.12}$$

Now, we add fifth and sixth equations of our model

$$\frac{d(C_2 + C_3)}{dt} \leq k_2 \lambda \bar{S} - \xi(C_2 + C_3), \text{where } \xi = min\{k_{-2}, k_4\}. \tag{2.3.13}$$

Solving the above inequality, we get

$$(C_2 + C_3)(t) \leq \frac{k_2 \lambda \bar{S}}{\xi} + (C_2 + C_3)(0) e^{-} \xi t, \tag{2.3.14}$$

for long time interval, we get

$$(C_2 + C_3)(t) \leq \frac{k_2 \lambda \bar{S}}{\xi}, \tag{2.3.15}$$

the maximum value of CYP3A4-Ethanol complex and CYP3A4-PI-Ethanol complex.

Similarly, using the maximum value of $C_3$, we get from last equation,

$$\frac{dP}{dt} \leq \frac{k_4 k_2 \lambda \bar{S}}{\xi} - \mu_4 P. \tag{2.3.16}$$

Solving the above inequality, we get the thresold value of product as follows,

$$P(t) \leq \frac{k_2 k_4 \lambda \bar{S}}{\xi \mu_4}. \tag{2.3.17}$$

Therefore, all solutions of the system (2.2.1) are bounded.

### 2.3.3 Equilibrium Analysis

In this section we analyze the stability of the endemic equilibrium of the system (2.2.1). The endemic equilibrium of the system (2.2.1) will be in the form $E(E^*, I^*, S^*, C_1^*, C_2^*, C_3^*, P^*)$, where, $E^* = \frac{\lambda}{\mu_1}$ , $I^* = \frac{\bar{I}-k_4 C_3^*}{\mu_2}$, $S^* = \frac{\bar{S}-k_4 C_3^*}{\mu_3}$, $C_1^* = \frac{\lambda k_1(\bar{I}-k_4 C_3^*)}{k_{-1}\mu_1\mu_2}$, $C_2^* = \frac{\lambda k_2 \bar{S} - \lambda k_2 k_4 C_3^* - \mu_1\mu_3 k_4 C_3^*}{k_{-2}\mu_1\mu_3}$, $P^* = \frac{k_4 C_3^*}{\mu_4}$ and the value of $C_3^*$ will be obtained from the equation:
$(\lambda k_2 k_3 k_4^2 + \mu_1\mu_3 k_3 k_4^2)C_3^{*2} - (\lambda k_2 k_3 k_4 \bar{S} + \lambda k_2 k_3 k_4 \bar{I} + \mu_1\mu_3 k_3 k_4 \bar{I} + k_2 k_3 \mu_1\mu_2\mu_3 + k_2 k_4 \mu_1\mu_2\mu_3)C_3^* + \lambda k_2 k_3 \bar{S}\bar{I} = 0$.
The Jacobian matrix at the equilibrium point is:

$$J = \begin{pmatrix} a_{11} & a_{12} & a_{13} & a_{14} & a_{15} & a_{16} & a_{17} \\ a_{21} & a_{22} & a_{23} & a_{24} & a_{25} & a_{26} & a_{27} \\ a_{31} & a_{32} & a_{33} & a_{34} & a_{35} & a_{36} & a_{37} \\ a_{41} & a_{42} & a_{43} & a_{44} & a_{45} & a_{46} & a_{47} \\ a_{51} & a_{52} & a_{53} & a_{54} & a_{55} & a_{56} & a_{57} \\ a_{61} & a_{62} & a_{63} & a_{64} & a_{65} & a_{66} & a_{67} \\ a_{71} & a_{72} & a_{73} & a_{74} & a_{75} & a_{76} & a_{77} \end{pmatrix},$$

where, $a_{11} = -k_1 I^* - k_2 S^* - \mu_1$, $a_{12} = -k_1 E^*$, $a_{13} = -k_2 E^*$, $a_{14} = k_{-1}$, $a_{15} = k_{-2}$, $a_{16} = k_4$, $a_{17} = 0$, $a_{21} = -k_1 I^*$, $a_{22} = -k_1 E^* - k_3 C_2^* - \mu_2$, $a_{23} = 0$, $a_{24} = k_{-1}$, $a_{25} = -k_3 I^*$, $a_{26} = k_{-3}$, $a_{27} = 0$, $a_{31} = -k_2 S^*$, $a_{32} = 0$, $a_{33} = -k_2 E^* - \mu_3$, $a_{34} = 0$, $a_{35} = k_{-2}$, $a_{36} = 0$, $a_{37} = 0$, $a_{41} = k_1 I^*$, $a_{42} = k_1 E^*$, $a_{43} = 0$, $a_{44} = -k_{-1}$, $a_{45} = 0$,

$a_{46} = 0$, $a_{47} = 0$, $a_{51} = k_2 S^*$, $a_{52} = -k_3 C_2^*$, $a_{53} = k_2 E^*$, $a_{54} = 0$, $a_{55} = -k_{-2} - k_3 I^*$, $a_{56} = k_{-3}$, $a_{57} = 0$, $a_{61} = 0$, $a_{62} = k_3 C_2^*$, $a_{63} = 0$, $a_{64} = 0$, $a_{65} = k_3 I^*$, $a_{66} = -k_{-3} - k_4$, $a_{67} = 0$, $a_{71} = 0$, $a_{72} = 0$, $a_{73} = 0$, $a_{74} = 0$, $a_{75} = 0$, $a_{76} = k_4$, $a_{77} = -\mu_4$.

Now the characteristic polynomial of the above matrix $J$ is:

$$det(J - uI_7) = (-\mu_4 - u)(u^6 + Au^5 + Bu^4 + Cu^3 + Du^2 + Eu + F). \quad (2.3.18)$$

Where the values of the coefficients $A$, $B$, $C$, $D$, $E$, $F$ are as follows:

$$\begin{aligned}
A &= -\sum a_{ii} \\
B &= \sum a_{ii}a_{jj} - \sum a_{ij}a_{ji} \\
C &= -\sum a_{ii}a_{jj}a_{kk} + \sum a_{ij}a_{ji}a_{kk} - \sum a_{ij}a_{jk}a_{ki} \\
D &= \sum a_{ii}a_{jj}a_{kk}a_{ll} + \sum a_{ij}a_{ji}a_{ki}a_{ll} + \sum a_{ij}a_{ji}a_{kl}a_{lk} - \sum a_{ij}a_{ji}a_{kk}a_{ll} - \sum a_{ij}a_{jk}a_{kl}a_{li} \\
E &= -\sum a_{ii}a_{jj}a_{kk}a_{ll}a_{mm} + \sum a_{ij}a_{ji}a_{kk}a_{ll}a_{mm} - \sum a_{ij}a_{jk}a_{kl}a_{li}a_{mm} - \sum a_{ij}a_{jk}a_{ki}a_{ll}a_{mm} \\
&\quad - \sum a_{ij}a_{ji}a_{kl}a_{lk}a_{mm} + \sum a_{ij}a_{jk}a_{kl}a_{lm}a_{mi} \\
F &= \sum a_{ii}a_{jj}a_{kk}a_{ll}a_{mm}a_{nn} + \sum a_{ij}a_{jk}a_{kl}a_{lm}a_{mi}a_{nn} + \sum a_{ij}a_{ji}a_{kl}a_{lk}a_{mm}a_{nn} \\
&\quad + \sum a_{ij}a_{jk}a_{ki}a_{lm}a_{mn}a_{nl} - \sum a_{ij}a_{ji}a_{kk}a_{ll}a_{mm}a_{nn} - \sum a_{ij}a_{ji}a_{kl}a_{lm}a_{mk}a_{nn}
\end{aligned} \quad (2.3.19)$$

Here A, B, C, D, E, F follows a rule: $i \neq j \neq k \neq l \neq m \neq n$. If $i = 1$ then $j$ can go to 2 or 3 or 4 or 5 or 6. Following same rule for $k, l, m, n$. Similarly, 2 can go to 1 or 4 or 5 or 6, 3 can go to 1 or 5, 4 can go to 1 or 2, 5 can go to 1 or 2 or 3 or 6, and 6 can go to 2 or 5.

Let $M_1 = \begin{pmatrix} A \end{pmatrix}$, $M_2 = \begin{pmatrix} A & 1 \\ 0 & B \end{pmatrix}$, $M_3 = \begin{pmatrix} A & 1 & 0 \\ C & B & A \\ 0 & 0 & C \end{pmatrix}$, $M_4 = \begin{pmatrix} A & 1 & 0 & 0 \\ C & B & A & 1 \\ 0 & D & C & B \\ 0 & 0 & 0 & D \end{pmatrix}$,

$M_5 = \begin{pmatrix} A & 1 & 0 & 0 & 0 \\ C & B & A & 1 & 0 \\ E & D & C & B & A \\ 0 & 0 & E & D & C \\ 0 & 0 & 0 & 0 & E \end{pmatrix}$ and $M_6 = \begin{pmatrix} A & 1 & 0 & 0 & 0 & 0 \\ C & B & A & 1 & 0 & 0 \\ F & E & D & C & B & A \\ 0 & F & E & D & C & B \\ 0 & 0 & 0 & F & E & D \\ 0 & 0 & 0 & 0 & 0 & F \end{pmatrix}$.

***Lemma:*** All roots of the characteristic equation are negative or negative real part if the determinants of all the Hurwitz matrices are positive, i.e., $det(M_j) > 0, j \in \{1, 2, ...6\}$. Thus from the Routh-Hurwitz criterion the system is asymptotically stable if $det(M_j) > 0, j \in \{1, 2, ...6\}$.

## 2.4 Numerical Analysis

In this section, we study the numerical simulations of our model system on the basis of analytical findings. Our numerical studies were done using MATLAB 2008a. For numerical simulations we take a set of parameter values given in Table (2.1). Most of the parameter values are taken from (Das and Arnold, 2013; Goudar et al., 1999; Kumar et al., 2012; Schulz, 1994; Segel, 1984), some are estimated and remaining values are assumed.

Table 2.1: Values of the parameters used in numerical simulation.

| Parameters | Values (Unit) |
|---|---|
| $k_1$ | (0.01-2.5) $(\mu\ mol/l)^{-1}h^{-1}$ |
| $k_2$ | (0-3) $(\mu\ mol/l)^{-1}h^{-1}$ |
| $k_3$ | (0-2.5) $(\mu\ mol/l)^{-1}h^{-1}$ |
| $k_4$ | (0-3) $(\mu\ mol/l)^{-1}h^{-1}$ |
| $k_{-1}$ | (0.001-0.3) $h^{-1}$ |
| $k_{-2}$ | (0-0.03) $h^{-1}$ |
| $k_{-3}$ | (0-0.09) $h^{-1}$ |

Figure (2.3) shows the reaction dynamics between protease inhibitors and cytochrome P3A4 (CYP3A4) enzyme in human liver in the absence of alcohol. While taking protease inhibitors ($I(t)$), the secretion of enzyme Cytochrome P3A4 ($E(t)$) occurs from the liver and it reacts with the drug forming CYP3A4-PI complex ($C_1(t)$). So, the enzyme ($E(t)$) concentration and the PI ($I(t)$) concentration decrease and the complex concentration ($C_1(t)$) increases with time in a particular rate. Further, a little portion of the complex ($C_1(t)$) reverts back to the enzyme ($E(t)$) and PI ($I(t)$).

So, the complex ($C_1(t)$) concentration decreases and as the enzyme ($E(t)$) is reversed, the enzyme ($E(t)$) concentration slightly increases. But changing in the concentration of the drug PI ($I(t)$) is not noticeable because of its higher concentration. Although we can study the effect of reversion of the drug PI ($I(t)$) in other way. If there is no reversion of the PI ($I(t)$) from the complex $C_1$, the PI ($I(t)$) concentration will decrease more rapidly. But since the drug ($I(t)$) is reversed, the PI ($I(t)$) concentration decreases very slowly.

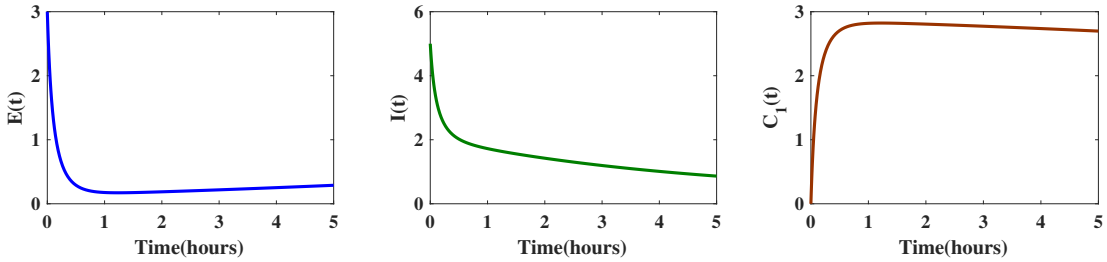


Figure 2.3: The nature of the curves of enzyme, protease inhibitor and complex $C_1$ without alcohol, using $E_0 = 3.0\ \mu mol/L$, $I_0 = 5.0\ \mu mol/L$, $S_0 = 0\ \mu mol/L$ and $C_{10} = 0$ as initial values.

Figure (2.4) describes the dynamics between protease inhibitor and cytochrome P3A4 enzyme in liver after consumption of alcohol. When an HIV-infected individual consumes alcohol ($S(t)$), it goes to the liver and reacts with the liver secreted enzyme cytochrome P3A4 ($E(t)$). So, the concentration of alcohol ($S(t)$) and enzyme ($E(t)$) decreases and the complex ($C_2(t)$) concentration increases with time at a particular rate. A little portion of the complex ($C_2(t)$) reverts. Now the drug Protease Inhibitor ($I(t)$) reacts with the complex ($C_2(t)$) forming a complex ($C_3(t)$). For this, the complex ($C_2(t)$) concentration decreases and as a little portion of the complex ($C_3(t)$) reverts, the concentration of complex ($C_2(t)$) slightly increases. Now, the complex ($C_3(t)$) is converted into the product ($P(t)$) and the enzyme ($E(t)$) is reversed. So, the complex ($C_3(t)$) concentration decreases when the product ($P(t)$) concentration increases and as the CYP3A4 enzyme ($E(t)$) is reversed, the enzyme ($E(t)$) concentration increases.
In figure (2.5), we compare the concentrations of enzyme CYP3A4, protease inhibitor and the complex $C_1$ in presence of alcohol and in the absence of alcohol. Here we

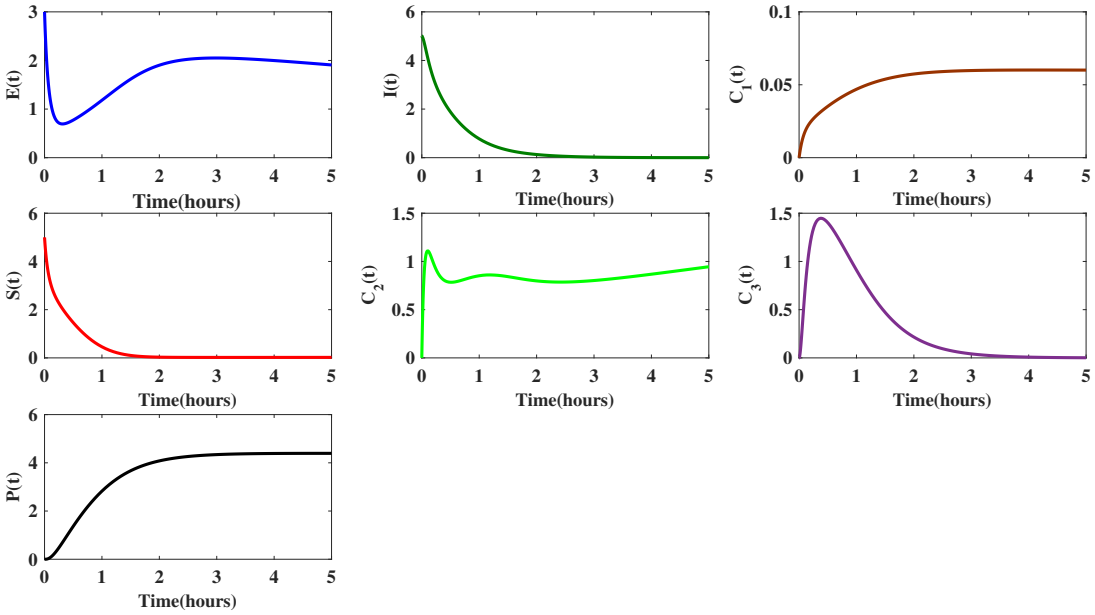


Figure 2.4: The nature of the curves of all reactance after alcohol consumption with the initial values $E_0 = 3.0\ \mu mol/L$, $I_0 = 5.0\ \mu mol/L$, $S_0 = 5.0\ \mu mol/L$ and $C_{10} = 0$.

observe that the formation of the complex $C_1$ slows down after consumption of alcohol. Because of the absorption of enzyme cytochrome P3A4 ($E(t)$) by alcohol as well as the reaction of the enzyme ($E(t)$) with the drug PI ($I(t)$), enzyme concentration decreases. But since the enzyme ($E(t)$) is reversed, the concentration of the enzyme ($E(t)$) increases. Also we can see that in presence of alcohol, the curve of protease inhibitor PI ($I(t)$) becomes lower that in absence of alcohol which is harmful for alcoholic HIV-infected individual. Until the complex $C_2$ is formed, PI reacts with the enzyme ($E(t)$) and produces the complex $C_1$. Hence, at first, in presence of alcohol the PI concentration slows down in a similar way that of the curve of PI in absence of alcohol. Another feature of the figure is that the curve of complex $C_1$ is like a horizontal curve in the presence of alcohol. Due to the presence of alcohol, the formation of complex $C_1$ is negligible and thus we see the impact of alcohol consumption on protease inhibitor for HIV-infected individuals.

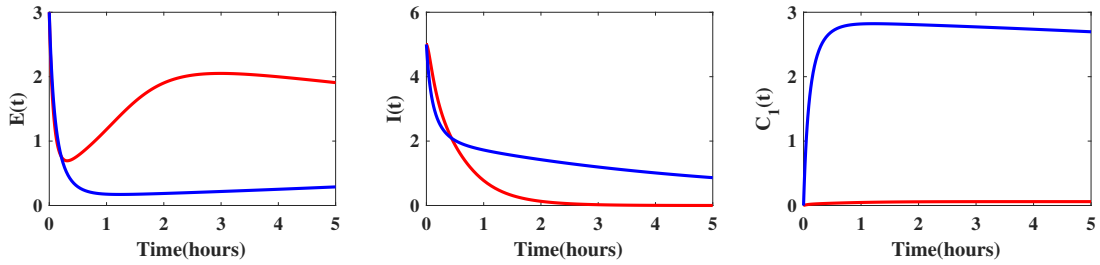


Figure 2.5: comparison study between absence of alcohol and presence of alcohol for enzyme, protease inhibitor and complex $C_1$ with the initial conditions $E_0 = 3.0\ \mu mol/L$, $I_0 = 5.0\ \mu mol/L$, $S_0 = 5.0\ \mu mol/L$ and $C_{10} = 0$

## 2.5 Conclusion

In this work, we mainly focus on the effect of alcohol consumption during antiretroviral therapy for HIV-infected individuals. The PIs used in the HAART regimen interact with alcohol, thereby altering their metabolism and antiviral activity. Here, we show that the alcohol and PIs interact with CYP3A4 physically causing complex alcohol–CYP3A4–PI, which results in altered metabolism of PI and NNRTI in the liver. In section 2.2, we have constructed a mathematical model using enzyme kinetic reaction, which seems to be rare in HIV disease dynamics. We can see from the figure (2.5) that for the consumption of alcohol, the PI concentration has been reduced. Thus, alcohol prevents the inhibition property of PI towards enzyme CYP3A4 and increases the metabolism rate of PI by CYP3A4. Conclusively, we expect that the conducted study and proposed mathematical model would help to explore new treatment strategy that effectively treats alcoholic HIV infected patients in a more balanced way.

# Chapter 3

# Impulsive differential equation model in HIV-1 inhibition: advances in dual inhibitors of HIV-1 RT and IN for the prevention of HIV-1 replication

## 3.1 Introduction

Acquired immunodeficiency syndrome (AIDS) is a lethal disease caused by human immunodeficiency virus (HIV) infection. According to Joint United Nations Programme on HIV and AIDS (UNAIDS), at the end of 2020, around 37.7 million people lived with HIV, among them 1.7 million people were newly infected (unaids, 2021). There are two main types of HIV: HIV-1 and HIV-2. HIV-1 has higher virulence with high infectivity, compared to HIV-2. Although no cure has yet been developed, the most effective treatment regimen for HIV-1 infection is HAART, a combination of 3 or 4 anti-AIDS drugs (Das and Arnold, 2013). HAART could successfully keep the viral

load low and evidently reduce the mortality of HIV-1 infected people, but it involves the difficulty of perfect adherence because of complicated dosing and intolerable toxicities. Recently, dual inhibitors of HIV-1 RT and IN (Portmanteau Inhibitors) to facilitate patient compliance have become a promising scientific endeavor (De and Camarasa, 2018; Gu et al., 2016).

A dual inhibitor of HIV-1 RT/IN is a single chemical entity capable of inhibiting both the enzymes RT and IN are less likely to develop drug resistance from the virus because of its multi-faceted approach and cost-effectiveness. RT inhibitors fall into two categories: nucleoside RT inhibitors (NRTIs) and non-nucleoside RT inhibitors (NNRTIs). NRTIs as competitive inhibitors act as chain terminators, whereas NNRTIs allosterically inhibit DNA polymerization. NRTIs not only interfere with the replication of viral DNA and RNA but also influence normal cell DNA replication due to its poor selectivity (Das and Arnold, 2013). NNRTIs target the allosteric site of the viral RT, change the conformation of the enzyme, interfere with the binding between the enzyme bonds and substrate, and inhibit in a non-competitive way (Rich, 2005; Schauer et al., 2014; Usach et al., 2013). Recently approved IN inhibitors (raltegravir and elvitegravir) bind the active site of HIV-1 IN in a pre-integration complex and block the viral DNA integration into host cell chromosomes (Anstett et al., 2017; Temesgen et al., 2008). In this paper, we have used dual inhibitor of HIV-1 RT/IN taking bis heteroaryl piperazine compounds (eg. delavirdine, atevirdine) as NNRTI and $\beta$-diketo acids (DKAs) group as IN inhibitor. For a better understanding of the inhibition mechanisms, it is important to have a clear view of the drug targets RT and IN and the roles they play in the viral life cycle.

Viral infections are initiated by the interactions of the envelope glycoprotein with the CD4 receptor on the surface of immune cells and a co-receptor either CCR5 or CXCR4 that leads to a fusion of the membranes of the host cell and the virion (Das and Arnold, 2013; Hu and Hughes, 2012; Sarafianos et al., 2009). This fusion introduces the viral core containing two copies of the single-stranded viral RNA genome, about fifty copies of RT, IN, and other viral entities into the cytoplasm of the

host cell (Das and Arnold, 2013; Hu and Hughes, 2012). RT copies the single-stranded viral RNA genome into double-stranded DNA. This double-stranded DNA is carried into the nucleus of the infected cell and integrated into the host cell chromosome by another viral enzyme, IN (Hu and Hughes, 2012; Sarafianos et al., 2009). RT has two catalytic domains: a DNA polymerase domain that can copy either an RNA or a DNA template and an RNase H domain that cleaves RNA from an RNA-DNA hybrid (Althaus et al., 1993; Hu and Hughes, 2012; Sarafianos et al., 2009). Reverse transcription by the enzyme RT needs both a primer and a template as well as deoxyribonucleotide triphosphates (dNTPs). The viral RNA genome serves as the template and the primer for synthesis of the first DNA strand (minus strand) is a host tRNA (Hu and Hughes, 2012; Sarafianos et al., 2009). The RNA template forms a complex with the tRNA primer and the complex binds to the polymerase domain of the enzyme, followed by the addition of dNTPs. The dNTPs bind separately to another binding site of the polymerase domain and are then catalytically added to the primer sequence (Rich, 2005). Hence, RT starts to copy the 5' end of the viral RNA genome and generates an RNA-DNA hybrid (Sarafianos et al., 2009). As soon as the hybrid is made, the RNase H domain degrades the 5' end of the RNA strand, making the newly synthesized minus-strand DNA single-stranded (Hu and Hughes, 2012). Now, RT starts to generate the second (plus) strand DNA by making a copy of the newly synthesized minus-strand DNA along with the first 18 nucleotides from the tRNA primer (Hu and Hughes, 2012; Sarafianos et al., 2009). As soon as tRNA has been copied into the DNA, the RNase H domain of RT cleaves the tRNA primer, and hence, finally double-stranded DNA is formed into the host cell cytoplasm (Hu and Hughes, 2012; Li et al., 2016; Sarafianos et al., 2009). Now this double-stranded DNA acts as a substrate for HIV-1 IN. The integration process consists of two catalytic steps: 3' processing (3'-P) and strand transfer (ST). The processing reaction first takes place in the cytoplasm of the infected cell. The enzyme removes two nucleotides from each 3' end of the viral DNA and forms IN-HIV DNA complex (pre-integration complex) (Engelman et al., 1991). The pre-integration complex is then transported into the nucleus of the host cell. Furthermore, the enzyme catalyzes the insertion of the two processed 3' ends of viral DNA into opposite strands of the host DNA 5'

phosphate ends by the reaction named strand transfer, and finally proviral DNA is formed (Craigie and Bushman, 2012). In the final stage of a viral life cycle, with the help of the Protease enzyme, the viral assembly process is complete.

A handful of analytical works based on constructing dual inhibitors of HIV-1 RT/IN in the treatment of AIDS have been performed and the efficacy of these HIV-1 RT/IN dual inhibitors in combating the HIV-1 infection have also been described theoretically (De and Camarasa, 2018; Gu et al., 2016). In 2007, Wang et al. (Wang et al., 2007) designed dual inhibitors of HIV-1 RT and IN by merging a NNRTI such as 1-[(2-hydroxyethoxy) methyl]-6-(phenylthio) thymine (HEPT) and $\beta$-diketo acid derivatives (DKAs) as IN inhibitors and showed that the merged compounds inhibited both the enzymes RT and IN at very low concentrations ($IC_{50RT} = 0.0092 - 0.23\mu M$, $IC_{50IN} = 1.8 - 7.7\mu M$). Next, in 2008, Wang and Vince (Wang and Vince, 2008) reported a new series of dual inhibitors of HIV-1 RT and IN by incorporating a diketo acid (DKA) fragment into the NNRTI delavirdine. With the aim to enhance the anti-HIV efficacy, in 2015, He and Chen group (Mao et al., 2015) hybridized the NNRTI etravirine and IN inhibitor GS-9137 to synthesize a new series of dual inhibitors of HIV-1 RT/IN. Despite having an ample number of theoretical works related to the anti-HIV activities of these dual inhibitors, a mathematical model-based analysis using HIV-1 RT/IN dual inhibitors is yet to be explored.

In this paper, we consider a mathematical model of HIV-1 RT and IN-catalyzed reaction for HIV-1 replication with the understanding of the Michaelis-Menten enzyme kinetic reaction. In the formulated model, we incorporate a dual inhibitor of HIV-1 RT/IN which simultaneously works as a NNRTI and an IN inhibitor. In order to determine an effective dosing regimen for applying the dual inhibitor of HIV-1 RT/IN, we use impulsive differential equations (IDEs) (Ghosh and Peters, 2020; Lakshmikantham and Simeonov, 1989) based on the steady-state Briggs-Haldane (Briggs and Haldane, 1925; Segel, 1975) approximation for an enzyme kinetic reaction. Furthermore, by using Lambert W function (Barry et al., 2000; Tang and Xiao, 2007) we have obtained the analytical periodic solution for multiple dose administration and also established

the expressions for maximum and minimum values of the periodic solution. Finally, we solve the model numerically and discuss the results from the biological aspect. We hope these results may help scientists to explore new treatment strategies in the fight against HIV-1 infection.

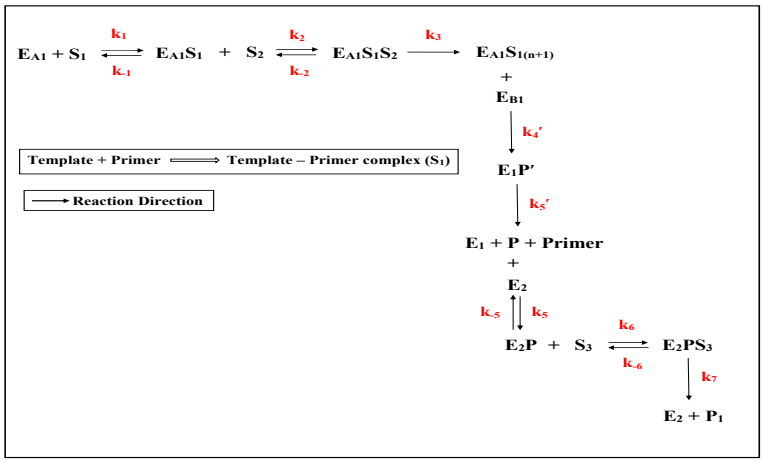


Figure 3.1: The schematic diagram of the enzymatic reactions.

## 3.2 Model Formulation

Let $E_1$ denote the concentration of HIV-1 RT, $S_1$ denote the concentration of viral single-stranded RNA template-primer complex and $S_2$ denote the concentration of dNTP. During reverse transcription, the polymerase domain of RT, i.e., $E_{A1}$ starts to copy the viral RNA genome generating RT-RNA template-primer complex ($E_{A1}S_1$), and little portion of the complex reverts. For this reaction, the forward and backward rate constants are $k_1$ and $k_{-1}$ respectively. The RT-RNA template-primer complex binds with dNTP ($S_2$) to yield RT-RNA template-primer-dNTP ($E_{A1}S_1S_2$) complex which finally formulates a new RT-RNA template-primer complex ($E_{A1}S_{1(n+1)}$). As DNA synthesis proceeds, the RNase H domain of RT, i.e., $E_{B1}$ binds with the complex $E_{A1}S_{1(n+1)}$ to produce linear single-stranded viral DNA ($P'$) with $k_4{}'$ rate constant. And from this viral single-stranded DNA ($P'$), viral double-stranded DNA ($P$) is formed and the free RT ($E_1$) along with the primer gets released. The rate constant for this reaction is $k_5{}'$. Now the enzyme HIV-1 IN ($E_2$) combines with the newly

formed double-stranded DNA (P) to yield IN-HIV DNA complex ($E_2P$). The IN-HIV DNA complex ($E_2P$) binds to the host DNA ($S_3$) inside the nucleus of the host cell and forms IN-HIV DNA-host DNA complex ($E_2PS_3$) that finally produces integrated proviral DNA ($P_1$) and releases free enzyme ($E_2$). The forward and backward rate constants for the integration process are $k_5$, $k_6$, $k_7$, $k_{-5}$, and $k_{-6}$ respectively. The above facts are represented by the schematic diagram 3.1.

Since we mainly focus on the polymerase chain reaction and integration process, we ignore the portion of RNase H mechanism from our model to reduce complexity during mathematical analysis. Here $E_{A1}$ is referred as $E_1$. Therefore the revised schematic diagram 3.2 is presented below.

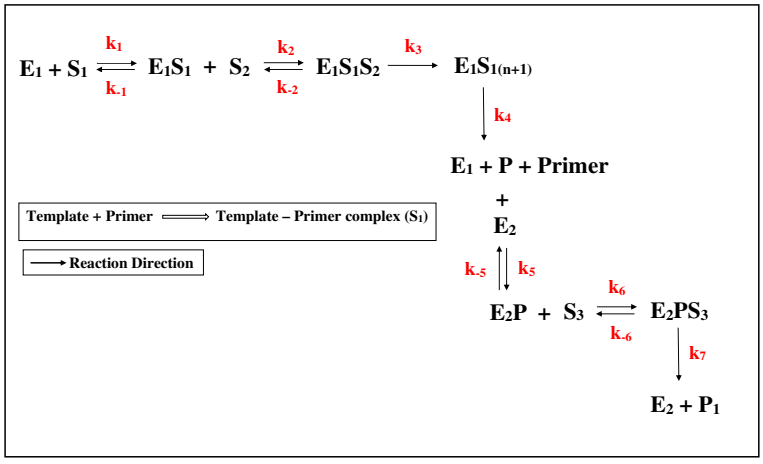


Figure 3.2: The schematic diagram of polymerase chain reaction and integration process.

Following the law of mass action, the set of non-linear differential equations describing the above enzymatic reactions is as follows:

$$
\begin{aligned}
\frac{d[E_1]}{dt} &= -k_1[E_1][S_1] + k_{-1}[E_1S_1] + k_4[E_1S_{1(n+1)}],\\
\frac{d[S_1]}{dt} &= \lambda_1 - k_1[E_1][S_1] + k_{-1}[E_1S_1] - \mu_1[S_1],\\
\frac{d[S_2]}{dt} &= \lambda_2 - k_2[E_1S_1][S_2] + k_{-2}[E_1S_1S_2] - \mu_2[S_2],\\
\frac{d[E_1S_1]}{dt} &= k_1[E_1][S_1] - k_{-1}[E_1S_1] - k_2[E_1S_1][S_2] + k_{-2}[E_1S_1S_2],\\
\frac{d[E_1S_1S_2]}{dt} &= k_2[E_1S_1][S_2] - k_{-2}[E_1S_1S_2] - k_3[E_1S_1S_2],\\
\frac{d[E_1S_{1(n+1)}]}{dt} &= k_3[E_1S_1S_2] - k_4[E_1S_{1(n+1)}],\\
\frac{d[P]}{dt} &= k_4[E_1S_{1(n+1)}] - k_5[P][E_2] + k_{-5}[E_2P] - \mu_3P,\\
\frac{d[E_2]}{dt} &= -k_5[E_2][P] + k_{-5}[E_2P] + k_7[E_2PS_3],\\
\frac{d[E_2P]}{dt} &= k_5[E_2][P] - k_{-5}[E_2P] - k_6[E_2P][S_3] + k_{-6}[E_2PS_3],\\
\frac{d[S_3]}{dt} &= \lambda_3 - k_6[E_2P][S_3] + k_{-6}[E_2PS_3] - \mu_4[S_3],\\
\frac{d[E_2PS_3]}{dt} &= k_6[E_2P][S_3] - k_{-6}[E_2PS_3] - k_7[E_2PS_3],\\
\frac{d[P_1]}{dt} &= k_7[E_2PS_3] - \mu_5[P_1],
\end{aligned}
\tag{3.2.1}
$$

where, $\lambda_i$ is the external source rate of $S_i$, $i = \{1, 2, 3\}$ and $\mu_i$ is the natural decay rate of $S_1$, $S_2$, $P$, $S_3$ and $P_1$ respectively.

In their original analysis, Michaelis and Menten (Michaelis and Menten, 1913) assumed that the substrate is in instantaneous equilibrium with the complex, which implies

$$k_1ES = k_{-1}C,$$

where $E$ and $S$ represents enzyme and substrate concentration respectively while $C$ is the complex concentration. Using the above mentioned condition, they obtained an expression for $V_{max}$, the maximum reaction velocity. (Reaction velocity is measured either as the rate of production of $P$, the product or as the rate of disappearance of $S$, the substrate.)
In 1925, Briggs-Haldane (Briggs and Haldane, 1925) suggested an alternative hypothesis, using an assumption known as the Quasi-Steady-State Assumption (QSSA):

$$k_1ES = k_{-1}C + k_2C.$$

The QSSA states that shortly after initiation of the reaction, the enzyme-substrate complex is in quasi-equilibrium with respect to the substrate and the product, due to

enzyme saturation. During the pre-steady state period, the QSSA does not hold, but it is assumed that the free substrate concentration is not decreased by any significant amount. The QSSA allowed Briggs-Haldane Briggs and Haldane (1925) to set $\frac{dC}{dt} = 0$ and to obtain

$$C = \frac{E_0 S}{K_M + S},$$

where

$K_M = \frac{k_1+k_2}{k_1}$ and $E_0$ is the initial concentration of the enzyme, $E$.

In order to simplify our model system, we use the steady-state Briggs-Haldane approximation (Briggs and Haldane, 1925; Segel, 1975), i.e., shortly after initiation of the reaction, an enzyme-substrate complex is formed at the same rate as it disappearances. Under this assumption, we get the following relations from the system (3.2.1):

$$\begin{aligned}
[E_1S_1] &= \frac{K_{M_{S_2}}[E_1][S_1]}{K_{S_1}K_{M_{S_2}} + K_{M_{S_1}}[S_2]}, \\
[E_1S_1S_2] &= \frac{[E_1][S_1][S_2]}{K_{S_1}K_{M_{S_2}} + K_{M_{S_1}}[S_2]}, \\
[E_1S_{1_{(n+1)}}] &= \frac{k_3[E_1][S_1][S_2]}{k_4(K_{S_1}K_{M_{S_2}} + K_{M_{S_1}}[S_2])}, \\
[E_2P] &= \frac{K_{M_{S_3}}[E_2][P]}{K_P K_{M_{S_3}} + K_{M_P}[S_3]}, \\
[E_2PS_3] &= \frac{[E_2][P][S_3]}{K_P K_{M_{S_3}} + K_{M_P}[S_3]}.
\end{aligned}$$

Substituting the expressions for $[E_1S_1]$, $[E_1S_1S_2]$, $[E_1S_{1_{(n+1)}}]$, $[E_2P]$, $[E_2PS_3]$ into (3.2.1) and using the relations $[E_1]_{10} = [E_1] + [E_1S_1] + [E_1S_1S_2] + [E_1S_{1_{(n+1)}}]$, and $[E_2]_{20} = [E_2]+[E_2P]+[E_2PS_3]$, we obtain the following five dimensional compartmental model:

$$\begin{aligned}
\frac{d[S_1]}{dt} &= \lambda_1 - \frac{k_3[E]_{10}}{f([S_1],[S_2])}[S_1][S_2] - \mu_1[S_1], \\
\frac{d[S_2]}{dt} &= \lambda_2 - \frac{k_3[E]_{10}}{f([S_1],[S_2])}[S_1][S_2] - \mu_2[S_2], \\
\frac{d[P]}{dt} &= \frac{k_3[E]_{10}}{f([S_1],[S_2])}[S_1][S_2] - \frac{k_7[E]_{20}}{g([P],[S_3])}[P][S_3] - \mu_3[P], \\
\frac{d[S_3]}{dt} &= \lambda_3 - \frac{k_7[E]_{20}}{g([P],[S_3])}[P][S_3] - \mu_4[S_3], \\
\frac{d[P_1]}{dt} &= \frac{k_7[E]_{20}}{g([P],[S_3])}[P][S_3] - \mu_5[P_1].
\end{aligned} \tag{3.2.2}$$

Where, $f([S_1],[S_2]) = K_{S_1}K_{M_{S_2}} + K_{M_{S_1}}[S_2] + K_{M_{S_2}}[S_1] + K_P{}'[S_1][S_2] + [S_1][S_2]$, $g([P],[S_3]) = K_PK_{M_{S_3}} + K_{M_P}[S_3] + K_{M_{S_3}}[P] + [P][S_3]$, $K_{S_1} = \frac{k_{-1}}{k_1}$, $K_{M_{S_1}} = \frac{k_3}{k_1}$, $K_{M_{S_2}} = \frac{k_{-2}+k_3}{k_2}$, $K_P{}' = \frac{k_3}{k_4}$, $K_P = \frac{k_{-5}}{k_5}$, $K_{M_P} = \frac{k_7}{k_5}$, $K_{M_{S_3}} = \frac{k_{-6}+k_7}{k_6}$ and $[E]_{i0}$ denotes the total concentration of the $i^{th}$ enzyme, $i = \{1, 2\}$.

In this article, we have introduced the dual inhibitor of HIV-1 RT/IN ($I$) into the system. Here the drug ($I$) works as a non-competitive, cooperatively binding inhibitor to bind $E_1$ and simultaneously inhibits $E_2$ in uncompetitive way. Since the dual inhibitor ($I$) of HIV-1 RT/IN manifests two different parallel inhibition mechanisms, we divide the inhibitor ($I$) into two portions $I_1$ and $I_2$, where $I_1 = \alpha I$ and $I_2 = (1-\alpha)I; 0 < \alpha < 1$. Therefore, clearly $I = I_1 + I_2$. Here $I_1$ represents non-competitive, cooperatively binding inhibitor to bind $E_1$ and hence inactivates it by forming enzyme-inhibitor complex ($E_1I_1$). The forward and backward rate constants of this reaction are $k_{i1}$ and $k_{-i1}$ respectively. The $E_1I_1$ complex could bind the substrate $S_1$ to yield a ternary complex $E_1S_1I_1$ and the reaction dissociation constant between the complex $E_1I_1$ and the substrate $S_1$ is $K_{S_1}{}'(= k_{-1}{}'/k_1{}')$. Alternatively, the inhibitor $I_1$ can bind to the preformed $E_1S_1$ complex and thus $E_1S_1I_1$ complex can also be generated with the rate constants $k_{i1}{}'$ and $k_{-i1}{}'$ respectively. In a similar manner, the $E_1S_1S_2I_1$ complex can be formed by binding the $E_1S_1I_1$ complex to the substrate $S_2$ or by binding the inhibitor $I_1$ to the preordained $E_1S_1S_2$ complex, in either way. The forward and backward rate constants for these reactions are $k_2{}', k_{-2}{}'$ or $k_{i1}{}''$ and $k_{-i1}{}''$ respectively. The complex $E_1S_1S_2I_1$ then can go on to yield the complex $E_1S_{1_{(n+1)}}$ at a reduced rate compared to the uninhibited reaction. The aforementioned reaction mechanism of $I_1$ can be described as

$$\frac{d[I_1]}{dt} = -k_3[E]_{10}\Big[\frac{1}{h_1(I_1)} + \frac{1}{h_2(I_1)} + \frac{1}{h_3(I_1)}\Big][I_1], \tag{3.2.3}$$

where $h_1(I_1) = (1 + \frac{I_1^n}{K_{i1}{}^n})$, $h_2(I_1) = (1 + \frac{I_1^n}{(K_{i1}{}')^n})$, $h_3(I_1) = (1 + \frac{I_1^n}{(K_{i1}{}'')^n})$, $n$ = hill coefficient of inhibitor binding and the equilibrium dissociation constants $K_{i1}$, $K_{i1}{}'$, $K_{i1}{}''$ are given by the following:

$$K_{i1} = \frac{k_{-i1}}{k_{i1}}, K_{i1}{}' = \frac{k_{-i1}{}'}{k_{i1}{}'}, K_{i1}{}'' = \frac{k_{-i1}{}''}{k_{i1}{}''}.$$

Besides acting as a non-competitive inhibitor toward $E_1$, the drug $I$ simultaneously inhibits the enzyme ($E_2$) in an uncompetitive way and here $I_2$ represents the uncompetitive binding inhibitor to bind $E_2$ by producing IN-HIV DNA-Inhibitor complex ($E_2PI_2$) and restrains the integration process. The forward and backward rate constants for this inhibition process are $k_{i2}$ and $k_{-i2}$ respectively. The dynamics of $I_2$ is represented by the following

$$\frac{d[I_2]}{dt} = -\frac{k_7[E]_{20}}{h_4(I_2)}[I_2], \tag{3.2.4}$$

where $h_4(I_2) = (1 + \frac{I_2}{K_{i2}})$ and the equilibrium dissociation constant $K_{i2}$ is given by the following:

$$K_{i2} = \frac{k_{-i2}}{k_{i2}}.$$

Therefore, from (3.2.3) & (3.2.4) we get the dynamics of $I$ as follows:

$$\frac{d[I]}{dt} = -k_3E_{10}[\frac{1}{h_1(I_1)} + \frac{1}{h_2(I_1)} + \frac{1}{h_3(I_1)}]I_1 - \frac{k_7E_{20}}{h_4(I_2)}I_2.$$

The entire system can be represented by the schematic diagram 3.3.

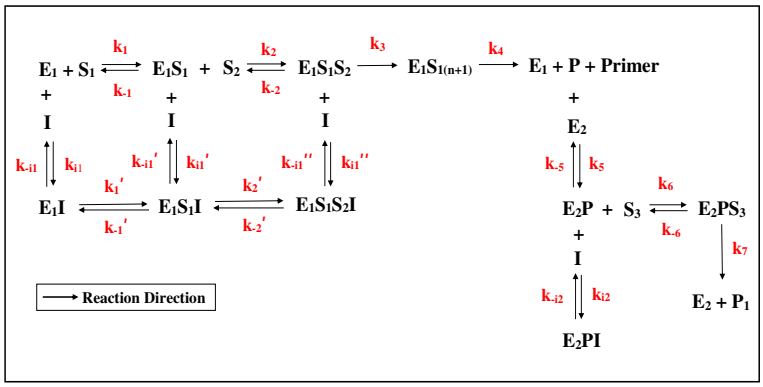


Figure 3.3: The schematic diagram of the inhibited enzymatic reactions.

Let, $[S_i] = S_i$, $i = \{1, 2, 3\}$, $[P] = P$, $[I] = I$ and $[E]_{j0} = E_{j0}, j = \{1, 2\}$. Using the steady state Briggs-Haldane kinetics, the model can be described as:

$$\begin{aligned}
\frac{dS_1}{dt} &= \lambda_1 - \frac{k_3E_{10}}{f_1(S_1,S_2,I)}S_1S_2 - \mu_1S_1,\\
\frac{dS_2}{dt} &= \lambda_2 - \frac{k_3E_{10}}{f_1(S_1,S_2,I)}S_1S_2 - \mu_2S_2,\\
\frac{dP}{dt} &= \frac{k_3E_{10}}{f_1(S_1,S_2,I)}S_1S_2 - \frac{k_7E_{20}}{g_1(P,S_3,I)}PS_3 - \mu_3P,\\
\frac{dS_3}{dt} &= \lambda_3 - \frac{k_7E_{20}}{g_1(P,S_3,I)}PS_3 - \mu_4S_3,\\
\frac{dP_1}{dt} &= \frac{k_7E_{20}}{g_1(P,S_3,I)}PS_3 - \mu_5P_1,\\
\frac{dI}{dt} &= I_c - \alpha k_3E_{10}[\frac{1}{h_1(I)} + \frac{1}{h_2(I)} + \frac{1}{h_3(I)}]I - \frac{(1-\alpha)k_7E_{20}}{h_4(I)}I - \mu_6I,
\end{aligned} \tag{3.2.5}$$

with the initial concentrations $S_1(0) = S_{10}$, $S_2(0) = S_{20}$, $S_3(0) = S_{30}$, $P(0) = 0$, $P_1(0) = 0$, and $I(0) = I_0$. Here, $f_1(S_1, S_2, I) = (K_{S_1}K_{M_{S_2}} + K_{M_{S_1}}S_2)h_1(I) + K_{M_{S_2}}S_1h_2(I) + S_1S_2h_3(I) + K_P{}'S_1S_2$, $g_1(P, S_3, I) = K_PK_{M_{S_3}} + K_{M_P}S_3 + PS_3 + PK_{M_{S_3}}h_4(I)$, $h_1(I) = (1 + \frac{\alpha^nI^n}{{K_{i1}}^n})$, $h_2(I) = (1 + \frac{\alpha^nI^n}{({K_{i1}}')^n})$, $h_3(I) = (1 + \frac{\alpha^nI^n}{({K_{i1}}'')^n})$, $h_4(I) = (1 + \frac{(1-\alpha)I}{K_{i2}})$, $n$ = hill coefficient of inhibitor binding.

### Non-negativity and boundedness of the model

In this section, we have studied the non-negativity and boundedness of the solutions of the system (3.2.5) using the following theorem.

**Theorem 3.2.1** *Solution of the system* (3.2.5) *for any non-negative initial condition, remains non-negative for all* $t \geq 0$ *and uniformly bounded in the region* $\Gamma$*, where,* $\Gamma = \Big\{(S_1, S_2, P, S_3, P_1, I) \in \mathbb{R}^6_+ \mid 0 < S_1(t) \leq \frac{\lambda_1}{\mu_1}, 0 < S_2(t) \leq \frac{\lambda_2}{\mu_2}, 0 \leq P(t) \leq \frac{M_1}{\mu_3}, 0 < S_3(t) \leq \frac{\lambda_3}{\mu_4}, 0 \leq P_1(t) \leq \frac{M_2}{\mu_5}, 0 < I(t) \leq \frac{I_c}{\mu_6}\Big\}$.

**Proof.** First, we show that $S_1(t)$ is positive for all $t \geq 0$. To see this, assume that $t_0$ be the first time when $S_1(t_0) = 0$. Now initially we have $S_1(t) > 0$ when $t = 0$. Therefore, $S_1(t) > 0$ for all $t \in [0, t_0)$. Substituting $t = t_0$ in the first equation of system (3.2.5), we get,

$$\frac{dS_1}{dt} = \lambda_1 - \frac{k_3E_{10}S_1(t_0)S_2(t_0)}{f_1(S_1(t_0),S_2(t_0),I(t_0)} - \mu_1S_1(t_0) = \lambda_1 \ \ (> 0).$$

This means $S_1(t)$ is an increasing function at $t = t_0$. So, there exists an arbitrarily small $\epsilon > 0$ such that for all $t \in (t_0 - \epsilon, t_0) \subset [0, t_0)$, we have $S_1(t) < 0$. This is a contradiction to the fact that $S_1(t) > 0, \forall t \in [0, t_0)$. Hence, $S_1(t) > 0, \forall t \geq 0$.

Similarly, we can show that the components $S_2(t)$, $S_3(t)$, $I(t)$, and $P(t)$) of our formulated model are positive for all $t \geq 0$. Again from the fifth equation of (3.2.5), we get

$$\frac{dP_1}{dt} = \frac{k_7 E_{20}}{g_1(P, S_3, I)} P S_3 - \mu_5 P_1 > -\mu_5 P_1.$$

But the initial value of $P_1$ is zero. So, we can write,

$$\frac{dP_1}{dt} \geq 0 \implies P_1 \geq 0.$$

Hence, we have the non-negativity of the solutions of the system (3.2.5) with the initial conditions.

Now we show that $S_1(t)$, $S_2(t)$, $P(t)$, $S_3(t)$, $P_1(t)$ and $I(t)$ are all bounded in their domains of definition. Taking first equation of (3.2.5), we get

$$\begin{aligned} &\tfrac{dS_1}{dt} = \lambda_1 - \tfrac{k_3 E_{10}}{f_1(S_1, S_2, I)} S_1 S_2 - \mu_1 S_1, \\ \implies \quad &\tfrac{dS_1}{dt} \leq \lambda_1 - \mu_1 S_1. \end{aligned}$$

After integration, we have

$$S_1(t) \leq \frac{\lambda_1}{\mu_1}(1 - e^{-\mu_1 t}) + S_{10} e^{-\mu_1 t}.$$

Thus, for sufficiently large $t$, we get the maximum value of template-primer complex presence in the case of HIV-1 infection as

$$\limsup_{t \to +\infty} S_1(t) \leq \frac{\lambda_1}{\mu_1}. \tag{3.2.6}$$

Similarly, from the second, fourth, and sixth equations of (3.2.5), we can determine

$$\limsup_{t \to +\infty} S_2(t) \leq \tfrac{\lambda_2}{\mu_2}, \quad \limsup_{t \to +\infty} S_3(t) \leq \tfrac{\lambda_3}{\mu_4}, \text{ and } \limsup_{t \to +\infty} I(t) \leq \tfrac{I_c}{\mu_6}. \tag{3.2.7}$$

Now considering the third equation of (3.2.5), we get the following inequality

$$\frac{dP}{dt} \leq \frac{k_3 E_{10} S_1 S_2}{f_1(S_1, S_2, I)} - \mu_3 P. \tag{3.2.8}$$

Using the results of (3.2.6) and (3.2.7) one can get from the inequality (3.2.8),

$$\frac{dP}{dt} \leq M_1 - \mu_3 P.$$

Solving the above inequality for sufficiently large $t$, we get the following result,

$$\limsup_{t\to+\infty} P(t) \leq \frac{M_1}{\mu_3},$$

where

$M_1 = \frac{k_3 E_{10}\lambda_1\lambda_2 {K_{i1}}^n ({K_{i1}}')^n ({K_{i1}}'')^n \mu_6^n}{\mu_1\beta_1\alpha_1 + K_{M_{S_2}}\lambda_1\mu_2\alpha_2 + \lambda_1\lambda_2\alpha_3 + {K_P}'\lambda_1\lambda_2\mu_6^n {K_{i1}}^n ({K_{i1}}')^n ({K_{i1}}'')^n}$,
with $\beta_1 = (\mu_2 K_{S_1} K_{M_{S_2}} + K_{M_{S_1}}\lambda_2)$, $\alpha_1 = (I_c^n + {K_{i1}}^n\mu_6^n)({K_{i1}}')^n({K_{i1}}'')^n$, $\alpha_2 = (I_c^n + ({K_{i1}}')^n\mu_6^n){K_{i1}}^n({K_{i1}}'')^n$, $\alpha_3 = (I_c^n + ({K_{i1}}'')^n\mu_6^n){K_{i1}}^n({K_{i1}}')^n$.

From the fifth equation of system (3.2.5) and using the maximum values of $P$ and $S_3$, the following inequality can be derived

$$\frac{dP_1}{dt} \leq M_2 - \mu_5 P_1.$$

In order to find the maximum value of proviral DNA in HIV-1 infected patient, we solve the above inequality for sufficiently large $t$ and get,

$$\limsup_{t\to+\infty} P_1(t) \leq \frac{M_2}{\mu_5},$$

where

$M_2 = \frac{k_7 E_{20} M_1 \lambda_3 \mu_6 K_{i2}}{\mu_3\mu_4\mu_6 K_P K_{M_{S_3}} + K_{M_P}\lambda_3\mu_3\mu_6 + M_1\lambda_3\mu_6 + M_1 K_{M_{S_3}}\mu_4(I_c + K_{i2})}$.
Therefore all solutions of the system (3.2.5) are bounded.

### 3.2.1 Equilibrium Analysis

The system (3.2.5) has at least one interior equilibrium, $E^* = ({S_1}^*, {S_2}^*, P^*, {S_3}^*, {P_1}^*, I^*)$, where ${S_1}^*$, ${S_2}^*$, $P^*$, ${S_3}^*$, ${P_1}^*$ and $I^*$ are the positive roots of the following set of equations:

$$\begin{aligned}
0 &= \lambda_1 - \tfrac{k_3 E_{10}}{f_1({S_1}^*, {S_2}^*, I^*)} {S_1}^* {S_2}^* - \mu_1 {S_1}^*,\\
0 &= \lambda_2 - \tfrac{k_3 E_{10}}{f_1({S_1}^*, {S_2}^*, I^*)} {S_1}^* {S_2}^* - \mu_2 {S_2}^*,\\
0 &= \tfrac{k_3 E_{10}}{f_1({S_1}^*, {S_2}^*, I^*)} {S_1}^* {S_2}^* - \tfrac{k_7 E_{20}}{g_1(P^*, {S_3}^*, I^*)} P^* {S_3}^* - \mu_3 P^*,\\
0 &= \lambda_3 - \tfrac{k_7 E_{20}}{g_1(P^*, {S_3}^*, I^*)} P^* {S_3}^* - \mu_4 {S_3}^*,\\
0 &= \tfrac{k_7 E_{20}}{g_1(P^*, {S_3}^*, I^*)} P^* {S_3}^* - \mu_5 {P_1}^*,\\
0 &= I_c - \alpha k_3 E_{10}[\tfrac{1}{h_1(I^*)} + \tfrac{1}{h_2(I^*)} + \tfrac{1}{h_3(I^*)}]I^* - \tfrac{(1-\alpha)k_7 E_{20}}{h_4(I^*)} I^* - \mu_6 I^*.
\end{aligned}$$

**Note:** As we explicitly couldn't determine the interior equilibrium point of the model (3.2.5), we used Maple Software to obtain interior equilibrium point numerically. We get the interior equilibrium point $E^* = (0.5582, 1.0223, 0.0548, 0.8146, 5.5489, 0.0146)$ for our considered parameter values from Table 2.1.

The Jacobin matrix $J^*$ at the interior equilibrium point $E^*$ is

$$J^* = \begin{bmatrix} -a_{11}-\mu_1 & -a_{12} & 0 & 0 & 0 & a_{16} \\ -a_{11} & -a_{12}-\mu_2 & 0 & 0 & 0 & a_{16} \\ a_{11} & a_{12} & -a_{33}-\mu_3 & -a_{34} & 0 & -a_{16}+a_{36} \\ 0 & 0 & -a_{33} & -a_{34}-\mu_4 & 0 & a_{36} \\ 0 & 0 & a_{33} & a_{34} & -\mu_5 & -a_{36} \\ 0 & 0 & 0 & 0 & 0 & -a_{66}-\mu_6 \end{bmatrix},$$

where

$$\begin{aligned}
a_{11} &= \frac{k_3 E_{10} h_1(I^*) {S_2}^* (K_{S_1} K_{M_{S_2}} + K_{M_{S_1}} {S_2}^*)}{(f_1({S_1}^*, {S_2}^*, I^*))^2}, \\
a_{12} &= \frac{k_3 E_{10} {S_1}^* K_{M_{S_2}} (K_{S_1} h_1(I^*) + {S_1}^* h_2(I^*))}{(f_1({S_1}^*, {S_2}^*, I^*))^2}, \\
a_{16} &= \frac{k_3 E_{10} {S_1}^* {S_2}^* \{(K_{S_1} K_{M_{S_2}} + K_{M_{S_1}} {S_2}^*)({K_{i1}}')^n ({K_{i1}}'')^n + K_{M_{S_2}} {S_1}^* {K_{i1}}^n ({K_{i1}}'')^n + {S_1}^* {S_2}^* {K_{i1}}^n ({K_{i1}}')^n\} n {I^*}^{(n-1)}}{(f_1({S_1}^*, {S_2}^*, I^*))^2 {K_{i1}}^n ({K_{i1}}')^n ({K_{i1}}'')^n}, \\
a_{33} &= \frac{k_7 E_{20} {S_3}^* (K_P K_{M_{S_3}} + K_{M_P} {S_3}^*)}{(g_1({P^*}, {S_3}^*, I^*))^2}, \\
a_{34} &= \frac{k_7 E_{20} {P^*} (K_P K_{M_{S_3}} + K_{M_{S_3}} {P^*} h_4(I^*))}{(g_1({P^*}, {S_3}^*, I^*))^2}, \\
a_{36} &= \frac{k_7 E_{20} {P^*}^2 {S_3}^* K_{M_{S_3}}}{(g_1({P^*}, {S_3}^*, I^*))^2 K_{i2}}, \\
a_{66} &= \alpha k_3 E_{10} \Big[ \frac{{K_{i1}}^n \{{K_{i1}}^n - (n-1)\alpha^n {I^*}^n\}}{({K_{i1}}^n + \alpha^n {I^*}^n)^2} + \frac{({K_{i1}}')^n \{({K_{i1}}')^n - (n-1)\alpha^n {I^*}^n\}}{\{({K_{i1}}')^n + \alpha^n {I^*}^n\}^2} \\
&\quad + \frac{({K_{i1}}'')^n \{({K_{i1}}'')^n - (n-1)\alpha^n {I^*}^n\}}{\{({K_{i1}}'')^n + \alpha^n {I^*}^n\}^2} \Big] \\
&\quad + \frac{(1-\alpha) k_7 E_{20} (K_{i2})^2}{\{K_{i2} + (1-\alpha) I^*\}^2}.
\end{aligned}$$

Now the characteristic equation at the interior equilibrium point $E^*$ is of the following form:

$$(\mu_5 + x)(a_{66} + \mu_6 + x)\{x^2 + A_1 x + B_1\}\{x^2 + A_2 x + B_2\} = 0,$$

where $A_1 = a_{33} + a_{34} + \mu_3 + \mu_4$, $B_1 = a_{33}\mu_4 + \mu_3(a_{34} + \mu_4)$, $A_2 = a_{11} + a_{12} + \mu_1 + \mu_2$, $B_2 = a_{11}\mu_2 + \mu_1(a_{12} + \mu_2)$.

All the six eigenvalues are always negative. Therefore, the interior equilibrium $E^*$ is locally asymptotically stable.

## 3.3 Impulsive Model

The one-dimensional impulsive differential equation takes the form:

$$\frac{dI}{dt} = \begin{cases} -\alpha k_3 E_{10}\left[\frac{1}{h_1(I)}+\frac{1}{h_2(I)}+\frac{1}{h_3(I)}\right]I-(1-\alpha)\frac{k_7 E_{20}}{h_4(I)}I-\mu_6 I, \text{ for } t\neq t_k, \\ I(t_k^+)-I(t_k^-)=I_c \text{ for } t=t_k. \end{cases} \tag{3.3.1}$$

Where $I$ is the concentration of the dual inhibitor of HIV-1 RT/IN with initial condition $I_0 > 0$. Here, $I^+$ and $I^-$ are the concentrations of the inhibitor after and before the impulse, respectively.

We calculate the rate equation of dual inhibitor of HIV-1 RT/IN in the following manner so that we can get some fruitful results from drug dynamics. The calculations are as follows:

$$\frac{dI}{dt} = -\alpha k_3 E_{10}\Big[\frac{1}{h_1(I)}+\frac{1}{h_2(I)}+\frac{1}{h_3(I)}\Big]I-(1-\alpha)\frac{k_7 E_{20}}{h_4(I)}I-\mu_6 I. \tag{3.3.2}$$

Where, $h_1(I) = (1+\frac{\alpha^n I^n}{{K_{i1}}^n})$, $h_2(I) = (1+\frac{\alpha^n I^n}{({K_{i1}}')^n})$, $h_3(I) = (1+\frac{\alpha^n I^n}{({K_{i1}}'')^n})$, $h_4(I) = (1+\frac{(1-\alpha)I}{K_{i2}})$, $n$ = hill coefficient of inhibitor binding.

We see from equation (3.3.2) that the dual inhibitor ($I$) of HIV-1 RT/IN exhibits simultaneous linear and nonlinear Michaelis-Menten elimination kinetics but the first-order elimination pathway is not very much important to determine the drug dose like the nonlinear Michaelis-Menten elimination pathway. So we can neglect the linear elimination part to avoid complexity in further calculations. Therefore, the rate equation of the inhibitor ($I$) takes the form:

$$\frac{dI}{dt} = -\alpha k_3 E_{10}\Big[\frac{1}{h_1(I)}+\frac{1}{h_2(I)}+\frac{1}{h_3(I)}\Big]I-(1-\alpha)\frac{k_7 E_{20}}{h_4(I)}I.$$

As earlier we described, the dual inhibitor ($I$) of HIV-1 RT/IN manifests two different parallel inhibition mechanisms therefore, from equations (3.2.3) and (3.2.4), we get the rate equations for $I_1(t)$ and $I_2(t)$ as follows:

$$\begin{aligned} \tfrac{dI_1}{dt} &= -k_3 E_{10}\Big[\tfrac{1}{h_1(I_1)}+\tfrac{1}{h_2(I_1)}+\tfrac{1}{h_3(I_1)}\Big]I_1, \\ \tfrac{dI_2}{dt} &= -\tfrac{k_7 E_{20}}{h_4(I_2)}I_2, \end{aligned} \tag{3.3.3}$$

where $I_1 = \alpha I$ and $I_2 = (1-\alpha)I$, $\alpha \in (0,1)$. Here $I_1$ working as a non-competitive binding inhibitor shows intermolecular cooperativity to inhibit the enzyme RT ($E_1$), whereas $I_2$ uncompetitively inhibits the enzyme IN ($E_2$).

Here, $h_1(I_1) = (1 + \frac{I_1^n}{{K_{i1}}^n})$, $h_2(I_1) = (1 + \frac{{I_1}^n}{({K_{i1}}')^n})$, $h_3(I_1) = (1 + \frac{{I_1}^n}{({K_{i1}}'')^n})$, $h_4(I_2) = (1 + \frac{I_2}{K_{i2}})$, ${K_{i1}}' = \beta_1 K_{i1}$ and ${K_{i1}}'' = \beta_2 K_{i1}$. ${K_{i1}}' \gtrless K_{i1}$ as well as ${K_{i1}}'' \gtrless K_{i1}$ according to $\beta_1 \gtrless 1$ and $\beta_2 \gtrless 1$ respectively. In our case, we choose $\beta_1$, $\beta_2$ such that $1 < \beta_2 < \beta_1$.

Using the above mentioned relations between $K_{i1}$, ${K_{i1}}'$ and ${K_{i1}}''$, we can derive

$$\begin{aligned} h_1(I_1) &= 1 + \frac{I_1^n}{{K_{i1}}^n} > 1 + \frac{{I_1}^n}{({K_{i1}}')^n} = h_2(I_1), \\ h_3(I_1) &= 1 + \frac{{I_1}^n}{({K_{i1}}'')^n} > 1 + \frac{{I_1}^n}{({K_{i1}}')^n} = h_2(I_1). \end{aligned}$$

Now replacing $h_1(I_1)$ and $h_3(I_1)$ by $h_2(I_1)$ in equation (3.3.3), we get the following inequality

$$\frac{dI_1}{dt} > \frac{-k_3 E_{10}}{h_2(I_1)} I_1, \text{ i.e., } \frac{dI_1}{dt} > \frac{-k_3 E_{10} ({K_{i1}}')^n}{({K_{i1}}')^n + {I_1}^n} I_1. \tag{3.3.4}$$

We have derived the inequality (3.3.4) from the above calculation to determine the minimum permitted dose for the maximum toxicity, as the inhibitor ($I$) itself can be toxic to the human body when present in excess amount. So we have considered the equality with equation (3.3.4) and formulated the impulsive differential equations for $I_1$ and $I_2$. Hence, the impulsive differential equations for $I_1$ and $I_2$ take the form

$$\frac{dI_1}{dt} = \begin{cases} \frac{-k_3 E_{10} ({K_{i1}}')^n}{({K_{i1}}')^n + {I_1}^n} I_1, \text{ for } t \neq t_k, \\ \\ I_1(t_k^+) - I_1(t_k^-) = \alpha I_c \text{ for } t = t_k \end{cases} \tag{3.3.5}$$

and

$$\frac{dI_2}{dt} = \begin{cases} \frac{-k_7 E_{20} K_{i2}}{K_{i2} + I_2} I_2, \text{ for } t \neq t_k, \\ \\ I_2(t_k^+) - I_2(t_k^-) = (1-\alpha) I_c \text{ for } t = t_k, \end{cases} \tag{3.3.6}$$

where $I_c$ is the fixed dose of dual inhibitor of HIV-1 RT/IN given on a fixed time interval $\tau$. Here we consider the single impulse cycle $t_k \leq t \leq t_{k+1}$ such that $t_{k+1} - t_k = \tau$ and $k = 0,\ 1,\ 2,\ \ldots$ The general integrated forms of the differential equations (3.3.5) and (3.3.6) are given by

$$\begin{aligned} \frac{1}{k_3 E_{10}} \left[ ln\left(\frac{I_1(t_k^+)}{I_1(t)}\right) + \frac{1}{n({K_{i1}}')^n} \left( I_1(t_k^+)^n - I_1(t)^n \right) \right] &= t - t_k \quad \text{and} \\ \frac{1}{k_7 E_{20}} \left[ ln\left(\frac{I_2(t_k^+)}{I_2(t)}\right) + \frac{1}{K_{i2}} (I_2(t_k^+) - I_2(t)) \right] &= t - t_k. \end{aligned} \tag{3.3.7}$$

However, (3.3.7) does not represent the completely analytical solutions of the differential equations (3.3.5) and (3.3.6). It is known that analytic solutions provide a clear and direct way to explore the underlying mechanisms and easily derive expressions of related pharmacological indices therefore, it is important to obtain closed form solutions of the equations (3.3.5) and (3.3.6). In 1997, Schnell and Mendoz (Schnell and Mendoza, 1997) first used Lambert W function for a model of enzyme reaction processes with Michaelis–Menten kinetics. In 2007, Tang and Xiao (Tang and Xiao, 2007) provided a detailed analytical solution for the one-compartment model with a Michaelis-Menten elimination kinetics, under different administrations by using the Lambert W function. In this paper, to derive the exact closed-form solutions for the differential equations (3.3.5)-(3.3.6), we use the properties of the Lambert W function (one can have a look at (Barry et al., 2000; Corless et al., 1996) for details), defined to be the multivalued inverse of the function $x \mapsto xe^x$ satisfying

$$\text{Lambert W(x)} \exp(\text{Lambert W(x)}) \quad = \quad x.$$

Now equations in (3.3.7) can be rewritten as:

$$\ln\left(\frac{I_1(t)^n}{I_1(t_k^+)^n}\right) + \frac{I_1(t)^n}{({K_{i1}}')^n} \quad = \quad \frac{I_1(t_k^+)^n - n({K_{i1}}')^n k_3 E_{10}(t-t_k)}{({K_{i1}}')^n} \tag{3.3.8}$$

and

$$\ln\left(\frac{I_2(t)}{I_2(t_k^+)}\right) + \frac{I_2(t)}{K_{i2}} \quad = \quad \frac{I_2(t_k^+) - K_{i2}k_7E_{20}(t-t_k)}{K_{i2}}, \tag{3.3.9}$$

respectively.

Taking exponents of both sides on the above equation (3.3.8) implies

$$\frac{I_1(t)^n}{({K_{i1}}')^n}\exp\left(\frac{I_1(t)^n}{({K_{i1}}')^n}\right) = \frac{I_1(t_k^+)^n}{({K_{i1}}')^n}\exp\left(\frac{I_1(t_k^+)^n - n({K_{i1}}')^n k_3 E_{10}(t-t_k)}{({K_{i1}}')^n}\right).$$

It follows from the definition of Lambert W function that we have the following explicit closed-form solution for model (3.3.5):

$$I_1(t)^n = ({K_{i1}}')^n \text{Lambert W}\left(\frac{I_1(t_k^+)^n}{({K_{i1}}')^n}\exp\left(\frac{I_1(t_k^+)^n - n({K_{i1}}')^n k_3 E_{10}(t-t_k)}{({K_{i1}}')^n}\right)\right). \tag{3.3.10}$$

Using a similar approach, we derive the analytical solution for model (3.3.6) from equation (3.3.9) as

$$I_2(t) \quad = \quad K_{i2}\text{Lambert W}\left(\frac{I_2(t_k^+)}{K_{i2}}\exp\left(\frac{I_2(t_k^+) - K_{i2}k_7E_{20}(t-t_k)}{K_{i2}}\right)\right). \tag{3.3.11}$$

Actually, here $I_1(t)^n \equiv I_1(t)$ because $I_1(t)^n$ represents the total amount of the dual inhibitor ($I$) of HIV-1 RT/IN in the body at time $t$. Hence, denoting $I_1(t)^n$ by $I_1(t)$ in equation (3.3.10) gives

$$I_1(t) = (K_{i1}{}')^n \text{Lambert W}\left(\frac{I_1(t_k^+)}{(K_{i1}{}')^n}\exp\left(\frac{I_1(t_k^+) - n(K_{i1}{}')^n k_3 E_{10}(t-t_k)}{(K_{i1}{}')^n}\right)\right). \quad (3.3.12)$$

Therefore, the solution of model (3.3.1) at any interval $(t_k, t_{k+1}]$ is:

$$\begin{aligned} I(t) &= I_1(t) + I_2(t) \\ &= (K_{i1}{}')^n \text{Lambert W}\left(\frac{I_1(t_k^+)}{(K_{i1}{}')^n}\exp\left(\frac{I_1(t_k^+) - n(K_{i1}{}')^n k_3 E_{10}(t-t_k)}{(K_{i1}{}')^n}\right)\right) \\ &+ K_{i2}\text{Lambert W}\left(\frac{I_2(t_k^+)}{K_{i2}}\exp\left(\frac{I_2(t_k^+) - K_{i2}k_7 E_{20}(t-t_k)}{K_{i2}}\right)\right). \end{aligned} \quad (3.3.13)$$

Now equation (3.3.13) implies that

$$I(t_{k+1}^-) = I_1(t_{k+1}^-) + I_2(t_{k+1}^-).$$

Therefore,

$$\begin{aligned} I(t_{k+1}^+) &= I(t_{k+1}^-) + I_c \\ &= I_1(t_{k+1}^-) + I_2(t_{k+1}^-) + \alpha I_c + (1-\alpha)I_c \\ &= (I_1(t_{k+1}^-) + \alpha I_c) + (I_2(t_{k+1}^-) + (1-\alpha)I_c) \\ \Rightarrow I(t_{k+1}^+) &= I_1(t_{k+1}^+) + I_2(t_{k+1}^+). \end{aligned} \quad (3.3.14)$$

We obtain the expressions for $I_1(t_{k+1}^-)$, $I_2(t_{k+1}^-)$ from equations (3.3.12) and (3.3.11) respectively. Equation (3.3.12) implies that

$$I_1(t_{k+1}^-) = (K_{i1}{}')^n \text{Lambert W}\left(\frac{I_1(t_k^+)}{(K_{i1}{}')^n}\exp\left(\frac{I_1(t_k^+) - n(K_{i1}{}')^n k_3 E_{10}(t_{k+1}-t_k)}{(K_{i1}{}')^n}\right)\right).$$

This implies

$$\begin{aligned} I_1(t_{k+1}^+) &= I_1(t_{k+1}^-) + \alpha I_c \\ &= (K_{i1}{}')^n \text{Lambert W}\left(\frac{I_1(t_k^+)}{(K_{i1}{}')^n}\exp\left(\frac{I_1(t_k^+) - n(K_{i1}{}')^n k_3 E_{10}(t_{k+1}-t_k)}{(K_{i1}{}')^n}\right)\right) + \alpha I_c. \end{aligned}$$

Similarly, considering equation (3.3.11) we can derive

$$I_2(t_{k+1}^+) = K_{i2}\text{Lambert W}\left(\frac{I_2(t_k^+)}{K_{i2}}\exp\left(\frac{I_2(t_k^+) - K_{i2}k_7 E_{20}(t_{k+1}-t_k)}{K_{i2}}\right)\right) + (1-\alpha)I_c.$$

Now, equation (3.3.14) implies that there is a positive periodic solution of model (3.3.1) if the model (3.3.14) has at least one positive steady state. To find the steady-state concentration at any time $t$, we denote $I_k = I(t_{k+1}^+)$, $I_{1_k} = I_1(t_{k+1}^+)$, $I_{2_k} = I_2(t_{k+1}^+)$. Then equation (3.3.14) reduces to

$$I_k = I_{1_k} + I_{2_k}, \tag{3.3.15}$$

where the expressions for $I_{1_k}$ and $I_{2_k}$ are represented by the following equations, substituting $t_{k+1} - t_k = \tau$

$$I_{1_k} = ({K_{i1}}')^n \text{Lambert W}\left(\frac{I_{1_{k-1}}}{({K_{i1}}')^n}\exp\left(\frac{I_{1_{k-1}} - n({K_{i1}}')^n k_3 E_{10}\tau}{({K_{i1}}')^n}\right)\right) + \alpha I_c \tag{3.3.16}$$

and

$$I_{2_k} = K_{i2}\text{Lambert W}\left(\frac{I_{2_{k-1}}}{K_{i2}}\exp\left(\frac{I_{2_{k-1}} - K_{i2}k_7E_{20}\tau}{K_{i2}}\right)\right) + (1-\alpha)I_c. \tag{3.3.17}$$

Let $k$ tend to infinity, the steady-state $I^*$ satisfies the following equation:

$$I^* = I_1^* + I_2^*. \tag{3.3.18}$$

$I_1^*$ and $I_2^*$ are the respective steady-states of equations (3.3.16)-(3.3.17) and satisfies

$$I_1^* = ({K_{i1}}')^n \text{Lambert W}\left(\frac{I_1^*}{({K_{i1}}')^n}\exp\left(\frac{I_1^* - n({K_{i1}}')^n k_3 E_{10}\tau}{({K_{i1}}')^n}\right)\right) + \alpha I_c, \tag{3.3.19}$$

$$I_2^* = K_{i2}\text{Lambert W}\left(\frac{I_2^*}{K_{i2}}\exp\left(\frac{I_2^* - K_{i2}k_7E_{20}\tau}{K_{i2}}\right)\right) + (1-\alpha)I_c. \tag{3.3.20}$$

Now equation (3.3.19) implies that

$$\frac{I_1^* - \alpha I_c}{({K_{i1}}')^n} = \text{Lambert W}\left(\frac{I_1^*}{({K_{i1}}')^n}\exp\left(\frac{I_1^* - n({K_{i1}}')^n k_3 E_{10}\tau}{({K_{i1}}')^n}\right)\right).$$

It follows from the definition of Lambert W function that

$$\frac{I_1^* - \alpha I_c}{({K_{i1}}')^n}\exp\left(\frac{I_1^* - \alpha I_c}{({K_{i1}}')^n}\right) = \frac{I_1^*}{({K_{i1}}')^n}\exp\left(\frac{I_1^* - n({K_{i1}}')^n k_3 E_{10}\tau}{({K_{i1}}')^n}\right),$$

which implies that there is a unique positive steady-state

$$I_1^* = \frac{\alpha I_c}{1-\exp\left(\frac{\alpha I_c - n(K_{i1}{}')^n k_3 E_{10}\tau}{(K_{i1}{}')^n}\right)} \text{ provided } \exp\left(\frac{\alpha I_c - n(K_{i1}{}')^n k_3 E_{10}\tau}{(K_{i1}{}')^n}\right) < 1. \tag{3.3.21}$$

Hence, we get the periodic solution of the model (3.3.5) as

$$I_1(t) = (K_{i1}{}')^n \text{Lambert W}\left(\frac{I_1^*}{(K_{i1}{}')^n}\exp\left(\frac{I_1^* - n(K_{i1}{}')^n k_3 E_{10}(t-t_k)}{(K_{i1}{}')^n}\right)\right). \tag{3.3.22}$$

Similarly, we can show that the difference equation (3.3.17) has a unique positive steady-state $I_2^*$ and satisfies

$$I_2^* = \frac{(1-\alpha)I_c}{1-\exp\left(\frac{(1-\alpha)I_c - K_{i2}k_7 E_{20}\tau}{K_{i2}}\right)} \text{ provided } \exp\left(\frac{(1-\alpha)I_c - K_{i2}k_7 E_{20}\tau}{K_{i2}}\right) < 1 \tag{3.3.23}$$

and thus the periodic solution of model (3.3.6) is

$$I_2(t) = K_{i2}\text{Lambert W}\left(\frac{I_2^*}{K_{i2}}\exp\left(\frac{I_2^* - K_{i2}k_7 E_{20}(t-t_k)}{K_{i2}}\right)\right). \tag{3.3.24}$$

Therefore, we can say that the difference equation (3.3.15) has a unique positive steady-state $I^*$ and verifies

$$I^* = \frac{\alpha I_c}{1 - exp\left(\frac{\alpha I_c - n(K_{i1}{}')^n k_3 E_{10}\tau}{(K_{i1}{}')^n}\right)} + \frac{(1-\alpha)I_c}{1 - exp\left(\frac{(1-\alpha)I_c - K_{i2}k_7 E_{20}\tau}{K_{i2}}\right)}, \tag{3.3.25}$$

if the following inequalities hold true:

$$\frac{\alpha I_c}{\tau} < n(K_{i1}{}')^n k_3 E_{10} \text{ and } \frac{(1-\alpha)I_c}{\tau} < K_{i2}k_7 E_{20}.$$

Adding the above two inequalities, we obtain

$$\begin{array}{l} \frac{I_c}{\tau} < n(K_{i1}{}')^n k_3 E_{10} + K_{i2}k_7 E_{20} \\ \text{or } \tau > \frac{I_c}{n(K_{i1}{}')^n k_3 E_{10} + K_{i2}k_7 E_{20}} = \tau_{min}. \end{array} \tag{3.3.26}$$

Thus, the periodic solution of model (3.3.1) is given by

$$\begin{array}{rcl} I(t) & = & (K_{i1}{}')^n \text{Lambert W}\left(\frac{I_1^*}{(K_{i1}{}')^n}\exp\left(\frac{I_1^* - n(K_{i1}{}')^n k_3 E_{10}(t-t_k)}{(K_{i1}{}')^n}\right)\right) \\ & + & K_{i2}\text{Lambert W}\left(\frac{I_2^*}{K_{i2}}\exp\left(\frac{I_2^* - K_{i2}k_7 E_{20}(t-t_k)}{K_{i2}}\right)\right), \end{array} \tag{3.3.27}$$

where the values of $I_1^*$, $I_2^*$ are expressed by equations (3.3.21), (3.3.23) respectively.

We see from the existence condition (3.3.26) that the model (3.3.1) has a unique periodic solution under the condition $\frac{I_c}{\tau} < (n(K_{i1}{}')^n k_3 E_{10} + K_{i2} k_7 E_{20})$. Moreover, we have shown the local stability of the periodic solution (3.3.27). Obviously, equation (3.3.25) implies that $I^* > I_c$. Hence, in order to design a periodic dosing regimen, one large initial dose $I^*$ should be administered, following with a small dose $I_c$.

Let us denote the steady-state minimum and maximum concentrations as $I^{ss}_{min}$ and $I^{ss}_{max}$, respectively. At the steady-state, these concentrations can be given by

$$\begin{aligned} I^{ss}_{min} &= (K_{i1}{}')^n \text{Lambert W}\left(\frac{I_1^*}{(K_{i1}{}')^n}\exp\left(\frac{I_1^* - n(K_{i1}{}')^n k_3 E_{10}\tau}{(K_{i1}{}')^n}\right)\right) \\ &+ K_{i2}\text{Lambert W}\left(\frac{I_2^*}{K_{i2}}\exp\left(\frac{I_2^* - K_{i2}k_7E_{20}\tau}{K_{i2}}\right)\right) \text{ and} \\ I^{ss}_{max} &= (K_{i1}{}')^n \text{Lambert W}\left(\frac{I_1^*}{(K_{i1}{}')^n}\exp\left(\frac{I_1^* - n(K_{i1}{}')^n k_3 E_{10}\tau}{(K_{i1}{}')^n}\right)\right) \\ &+ K_{i2}\text{Lambert W}\left(\frac{I_2^*}{K_{i2}}\exp\left(\frac{I_2^* - K_{i2}k_7E_{20}\tau}{K_{i2}}\right)\right) + I_c \equiv I^*. \end{aligned} \tag{3.3.28}$$

### 3.3.1 Corollary

**Local stability of the periodic solution**

**Theorem 3.3.1** *The periodic solution given by equation* (3.3.27) *is locally stable.*

**Proof.** We will show that any solution of model (3.3.1) will asymptotically approach the periodic solution (3.3.27), for any given initial dose. To do this, we first prove that the solutions given by equations (3.3.22) and (3.3.24) are locally stable. Now, solution $I_1^*$ at equilibrium is locally stable if the following condition

$$\frac{\partial(I_1(t_{k+1}^+))}{\partial(I_1(t_k^+))}\Big|_{I_1(t_k^+)=I_1^*} < 1 \text{ is satisfied.}$$

Solving the above inequality by applying the chain rule, we have

$$\begin{aligned} \frac{(K_{i1}{}')^n \text{Lambert W}_{(Z)}}{1+\text{Lambert W}_{(Z)}}\left[\frac{1}{(K_{i1}{}')^n} + \frac{1}{I_1^*}\right] &< 1, \\ i.e., \frac{\text{Lambert W}_{(Z)}}{1+\text{Lambert W}_{(Z)}}\left[\frac{(K_{i1}{}')^n}{I_1^*} + 1\right] &< 1, \end{aligned} \tag{3.3.29}$$

where $Z = \frac{I_1^*}{(K_{i1}{}')^n}\exp\left(\frac{I_1^* - n(K_{i1}{}')^n k_3 E_{10}\tau}{(K_{i1}{}')^n}\right)$. Now we show that, if the positive steady-state $I_1^*$ exists then the inequality (3.3.29) always holds true. It follows from equation

(3.3.19) that we have

$$\begin{aligned}\frac{I_1^*}{(K_{i1}')^n} &= \text{Lambert W}\left(\frac{I_1^*}{(K_{i1}')^n}\exp\left(\frac{I_1^*-n(K_{i1}')^n k_3 E_{10}\tau}{(K_{i1}')^n}\right)\right)+\frac{\alpha I_c}{(K_{i1}')^n}\\ &= \text{Lambert W}(Z)+\frac{\alpha I_c}{(K_{i1}')^n}.\end{aligned}$$

Substituting the above expression for $\frac{I_1^*}{(K_{i1}')^n}$ into (3.3.29), we obtain

$$\begin{aligned}&\frac{\text{Lambert W}(Z)}{1+\text{Lambert W}(Z)}\left[\frac{1}{\text{Lambert W}(Z)+\frac{\alpha I_c}{(K_{i1}')^n}}+1\right] < 1,\\ &\Rightarrow \frac{\text{Lambert W}(Z)}{(1+\text{Lambert W}(Z))}\frac{(1+\text{Lambert W}(Z)+\frac{\alpha I_c}{(K_{i1}')^n})}{(\text{Lambert W}(Z)+\frac{\alpha I_c}{(K_{i1}')^n})} < 1.\end{aligned} \tag{3.3.30}$$

Let us define a function

$$f(x)=\frac{1+\text{Lambert W}(Z)+x}{\text{Lambert W}(Z)+x}, x\geq 0 \text{ with } f(0)=\frac{1+\text{Lambert W}(Z)}{\text{Lambert W}(Z)}.$$

This implies

$$\frac{\text{Lambert W}(Z)}{1+\text{Lambert W}(Z)}f(0)=1.$$

Since

$$\frac{d(f(x))}{dx}=\frac{-1}{(\text{Lambert W}(Z)+x)^2}<0.$$

We can say that $f(x)$ is a monotonically decreasing function. This implies that the inequality (3.3.30) holds true and hence, the local stability of the steady-state $I_1^*$ is proved. Similarly, we can show that the steady-state $I_2^*$ is also locally stable. Now we prove the local stability of the steady-state $I^*$. Since $I(t)=I_1+I_2(t)$ (3.3.13) and $I^*=I_1^*+I_2^*$ (3.3.18), therefore, by applying the $\epsilon-\delta$ definition for stability one can prove that $I^*$ is stable, provided both the steady-states $I_1^*$ and $I_2^*$ are stable.

**Definition 3.3.1** *The equilibrium $X_e$ of an nonlinear autonomous system $X'=f(X)$, $f:D\to\Re^n$ (a locally Lipschitz map from domain $D\subseteq\Re^n$) is*

*(i)* ***stable*** *if for each $\epsilon>0$ there exists a $\delta(\epsilon)>0$ such that*

$$\| X(t_0)-X_e \|<\delta(\epsilon)\Longrightarrow\| X(t)-X_e \|<\epsilon,$$

*(ii)* ***asymptotically stable*** *if it is stable and in addition* $\delta(\epsilon)$ *can be chosen such that*

$$\| X(t_0) - X_e \| < \delta(\epsilon) \Longrightarrow \lim_{t \to \infty} \| X(t) - X_e \| = 0.$$

## 3.4 Results and Discussion

To illustrate the behavior of our models (3.2.3) and (3.2.5), we give numerical simulations with the set of parameter values in Table 3.1. Some of these values are taken from (Althaus et al., 1993; Brussel and Sonigo, 2004; Butler et al., 2001; De and Camarasa, 2018; Gu et al., 2016; Kustikova et al., 2003; Mislak et al., 2014; Mohammadi et al., 2013; Murray et al., 2012; Shcherbatova et al., 2020; Siliciano et al., 2003; Vandegraaff et al., 2012; Zarrabi et al., 2010), while some parameter values are hypothetically assumed. We begin by simulating the system without impulse, then with impulse. We used MATLAB 2016A to perform our numerical studies.

Figure 3.4 represents the variations of reactants' concentration over time $t$ with and without the introduction of dual inhibitor of HIV-1 RT and IN into the system. When an individual gets infected, a viral enzyme RT starts to synthesize double-stranded DNA ($P(t)$) from a viral single-stranded RNA genome with the help of dNTPs. The viral genome serving as an RNA template binds into a host tRNA primer and forms a template-primer complex ($S_1(t)$) that starts to interact with the dNTPs ($S_2(t)$). Hence, the synthesis of viral double-stranded DNA ($P(t)$) begins in the host cell cytoplasm. So, the complex ($S_1(t)$) concentration and the dNTPs ($S_2(t)$) concentration decrease, whereas, the concentration of double-stranded DNA ($P(t)$) increases with time at a particular rate. Further, the double-stranded DNA ($P(t)$) is transported into the nucleus of the infected cell and transformed into integrated pro-viral DNA ($P_1(t)$) after making integration with the host cell chromosome ($S_3(t)$) by another viral enzyme, IN. So, the concentration of viral double-stranded DNA ($P(t)$) and the host DNA ($S_3(t)$) concentration decrease while the integrated pro-viral DNA ($P_1(t)$) concentration increases. For being the product of one reaction and substrate of another, the progress curve of viral double-stranded DNA ($P(t)$) first increases

Table 3.1: List of parameters for model (3.2.5).

| Parameter | Parameter description | Value (Unit) | References |
|---|---|---|---|
| $k_3$ | Rate of forward reaction from $E_1S_1S_2$ to $E_1S_{1_{n+1}}$ | $0.8 - 2.7\ sec^{-1}$ | Althaus et al. (1993); Hu and Hughes (2012); Shcherbatova et al. (2020); Zarrabi et al. (2010) |
| $K_7$ | Rate of forward reaction from $E_2PS_3$ to $E_2$ and $P_1$ | $0.7 - 4.6\ hr^{-1}$ | Butler et al. (2001); Kustikova et al. (2003); Shcherbatova et al. (2020) |
| $K_{S_1}$ | Reaction dissociation constant between $S_1$ and $E_1$ | $0.00001 - 2.05\ \mu M$ | Althaus et al. (1993) |
| $K_{M_{S_1}}$ | Michaelis constant for $S_1$ | $1.002 - 2.08\ \mu M$ | Estimated |
| $K_{M_{S_2}}$ | Michaelis constant for $S_2$ | $0.005 - 1.8\ \mu M$ | Estimated |
| $K_{M_{S_3}}$ | Michaelis constant for $S_3$ | $1.0 - 3.5\ \mu M$ | Estimated |
| $K_{M_P}$ | Michaelis constant for $P$ | $0.002 - 0.20\ \mu M$ | Estimated |
| $K_P{}'$ | Ratio of forward rate constant from $E_1S_1S_2$ to $E_1S_{1_{n+1}}$ and from $E_1S_{1_{n+1}}$ to $E_1 + P$ | $0.1 - 0.8\ \mu M$ | Estimated |
| $K_P$ | Reaction dissociation constant between $P$ and $E_2$ | $0.002 - 1.03\ \mu M$ | Estimated |
| $K_{i1}$ | Reaction dissociation constant between $E_1$ and $I$ | $1.8 - 5.5\ \mu M$ | Althaus et al. (1993); Mislak et al. (2014) |
| $K_{i1}{}'$ | Reaction dissociation constant between $E_1S_1$ and $I$ | $10.0 - 15.0\ \mu M$ | Althaus et al. (1993); Mislak et al. (2014) |
| $K_{i1}{}''$ | Reaction dissociation constant between $E_1S_1S_2$ and $I$ | $5.7 - 10.0\ \mu M$ | Althaus et al. (1993) |
| $K_{i2}$ | Reaction dissociation constant between $E_2P$ and $I$ | $1.3 - 5.8\ \mu M$ | De and Camarasa (2018); Gu et al. (2016) |
| $\mu_1$ | Degradation rate of $S_1$ | $0.001 - 0.28\ hr^{-1}$ | Brussel and Sonigo (2004) |
| $\mu_2$ | Degradation rate of $S_2$ | $0.02 - 0.5\ hr^{-1}$ | Assumed |
| $\mu_3$ | Degradation rate of $P$ | $0.0001 - 0.4\ hr^{-1}$ | Mohammadi et al. (2013); Murray et al. (2012); Vandegraaff et al. (2012) |
| $\mu_4$ | Degradation rate of $S_3$ | $0.001 - 0.18\ hr^{-1}$ | Assumed |
| $\mu_5$ | Degradation rate of $P_1$ | $0.002 - 0.3\ hr^{-1}$ | Siliciano et al. (2003) |

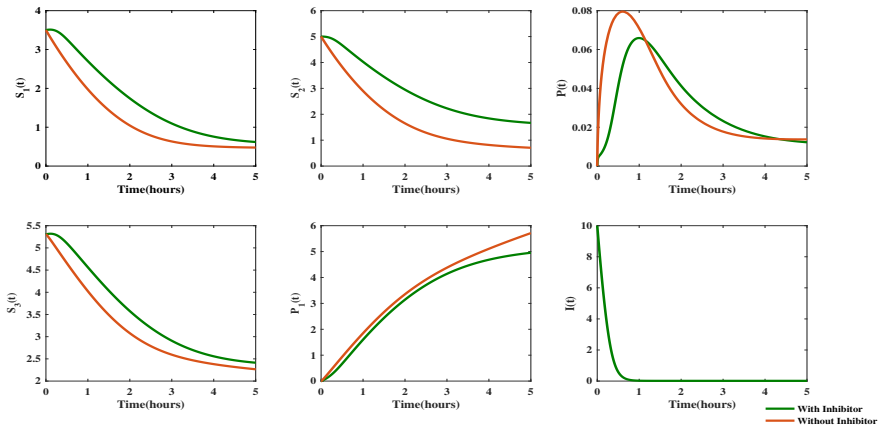


Figure 3.4: Comparison study between the absence of HIV-1 RT/IN dual inhibitor and presence of HIV-1 RT/IN dual inhibitor for each reactant with initial conditions $[S_1, S_2, S_3, E_1, E_2, I](0) = [3.5, 5, 5.3, 3, 1.8, 10]\mu M$. Here also the parameter values are taken from Table (3.1). For both with and without HIV-1 RT/IN dual inhibitor the substrates $S_1$, $S_2$ and $S_3$ concentration decreases over time, but at a slower rate in the case of with inhibitor compared to without inhibitor. The progress curve of viral double-standed DNA ($P(t)$) first increases with time and then decreases, whereas, concentration of pro-viral DNA ($P_1(t)$) increases over time in both the cases.

with time and then decreases. Here we introduce dual inhibitor ($I(t)$) of HIV-1 RT and IN in the system immediately after infection and see that the formation of viral double-stranded DNA ($P(t)$) reduces at a higher rate in comparison to the uninhibited reaction. Since the formation of the viral double-stranded DNA ($P(t)$) drops after applying the inhibitor therefore, a similar declination is seen in the progress curve of integrated pro-viral DNA ($P_1(t)$). Due to the non-competitive binding phenomena of the inhibitor ($I(t)$) towards enzyme RT, the progress curves of template-primer complex ($S_1(t)$) and the dNTPs ($S_2(t)$) go down at a slower rate relative to the uninhibited reaction. A similar thing happens to the host DNA ($S_3(t)$) concentration curve as the drug simultaneously inhibits the enzyme IN in an uncompetitive way. The effect of slower reduction of the substrates ($S_1, S_2, S_3$) concentration is reflected on the other two components ($P, P_1$) participating in HIV-1 life cycle. Integrated pro-viral DNA ($P_1$) further takes part in HIV-1 replication process therefore, the reduction of $P_1$ concentration creates a favorable condition for suppressing the viral load at a low level. However, the effect of a single dose of a dual inhibitor of HIV-1 RT/IN on HIV-1

replication has been shown in Fig. 3.4 and we can see the benefits of using it for an HIV-1 infected individual introducing only once at intermediate stages of the viral life cycle.

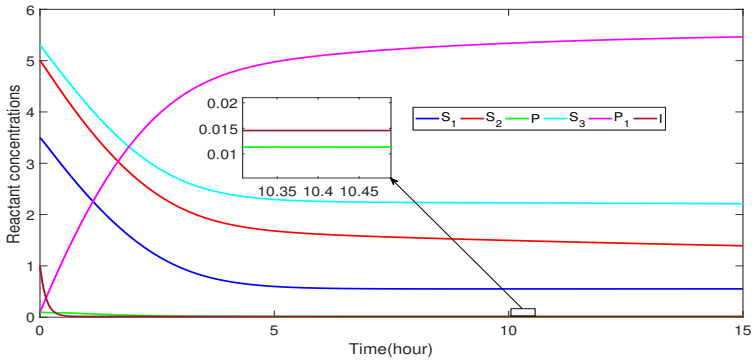


Figure 3.5: Persistence of the system 3.2.5. The initial conditions and the parameter values are same as Fig. 3.4.

Figure 3.5 illustrates the variations of reactants' concentration over time in a single figure and we see that the reactants do not go to extinction, thereby confirming the persistence of the system 3.2.5.

From Figure 3.6 we can get an overview of how fast the substrate template-primer complex ($S_1$) disappearances in the reaction pathway as well as how fast the viral double-stranded DNA ($P$) is turned into the product integrated proviral DNA ($P_1$). The rate of disappearance of the substrate $S_1$ starts in a hyperbolic way because the velocity decreases proportionately with the substrate concentration. However, with further increment in substrate ($S_1$) concentration, the velocity begins to slow down until a plateau is reached as the enzyme RT ($E_1$) becomes saturated. It is worth noting that in the presence of dual inhibitor of HIV-1 RT and IN, the rate of disappearance of substrate $S_1$ occurs in a slower motion than in the absence of the inhibitor ($I$) because of the non-competitive binding property of the inhibitor ($I$) towards enzyme RT ($E_1$). As a result, the saturation point $C_1(10, 0.6851)$ exists at a considerably upper position than the saturation point in absence of the dual inhibitor of HIV-1 RT/IN ($I$). In Fig. 3.6(b) we see an exact opposite nature between the positions of the saturation points from Fig. 3.6(a). Here the rate of reaction

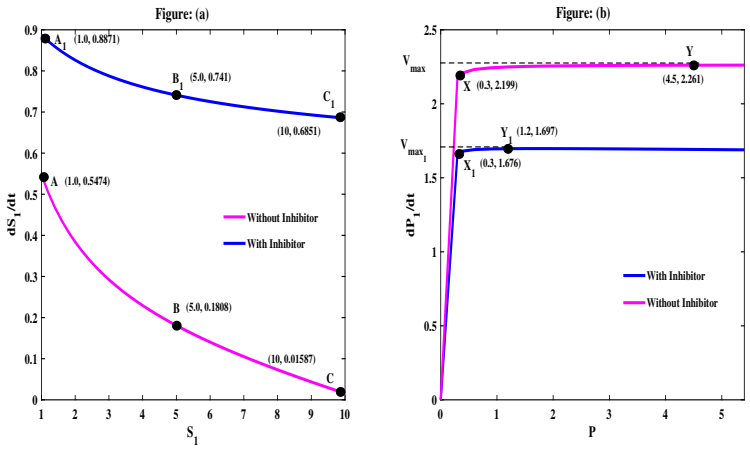


Figure 3.6: Comparison study between the plot of initial velocity as a function of substrate concentration in the presence of HIV-1 RT/IN dual inhibitor and in absence of HIV-1 RT/IN dual inhibitor. The parameter values are taken from Table 3.1. Disappearance of $S_1$ starts in a hyperbolic way but at a slower motion, in the presence of dual inhibitor than in the absence. Saturation of substrate $(P)$ concentration behavior is opposite, i.e., saturation concentration is much lower in the presence of dual inhibitor than in its absence. Moreover, the rate of reaction does not grow in a hyperbolic manner.

increases with the increasing value of substrate $(P)$ concentration until the velocity reaches a maximum level $(V_{max})$A. Further increment in substrate $(P)$ concentration produces no significant change in the reaction rate as there are not enough enzyme IN $(E_2)$ molecules available to break down the excess substrate $(P)$ molecules. Since the dual inhibitor of HIV-1 RT/IN $(I)$ simultaneously binds the enzyme IN $(E_2)$ in an uncompetitive way, the saturation point $Y_1(1.2, 1.697)$ exists at a lower position than the point $Y(4.5, 2.261)$ in absence of the dual inhibitor of HIV-1 RT/IN $(I)$. Another noticeable feature of Fig. 3.6(b) is that unlike Fig. 3.6$(a)$, the rate of reaction does not grow in a hyperbolic manner. Instead, the initial velocity tracks linearly with substrate $(P)$ concentration as the enzyme $(E_2)$ concentration is fixed at a higher value than the substrate $(P)$ concentration and the concentration of substrate $(P)$ is then titrated. However, both the figures 3.6(a) and 3.6(b) confirm the therapeutic efficacy of dual inhibitor of HIV-1 RT and IN against HIV-1 replication.

We can notice as displayed in Fig. 3.7 that $I^{ss}_{min}$ and $I^{ss}_{max}$ increase in a non-linear

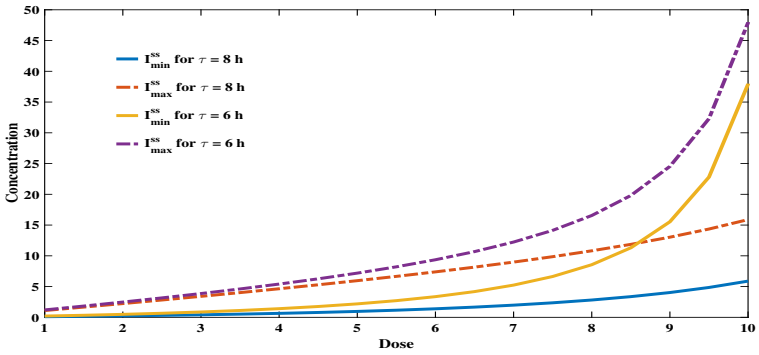


Figure 3.7: The relationships among the steady state, dose interval $\tau$ and dose $I_c$. Here we have taken $E_1(0) = 3\mu M$, $E_2(0) = 1.8\mu M$ and the parameter values are taken from Table 3.1. $I^{ss}_{\min}$ and $I^{ss}_{\max}$ increase in a non-linear way with respect to dose. As the period of dosing $\tau$ increases the concentration of $I^{ss}_{\min}$ and $I^{ss}_{\max}$ decreases. The above curves also confirm that the longer the dosing interval is, the larger the dose can be used.

way with respect to dose. However, for a fixed dose these concentrations are decreasing with respect to dosing interval $\tau$. Here, we have taken a period of dosing $\tau$ as 6 hr., 8 hr. and observed the nature of the curves of $I^{ss}_{min}$ and $I^{ss}_{max}$. Now, equation (3.3.28) clarify that $I^{ss}_{min}$ or $I^{ss}_{max}$ depends on the steady-state $I^*$. In combination with the existing condition (3.3.26), Fig. 3.7 also describes that for a given dose interval $\tau$, the small dose $I_c$ results in a small steady-state $I^*$ as well as a small maximum value of the periodic solution (3.3.27). This means that any solution of model (3.3.1) approaches the periodic solution (3.3.27) at a higher speed in response to a smaller dose $I_c$. Fig. 3.7 also confirms that the longer the dosing interval is, the larger the dose can be used.

Figure 3.8 illustrates the patterns of the progress curves of the components (viral single-stranded RNA ($S_1$), dNTPs ($S_2$), viral double-stranded DNA ($P$), host DNA ($S_3$), integrated proviral DNA ($P_1$)) involved in HIV-1 replication with the presence of dual inhibitor ($I$) of HIV-1 RT and IN. Here considering the dosing interval $\tau = 8$ hr as fixed and varying the initial value $I_0$(= $10\mu M$, $25\mu M$, $30\mu M$, $35\mu M$, $40\mu M$ respectively) of the inhibitor ($I$) as well as the impulse dose amount $I_c$ (= $5\mu M$, $20\mu M$, $25\mu M$, $30\mu M$, $35\mu M$) in each respective graph. We can notice as displayed in figure 3.8 that for $I_c = 5\mu M$ and $I_0 = 10\mu M$, the concentration of viral double-stranded

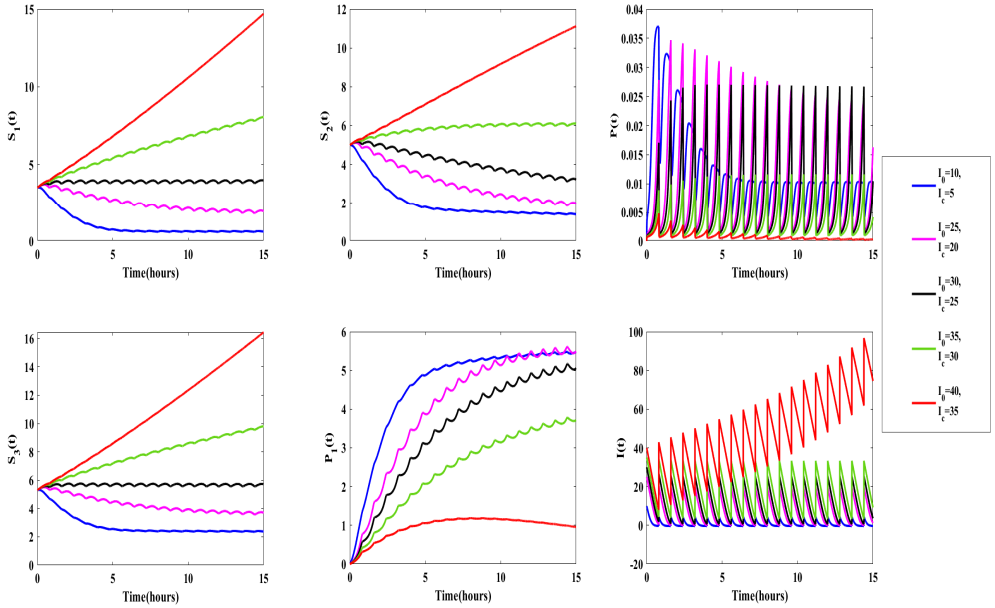


Figure 3.8: Concentration-time curves of the components of model (3.2.5) for the impulsive dosing of dual inhibitor of HIV-1 RT/IN with the initial conditions $[S_1, S_2, S_3, E_1, E_2, I](0) = [3.5, 5, 5.3, 3, 1.8, 10]\mu M$, impulse dose input $I_c = 5\mu M$ and the time interval of dosing $\tau = 8$ hr. We have taken the parameter values from Table 3.1.

DNA ($P$) decreases after applying the HIV-1 RT/IN dual inhibitor ($I$) for the first time and then increases again participating in the reaction mechanism for a while until the second dose of the inhibitor ($I$) is administered. It is worth noting that for $(I_c, I_0) = (5\mu M, 10\mu M)$ the inhibitor ($I$) concentration first reduces to zero but it does not rise up immediately, rather it becomes steady until the next dose is administered while for $(I_c, I_0) = (20\mu M, 25\mu M)$, the concentration of the inhibitor $I$ immediately speeds up after being reduced to zero. Also, it is noticeable from Fig. 3.8 that the progress curves of the components $S_1(t), S_2(t), S_3(t), P_1(t)$ for impulse dose $I_c = 20\mu M$ slow down at a reduced rate compared to those curves representing $I_c = 5\mu M$, and create a more favourable condition to combating HIV-1 replication. From $(I_c, I_0) = (25\mu M, 30\mu M)$ the dual inhibitor ($I$) of HIV-1 RT/IN starts to dominate the viral replication process and as a result, we can see that for impulse dose $I_c = 25\mu M$ that the progress curves of the components viral single-stranded RNA ($S_1$) and host DNA ($S_3$) increase whereas, the concentration of dNTPs ($S_2$) decreases. This is because the dual inhibitor ($I$) of HIV-1 RT/IN first binds to the enzyme RT ($E_1$) forming a complex $E_1I_1$ and makes it difficult for $S_1$ to participate in the replication process. Since the inhibitor $I$ simultaneously inhibits the enzyme IN ($E_2$) therefore, a similar increment is seen in $S_3$'s progress curve thereby, confirming the dual inhibitory property of $I$ towards the enzymes RT and IN respectively. On the other hand, the concentration of $S_2$ decreases for $I_c = 25\mu M$ because the impulse dose input $I_c = 25\mu M$ is not sufficient for the considered dosing interval to completely conquering the HIV-1 replication. In curves representing $(I_c, I_0) = (30\mu M, 35\mu M)$ and $(I_c, I_0) = (35\mu M, 40\mu M)$, a complete dominating property of the inhibitor ($I$) to controlling the enzymatic reactions of RT and IN is seen, and the reactants $(S_1, S_2, P, S_3)$ do not get scope to take part in the reaction mechanism at all. A noticeable feature in the curves for $(I_c, I_0) = (30\mu M, 35\mu M)$ and $(I_c, I_0) = (35\mu M, 40\mu M)$ is that before the inhibitor ($I$) concentration could completely reduce to zero, the next dose is applied and hence, an immediate rise is seen in the inhibitor ($I$) concentration. Therefore, we can conclude from Fig. 3.8 that the impulse dose amount $I_c = 5\mu M$ (with dosing interval $\tau = 8hr$) is not too effective to combating the viral replication; whereas, the inhibitor ($I$) could reach the maximum therapeutic level for $I_c = 25\mu M$ and it could

exceed the maximum tolerance level of the human body for $(I_c, I_0) = (30\mu M, 35\mu M)$ and $(I_c, I_0) = (35\mu M, 40\mu M)$.

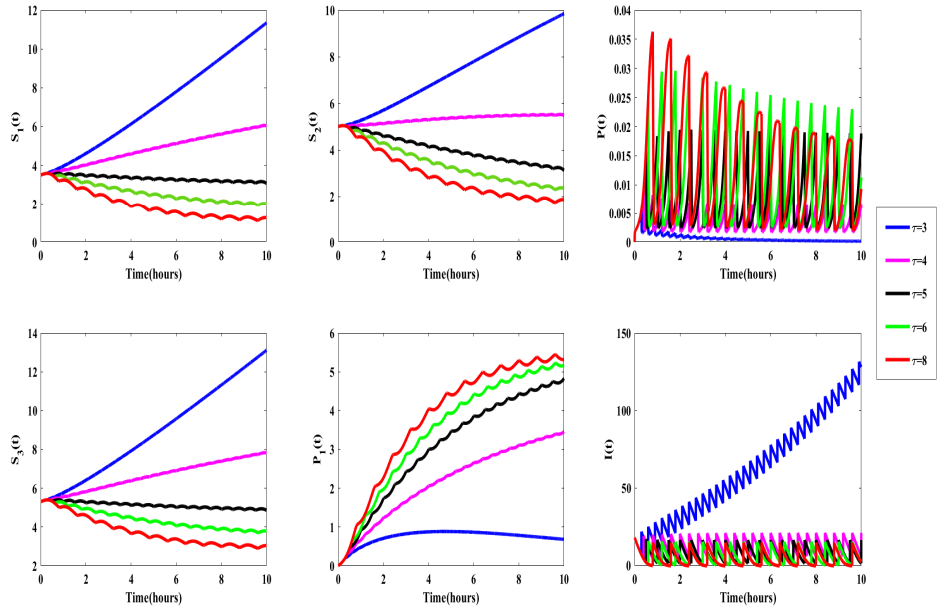


Figure 3.9: Concentration-time curves of the components of model (3.2.5) for the impulsive dosing of dual inhibitor of HIV-1 RT/IN with the initial conditions $[S_1, S_2, S_3, E_1, E_2, I_0](0) = [3.5, 5, 5.3, 3, 1.8, 18]\mu M$, impulse dose input $I_c = 15\mu M$ and the time interval of dosing $\tau = 3$ hr. We have taken the parameter values from Table 3.1.

In figures 3.9, we fix the initial value of the dual inhibitor $(I)$ of HIV-1 RT/IN to $18\mu M$ as well as the impulse dose $I_c$ to $15\mu M$ and vary the dosing interval $\tau$ (= 3 hr, 4 hr, 5 hr, 6 hr, 8 hr respectively) to observe the change in nature of the reactants' progress curves in each respective curves. It is worth noting that the figure 3.9 follows a reverse order in illustrating the nature of the curves of the components as in figure 3.8, i.e, the curves of the figures representing $\tau$ (= 3 hr, 4 hr, 5 hr, 6 hr, 8 hr respectively) follow the patterns of the curves of figures representing $(I_c, I_0) = (35\mu M, 40\mu M)$ - $(I_c, I_0) = (5\mu M, 10\mu M)$ respectively. Hence, a detailed description is not needed here.

In figure 3.10, we compare the progress curves of the components viral double-stranded DNA $(P)$ and integrated proviral DNA $(P_1)$ in absence of dual inhibitor

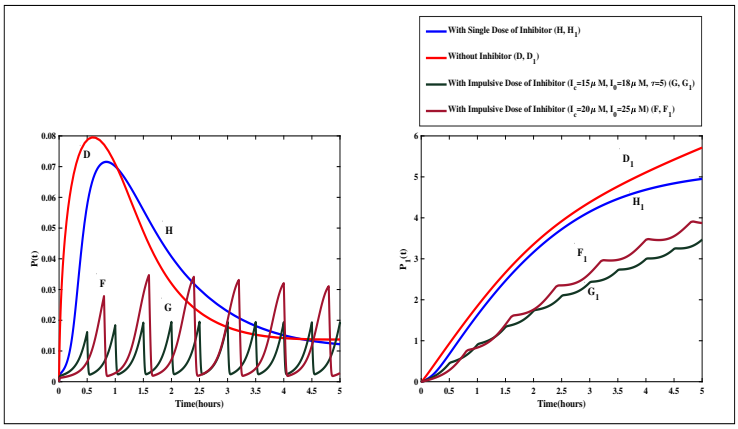


Figure 3.10: Variations of the curves for viral double-stranded DNA concentration and integrated proviral DNA concentration in a different situation (without HIV-1 RT/IN dual inhibitor, in the presence of HIV-1 RT/IN dual inhibitor with a single dose and with multiple doses in an impulsive way) are seen in this figure using the initial conditions and parameter values same as in Fig. 3.9.

$(I)$ of HIV-1 RT/IN, in presence of dual inhibitor $(I)$ of HIV-1 RT/IN with a single dose and in presence of dual inhibitor $(I)$ of HIV-1 RT/IN with multiple doses in impulsive way (taking the values for $(I_c, I_0) = (20\mu M, 25\mu M)$ in Fig. 3.8 and $(I_c, I_0, \tau) = (15\mu M, 18\mu M, 5hr)$ in Fig. 3.9 respectively). Here we omit the curves of other components (viral single-stranded RNA $(S_1)$, dNTPs $(S_2)$, host DNA $(S_3)$, dual inhibitor $(I)$ of HIV-1 RT/IN) to observe the changes in nature of the progress curves of viral double-stranded DNA $(P)$ and integrated proviral DNA $(P_1)$ explicitly. We can see that the concentration of viral double-stranded DNA $(P)$ in the presence of the inhibitor $(I)$ with a single dose remains lower than the concentration without inhibitor $(I)$. Furthermore, for impulsive dosing the formation of viral double-stranded DNA $(P)$ decreases rapidly as compared to the other two. A similar thing happens for the curves representing the integrated proviral DNA $(P_1)$ concentration. Here, we take two different impulse doses of the dual inhibitor $(I)$ of HIV-1 RT/IN as well as two different dosing intervals to perform the impulse. Curve $F$ and curve $F_1$ represent the nature change in the concentrations of viral double-stranded DNA $(P)$ and integrated proviral DNA $(P_1)$ respectively in the presence of the inhibitor $(I)$ with the impulse dose $20\mu M$ and the time interval of dosing is 8 hr; whereas, curves $G$ and $G_1$ illustrate the same

thing for the impulse drug dose $15\mu M$ and the dosing interval, in this case, is 5 hr. It is noticeable in Fig. 3.10 that the peak point of the progress curve (represented by the curve $G$) of $P$ stays quite below the curve $F$ and creates a favourable condition for considering the impulse drug dose $15\mu M$ while the dosing interval is $\tau = 5hr$. We can see similar pattern in the progress curves of $P_1$ illustrated by $F_1$ and $G_1$ respectively. Therefore, from this figure, we can conclude that for the impulse dose ($I_c = 15\mu M$) of HIV-1 RT/IN dual inhibitor, dosing interval $\tau = 5hr$ is more appreciable for HIV-1 infected patients.

### 3.4.1 Comparison of the present work with existing studies

In the existing literature, although there exist a handful of mathematical models describing the dynamics of viral replication during HIV-1 infection supplemented by various treatment strategies and the effects of different drug therapies as well (Lakshmikantham and Simeonov, 1989; Majumder et al., 2022; Pal and Mitra, 2006; Perelson, 2002; Smith, 2006), none of them has extensively addressed the HIV-1 reverse transcription and integration process through enzyme kinetic reaction. Here we compare the proposed methods and results with state-of-art in detail: ($a$) The aforementioned mathematical models described the "within-host population" dynamics of HIV-1, while in this research, we consider the "within-infected-cell" replication of HIV-1. ($b$) In 2023, S. Pal (Pal and Mitra, 2006) introduced an awareness-induced transmission function associated with nonlinear infection rate in their mathematical model; whereas, in the present work, we formulate a mathematical model on the HIV-1 Reverse Transcriptase (RT) and Integrase (IN) catalyzed biochemical reaction with the understanding of Michaelis-Menten enzyme kinetic reaction. ($c$) The present chapter introduces an impulsive differential equation framework for calculating an effective dosing regimen for applying the dual inhibitors of HIV-1 RT/IN, while in the existing studies (De and Camarasa, 2018; Gu et al., 2016), theoretical works describing the efficacy of HIV-1 RT/IN dual inhibitors in combating HIV-1 infection have been performed. ($d$) In order to obtain the closed-form solution of the proposed impulsive differential equation model, We introduce the Lambert W function and obtained an effective dosing regimen

for applying the dual inhibitor of HIV-1 RT/IN; whereas, an optimal control model was employed by S. Mondal (Mondal et al., 2023) to find the strategy of applying treatment considering spontaneous response of people towards HIV-1 infection . These four facets of the work undertaken lead to the novelty of the present article.

## 3.5 Conclusion

In this chapter, we formulated a mathematical model on the HIV-1 RT and IN catalyzed biochemical reaction for HIV-1 replication and studied the effectiveness of dual inhibitor of HIV-1 RT and IN which simultaneously works as a NNRTI and IN inhibitor to combat HIV-1 infection. At first, we analyzed the model introducing dual inhibitor of HIV-1 RT/IN with a single dose and analytically it is shown that the solutions of the model are bounded and non-negative. Moreover, the local stability of the interior equilibrium point of the model is also established. Furthermore, we incorporated a one-dimensional impulsive differential equation to model the drug dynamics for multiple dose administration. By using the Lambert W function, we explicitly expressed the closed-form solution of the impulsive differential equation model and obtained the existence condition ($\frac{I_c}{\tau} < n(K_{i1}{}')^n k_3 E_{10} + K_{i2} k_7 E_{20}$) for the periodic solution. It is shown that in order to design a periodic dosing regimen, one large initial dose $I^*$ should be applied followed by a smaller dose $I_c$ in each dosing interval $\tau$. Our numerical findings also justify the analytical results.

A noticeable observation from numerical discussion is that impulse dose $5\mu M$ as well as $15\mu M$ is not sufficient to suppress the viral load for a large time interval 8 hr (see Fig. 3.8 (blue curve), Fig. 3.9 (red curve)); whereas, dosing amount $30\mu M$ and $35\mu M$ may exceed the human body tolerance level for the same dosing period $\tau$ which is identified in Fig. 3.8 (green curve & red curve respectively). Similarly, we observe from figure 3.9 that for a shorter dosing interval like 3 hr (blue curve) or 4 hr (purple curve), $15\mu M$ dose can overpower the entire system which is also not safe for a human body; whereas, the curves representing $(I_c, I_0) = (20\mu M, 25\mu M)$ in Fig. 3.8 and $(I_c, I_0, \tau) = (15\mu M, 18\mu M, 5hr)$ in Fig. 3.9 provide a satisfactory visualization

towards obtaining a safe and effective dosing regimen for HIV-1 infected individuals. These results imply that for a longer time interval $\tau$, a larger dose is required to maintain a therapeutic effect which is also confirmed in Fig. 3.7. Moreover, as small as the dose $I_c$ is, less time is required to approach the steady state for a given dosing interval $\tau$ (Fig. 3.7).

The main focus of the present research is on determining the completely analytical solutions for a two-compartment model exhibiting nonlinear Michaelis-Menten elimination kinetics and to provide a basic idea on obtaining an effective dosing regimen for applying dual inhibitor of HIV-1 RT/IN to treating HIV-1 infection. It is anticipated that the conducted study and the advocated mathematical model would guide toward expanding the treatment options to HIV-1 infected patients belonging to the complex HAART therapy.

Although the present chapter steps into expanding the treatment options to HIV-1 infected patients and determines an effective dosing regimen for applying the dual inhibitor of HIV-1 RT/IN, it has several limitations: (*i*) The interior equilibrium point of the model (3.2.5) is difficult to obtain analytically due to the non-linearity of the model (3.2.5). Therefore, existence of the interior equilibrium point is shown numerically. (*ii*) To obtain the explicit expression for the inhibitor $I$, we had to determine the analytical solutions for $I_1$ and $I_2$ individually due to the difficulty of the system (3.3.1). (*iii*) Although by using the Lambert W function, we are able to obtain the closed-form solution of the impulsive differential equation model, we couldn't determine the maximum time interval between two consecutive drug doses. We hope that we would be able to bridging the aforementioned limitations in our future work.

# Chapter 4

# Mathematical modelling of HIV-1 transcription inhibition: a comparative study between optimal control and impulsive approach

## 4.1 Introduction

Undoubtedly, the persistence of infection stemming from Human Immunodeficiency Virus type-1 (HIV-1) stands as an established and substantive concern within the global landscape of morbidity and mortality. Statistical evidence underscores this issue, with an estimated 38 million individuals currently afflicted by HIV-1 infection. Notably, within the year 2021 alone, there were 1.5 million newly recorded cases of HIV-1 infection, as documented in the UNAIDS Global AIDS Update of 2022. The emergence of these new cases of infection presents a palpable and substantial threat to worldwide public health. Thus, it becomes imperative to allocate significant intellectual resources toward the comprehensive understanding and resolution of this issue. A thorough grasp of the intricate biological, physical, and chemical

underpinnings of the phenomenon becomes a paramount requirement in the pursuit of mitigating HIV-1's impact. While the infection dynamics of HIV-1 are multifaceted and intricate, a simplified framework suggests that the infection's consequence involves the progressive depletion of $CD4^{+}T$ lymphocytes. This well-coordinated depletion precipitates a state of immunodeficiency, culminating in the eventual manifestation of the chronic malady recognized as Acquired Immunodeficiency Syndrome (AIDS). In this context, apprehending the orchestrated sequence of events at the molecular, cellular, and immunological levels is of profound significance for devising effective strategies against HIV-1 infection.

Prior to delving into the intricate realm of relevant mathematical models and their associated computational intricacies, it is imperative to establish a simplified conceptual framework elucidating the underlying biochemical intricacies organizing viral replication. Viral initiation hinges upon the binding interaction between the envelope glycoprotein and the CD4 receptor, concomitant with a co-receptor interaction on the surface of immune cells. This binding event culminates in the fusion of the cellular and viral membranes, resulting in the merger of the host cell and virion (Das and Arnold, 2013; Friedrich et al., 2011; Sarafianos et al., 2009). This membrane fusion event facilitates the intrusion of HIV-1 into the host cell, subsequently instigating the uncoating of the viral core. Within this core lie pivotal components, including the viral single-stranded RNA genome, reverse transcriptase (RT), integrase (IN), and various other virion components (Das and Arnold, 2013; Friedrich et al., 2011). The ensuing steps involve the reverse transcriptase enzyme (RT) transcribing the viral single-stranded RNA genome into a more stable double-stranded DNA configuration. This double-stranded DNA molecule is subsequently transported to the host cell nucleus, where the enzyme integrase (IN) orchestrates its integration into the host cell's chromosomal DNA (Engelman et al., 1991; Sarafianos et al., 2009). This integration into the host DNA prompts the commencement of the transcription process, where the integrated pro-viral DNA is transcribed into full-length messenger RNA (mRNA) under the catalytic auspices of the host enzyme RNA polymerase II (Pol II) (Likhoshvai et al, 2014; Ott et al., 2011). However, despite the successful

initiation of transcription and the formation of the elongation complex by the host Pol II enzyme, the process encounters eventual termination, culminating in the cessation of RNA Pol II activity (Likhoshvai et al, 2014; Ott et al., 2011). Subsequent to this stage, the transcriptional elongation process is meticulously regulated by an essential auxiliary protein known as the transcriptional trans-activator Tat. Moving forward, an intricate sequence of events involving the formation of intermediate complexes culminates in the maturation of a 9kb messenger RNA (mRNA) species within the host cell nucleus. This mature mRNA is either transported intact to the cytoplasm or undergoes splicing prior to cytoplasmic transport, in accordance with (Likhoshvai et al, 2014; Reddy and Yin, 1999). As the HIV-1 life cycle progresses, the latter stages involve cytoplasmic translation of the synthesized mRNAs, yielding specific proteins that ultimately undergo various modifications. These modified proteins collectively contribute to the assembly and maturation of new virions, thereby completing the viral life cycle.

The current endeavour involves a thorough exploration aimed at identifying potential solutions for promoting compliance among AIDS patients. While available medications don't offer a permanent eradication of HIV-1 infection, they do hold the capacity to significantly suppress the viral load to an undetectable level. This suppression notably decreases mortality rates and the probability of secondary infections emerging. However, it's important to note that HIV still remains latent within integrated proviruses within $CD4^{+}T$ cells, necessitating indefinite continuation of antiretroviral therapy (ART) (Mousseau et al., 2015). Discontinuation of treatment could trigger the activation of latent proviruses, resulting in swift viral replication and severe compromise of the immune system (Arlen et al., 2006; Mousseau et al., 2015). Given that existing anti-HIV drugs don't impede the transcription process, efforts should be directed towards permanent inhibition of this process. Multiple strategies have been employed to target the Tat/TAR interaction with the goal of controlling HIV-1 transcription (Cecchetti et al., 2000; Mousseau et al., 2012, 2015; Wan and Chen, 2014). Contemporary clinical investigations have demonstrated the potential effectiveness of combining transcription inhibitors with antiretroviral

drugs (ARVs) to manage HIV-1 replication (Mousseau et al., 2012, 2015). Studies indicate that employing Tat inhibitors for treating HIV-1 infection leads to a reduction in messenger RNA (mRNA) synthesis, thereby curbing viral replication. Despite substantial clinical and experimental studies on the efficacy of transcription inhibitors, a comprehensive exploration through mathematical modelling remains relatively limited. Addressing this gap, the current focus lies in constructing a mathematical model that encompasses the entire system's mechanics. This proposed model is anticipated to serve as a fundamental framework not only for enhancing comprehension of infection transmission dynamics but also for furnishing strategic guidelines to effectively manage the infection. This marks the innovative essence of the undertaken study.

Several mathematical models have been established to elucidate the intricate dynamics of viral replication during HIV-1 infection (Covert and Kirschner, 2000; Nowak and May, 2000; Perelson, 2002). These models have been supplemented with diverse treatment strategies, encompassing the effects of various drug therapies (Nowak and May, 2000; Perelson, 2002; Wahl and Nowak, 2000). The ramifications of impeccable adherence to antiretroviral therapy have been explored through impulsive differential equations (Lou and Smith, 2011; Smith, 2006). By employing this method, precise estimations of dosing intervals and threshold dosage values can be obtained. Likhoshval et al. (Likhoshvai et al, 2014) undertook a mathematical scrutiny of Tat's regulatory influence on HIV-1 replication, specifically investigating the potential existence of oscillatory patterns within the viral dynamics. Furthermore, numerous theoretical investigations have affirmed the inhibitory impact of Tat inhibitors on HIV-1 transcription, highlighting their ability to curtail mRNA production (Cecchetti et al., 2000; Mousseau et al., 2012, 2015; Wan and Chen, 2014). The present study involves the formulation of an enzyme kinetics model to scrutinize the influence of viral Tat protein on the synthesis of mRNA derived from integrated pro-viral DNA. Leveraging an optimal control approach, the Pontryagin minimum principle is applied to ascertain the optimal drug conditions for HIV-1 treatment (Kirschneret al., 1997). In this context, the drug of interest, namely the Tat inhibitor, functions as the control variable within the model. To determine an effective dosing regimen for the Tat inhibitor, impulsive differential

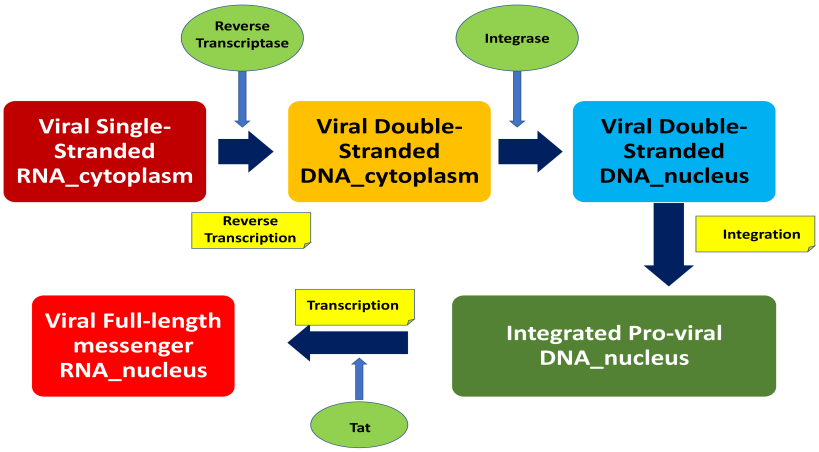


Figure 4.1: A schematic representation of HIV-1 life-cycle.

equations are employed (Lakshmikantham and Simeonov, 1989; Smith?, 2008), incorporating the therapeutic efficacy of the Tat inhibitor on Tat/TAR interactions. Moreover, this study seeks to investigate the impact of the Tat inhibitor both under continuous and impulsive administration modes, aiming to compare the outcomes of these two strategies. The anticipated results from this model system are expected to provide insights beneficial to both theoretical model developers and clinical practitioners alike.

## 4.2 The ODE Model

In this section of the **chapter (4)**, a comprehensive mathematical model is constructed, encapsulating the intricate biochemical interactions involving the host enzyme RNA polymerase II, the Trans Activation Response (TAR) element located on the HIV-1 pro-viral DNA promoter region, and the Tat protein. Within this framework, one may denote the concentrations of the host enzyme RNA polymerase II and the TAR element as $E$ and $S$, respectively. At the outset of HIV-1 transcription, the enzyme RNA polymerase II ($E$) initiates binding with the TAR element on the HIV-1 LTR promoter region. This interaction yields an RNA polymerase II-HIV-1 pro-viral DNA LTR promoter complex ($ES$), which subsequently gives rise to the TAR-RNA polymerase II_

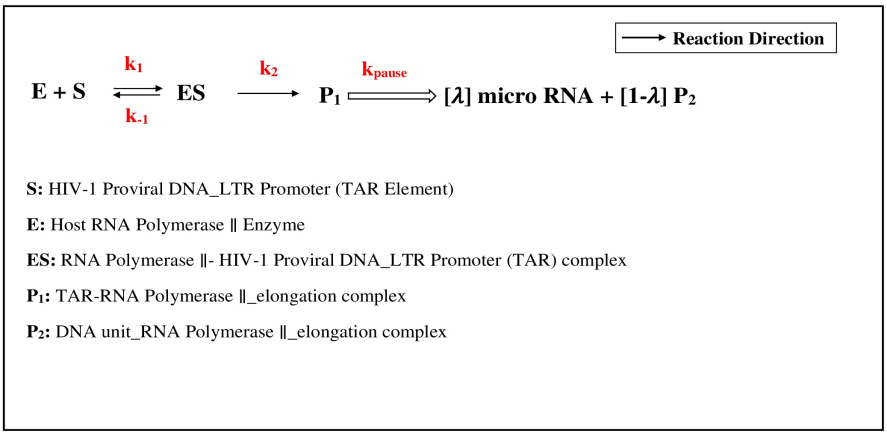


Figure 4.2: The schematic diagram of the enzymatic reactions.

elongation complex ($P_1$). The associated forward and backward rate constants for this process are denoted as $k_1$, $k_2$, and $k_{-1}$, respectively. During this sequence of events, the activity of RNA polymerase II ($E$) briefly pauses, culminating in the termination of the enzyme. It is postulated that, with a probability labelled as $\lambda$, RNA polymerase II ($E$) undergoes termination, leading to the formation of micro RNA. Conversely, the complementary probability $(1 - \lambda)$ accounts for the production of a DNA unit that comprises the RNA polymerase II_ elongation complex ($P_2$). The rate constant governing the resumption of RNA polymerase II activity after the pause is represented as $k_{pause}$. The intricacies elucidated above find visual representation in schematic diagram 4.2, effectively encapsulating the molecular interactions and transitions inherent in this process.

Furthermore, the process of HIV-1 transcription elongation is facilitated by the viral protein Tat ($T$), which engages in the activation of this transcriptional phase. Initially, Tat ($T$) attaches to TAR located at the TAR-RNA polymerase II_ elongation site ($P_1$), leading to the formation of the Tat-TAR complex ($TP_1$). This complex subsequently undergoes conversion into the DNA unit RNA polymerase II_ elongation complex ($P_2$). The reaction dynamics are characterized by forward and backward rate constants, denoted as $k_3$, $k_4$, and $k_{-3}$ respectively. Within the elongation complex $P_2$, there is a continuous formation of immature 9kb RNA ($P_3$) at a steady rate of $k_5$, concurrent with the release of enzyme RNA polymerase II ($E$). Ultimately, the immature 9kb RNA ($P_3$) undergoes a transformation into mature 9kb messenger RNA ($P_4$) within the nucleus of

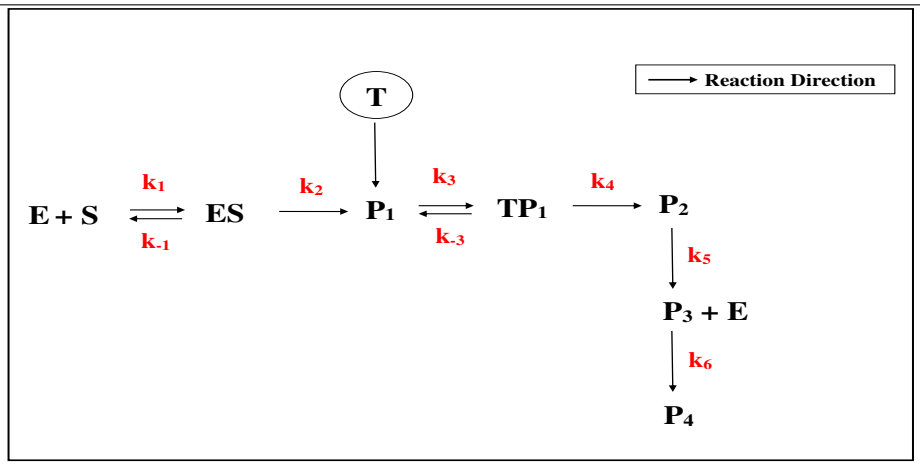


Figure 4.3: The schematic diagram of Tat-mediated reactions.

the host cell, facilitated by the rate constant $k_6$. The accompanying schematic diagram, depicted in Figure 4.3, serves to illustrate the process of Tat-mediated transcription.

Moreover, in accordance with the principles of the Law of Mass Action, the system of nonlinear differential equations that delineates the enzymatic reactions detailed above can be articulated as follows:

$$\begin{aligned}
\frac{dS}{dt} &= \alpha_1 - k_1.E.S + k_{-1}.ES - \beta_1 S, \\
\frac{dE}{dt} &= -k_1.E.S + k_{-1}.ES + k_5.P_2 - \beta_2 E, \\
\frac{dES}{dt} &= k_1.E.S - k_{-1}.ES - k_2.ES, \\
\frac{dP_1}{dt} &= k_2.ES - k_3.T.P_1 + k_{-3}.TP_1 - \beta_3 P_1, \\
\frac{dTP_1}{dt} &= k_3.P_1.T - k_{-3}.TP_1 - k_4.TP_1, \\
\frac{dT}{dt} &= \alpha_2 - k_3.T.P_1 + k_{-3}.TP_1 - \beta_4 T, \\
\frac{dP_2}{dt} &= k_4.TP_1 - k_5.P_2 - \beta_5 P_2, \\
\frac{dP_3}{dt} &= k_5.P_2 - k_6.P_3 - \beta_6 P_3, \\
\frac{dP_4}{dt} &= k_6.P_3 - \beta_7 P_4.
\end{aligned} \tag{4.2.1}$$

where $\alpha_i$, $i = \{1, 2\}$ are the respective rates of the external source of $S$, synthesis of $T$ while $\beta_j$, $j = \{1, 2, ..., 7\}$ are the natural degradation rates of $S, E, P_1, T, P_2, P_3$ and $P_4$ respectively.

The above system (4.2.1) involves several time scales. The binding and unbinding of the viral protein Tat to TAR-RNA polymerase II_elongation complex can occur on

a time scale of seconds, whereas the synthesis of messenger RNA lasts over a period of several minutes (Gonze and Kaufman, 2016). With the aim of simplifying the presently formulated model system, one may use quasi-steady-state approximations (QSSA) for the concentration of substrate-catalyst complexes (Briggs and Haldane, 1925; Segel, 1975). Under this assumption, denoting $P_{1_{Tot}} = P_1 + TP_1$, one may get the following relations from system (4.2.1):

$$ES = \frac{E.S}{K_M}, \text{ and } TP_1 = \frac{T.P_{1_{Tot}}}{K_3 + T},$$

where $K_M = \frac{k_{-1}+k_2}{k_1}, K_3 = \frac{k_{-3}}{k_3}$. Substituting the expressions for $ES$ and $TP_1$ into (4.2.1), one may obtain the following seven-dimensional compartmental model:

$$\begin{aligned}
\frac{dS}{dt} &= \alpha_1 - k_2\frac{E.S}{K_M} - \beta_1 S, \\
\frac{dE}{dt} &= -k_2\frac{E.S}{K_M} + k_5 P_2 - \beta_2 E, \\
\frac{dP_1}{dt} &= k_2\frac{E.S}{K_M} - \beta_3 P_1, \\
\frac{dT}{dt} &= \alpha_2 - \beta_4 T, \\
\frac{dP_2}{dt} &= k_4\frac{P_{1_{Tot}}.T}{K_3+T} - k_5 P_2 - \beta_5 P_2, \\
\frac{dP_3}{dt} &= k_5 P_2 - k_6 P_3 - \beta_6 P_3, \\
\frac{dP_4}{dt} &= k_6 P_3 - \beta_7 P_4,
\end{aligned} \tag{4.2.2}$$

with the initial conditions $S(0) = S_0$, $E(0) = E_0$, $P_1(0) = P_{10}$, $T(0) = T_0$, $P_2(0) = 0$, $P_3(0) = 0$, and $P_4(0) = 0$.

### Non-negativity and Boundedness

In this section, the non-negativity and boundedness of the solutions of the system (4.2.2) are studied using the following theorem.

**Theorem 4.2.1** *Each solution of the system* (4.2.2) *with initial conditions, remains non-negative for all* $t \geqslant 0$ *and uniformly bounded in the region* $\Gamma$*, where,* $\Gamma = \Big\{\big(S, E, P_1, T, P_2, P_3, P_4\big) \in \mathbb{R}^7_+ \mid 0 < S(t) \leq \frac{\alpha_1}{\beta_1}, 0 < E(t) \leq \frac{M_2}{\beta_2}, 0 < P_1(t) \leq \frac{\alpha_1 k_2 M_2}{\beta_1\beta_2\beta_3 K_M}, 0 < T(t) \leq \frac{\alpha_2}{\beta_4}, 0 \leq P_2(t) \leq \frac{M_1}{k_5+\beta_5}, 0 \leq P_3(t) \leq \frac{k_5 M_1}{(k_5+\beta_5)(k_6+\beta_6)}, 0 \leq P_4(t) \leq \frac{k_5 k_6 M_1}{\beta_7(k_5+\beta_5)(k_6+\beta_6)}\Big\}$.

**Proof.** First one can show that $S(t)$ is positive for all $t \geq 0$. If not, one may assume that $t_0$ is the first time when $S(t_0) = 0$. Now initially it is taken $S(t) > 0$ when $t = 0$. Therefore, $S(t) > 0$ for all $t \in [0, t_0)$. Substituting $t = t_0$ in the first equation of system (4.2.2), one gets

$$\frac{dS}{dt} = \alpha_1 - k_2 \frac{E(t_0)S(t_0)}{K_M} - \beta_1 S(t_0) = \alpha_1 > 0.$$

It means $S(t)$ is an increasing function at $t = t_0$. So, there exists an arbitrarily small $\epsilon > 0$ such that for all $t \in (t_0 - \epsilon, t_0) \subset [0, t_0)$, one should have $S(t) < 0$. This is a contradiction to the fact that $S(t) > 0, \forall t \in [0, t_0)$. Hence $S(t) > 0, \forall t \geqslant 0$. In a similar way, one may show that the components $E(t)$, $P_1(t)$, and $T(t)$ are positive for all $t \geq 0$. Again from the fifth equation of (4.2.2), one gets

$$\frac{dP_2}{dt} = k_4 \frac{P_{1_{Tot}}.T}{K_3 + T} - k_5 P_2 - \beta_5 P_2 > -(k_5 + \beta_5)P_2.$$

But the initial value of $P_2$ is zero. So, one can write,

$$\frac{dP_2}{dt} \geq 0 \implies P_2 \geq 0.$$

Similarly, one can show that $E(t)$, $P_3(t)$, $P_4(t) > 0, \forall t \geqslant 0$. Thus, the non-negativity of the solutions of the system (4.2.2) with the initial conditions is established.

Now one may show that $S(t)$, $E(t)$, $P_1(t)$, $T(t)$, $P_2(t)$, $P_3(t)$ and $P_4(t)$ are all bounded in their domains of definition. Taking first equation of (4.2.2), one gets

$$\frac{dS}{dt} = \alpha_1 - k_2 \frac{E.S}{K_M} - \beta_1 S \leq \alpha_1 - \beta_1 S.$$

The Gronwall Lemma guarantees that

$$S(t) \leq \frac{\alpha_1}{\beta_1}(1 - e^{-\beta_1 t}) + S_0 e^{-\beta_1 t}.$$

Thus, for sufficiently large $t$, one obtains

$$\limsup_{t \to +\infty} S(t) \leq \frac{\alpha_1}{\beta_1}.$$

Similarly, from fourth equation of (4.2.2), one can determine

$$\limsup_{t \to +\infty} T(t) = \frac{\alpha_2}{\beta_4}.$$

Now considering the fifth equation of (4.2.2) and using the maximum value of $T(t)$, one may get the following inequality:

$$\frac{dP_2}{dt} \leq M_1 - (k_5 + \beta_5)P_2.$$

Solving the above inequality for sufficiently large $t$, one can get the following result,

$$\limsup_{t\to+\infty} P_2(t) \leq \frac{M_1}{k_5+\beta_5}, \text{ where } M_1 = \frac{\alpha_2 k_4 P_{1_{Tot}}}{K_3\beta_4+\alpha_2}. \tag{4.2.3}$$

Now, from the second equation of system (4.2.2) and using the maximum value of $P_2$, the following inequality can be derived

$$\frac{dE}{dt} \leq M_2 - \beta_2 E.$$

Solving the above inequality for sufficiently large $t$, one may get

$$\limsup_{t\to+\infty} E(t) \leq \frac{M_2}{\beta_2}, \text{ where } M_2 = \frac{k_5 M_1}{k_5+\beta_5}.$$

Similarly substituting the maximum values of $E$ and $S$ in third equation of system (4.2.2), one can obtain the following result:

$$\limsup_{t\to+\infty} P_1(t) \leq \frac{\alpha_1 k_2 M_2}{\beta_1\beta_2\beta_3 K_M}.$$

Using a similar argument one may obtain the maximum values of $P_3$, $P_4$ as

$$\limsup_{t\to+\infty} P_3(t) \leq \frac{k_5 M_1}{(k_5+\beta_5)(k_6+\beta_6)}, \text{ and}$$

$$\limsup_{t\to+\infty} P_4(t) \leq \frac{k_5 k_6 M_1}{\beta_7(k_5+\beta_5)(k_6+\beta_6)}.$$

Therefore all solutions of the system (3.2.2) are bounded.

### 4.2.1 Equilibrium Analysis

The system (4.2.2) has a unique interior equilibrium $E_1^* = (S^*, E^*, P_1^*, T^*, P_2^*, P_3^*, P_4^*)$, which satisfies

$$\begin{aligned}
T^* &= \frac{\alpha_2}{\beta_4}, \\
P_2^* &= \frac{\alpha_2 k_4 P_{1_{Tot}}}{(K_3\beta_4+\alpha_2)(k_5+\beta_5)}, \\
P_3^* &= \frac{\alpha_2 k_4 k_5 P_{1_{Tot}}}{(K_3\beta_4+\alpha_2)(k_5+\beta_5)(k_6+\beta_6)}, \\
P_4^* &= \frac{\alpha_2 k_4 k_5 k_6 P_{1_{Tot}}}{\beta_7(K_3\beta_4+\alpha_2)(k_5+\beta_5)(k_6+\beta_6)}, \\
P_1^* &= \frac{\alpha_2 k_2 k_4 k_5 P_{1_{Tot}} S^*}{\beta_3(K_3\beta_4+\alpha_2)(k_5+\beta_5)(\beta_2 K_M+k_2 S^*)}, \\
E^* &= \frac{\alpha_2 k_4 k_5 P_{1_{Tot}} K_M}{(K_3\beta_4+\alpha_2)(k_5+\beta_5)(\beta_2 K_M+k_2 S^*)},
\end{aligned}$$

and $S^*$ satisfies the following quadratic equation:

$$\beta_1 Z k_2 S^{*2} + (\beta_1 Z \beta_2 K_M - \alpha_1 Z k_2 + \alpha_2 k_2 k_4 k_5 P_{1_{Tot}}) S^* - \alpha_1 Z \beta_2 K_M = 0,$$

where $Z = (K_3\beta_4 + \alpha_2)(k_5 + \beta_5)$. The above quadratic equation always has a unique positive real root.

The Jacobin matrix at the unique interior equilibrium $E_1^*$ is

$$J_{E_1^*} = \begin{bmatrix} -\frac{k_2 E^*}{K_M} - \beta_1 & -\frac{k_2 S^*}{K_M} & 0 & 0 & 0 & 0 & 0 \\ -\frac{k_2 E^*}{K_M} & -\frac{k_2 S^*}{K_M} - \beta_2 & 0 & 0 & k_5 & 0 & 0 \\ \frac{k_2 E^*}{K_M} & \frac{k_2 S^*}{K_M} & -\beta_3 & 0 & 0 & 0 & 0 \\ 0 & 0 & 0 & -\beta_4 & 0 & 0 & 0 \\ 0 & 0 & 0 & \frac{k_4 P_{1_{Tot}} K_3}{(K_3+T^*)^2} & -k_5 - \beta_5 & 0 & 0 \\ 0 & 0 & 0 & 0 & k_5 & -k_6 - \beta_6 & 0 \\ 0 & 0 & 0 & 0 & 0 & k_6 & -\beta_7 \end{bmatrix}.$$

Now the characteristic equation at the interior equilibrium point $E_1^*$ is of the following form:

$$(k_5 + \beta_5 + x)(k_6 + \beta_6 + x)(\beta_3 + x)(\beta_4 + x)(-\beta_7 - x)(x^2 + A_1 x + A_2) = 0,$$

where, $A_1 = \left(\beta_1 + \beta_2 + \frac{k_2 S^*}{K_M} + \frac{k_2 E^*}{K_M}\right)$ and $A_2 = \left(\frac{k_2 S^*}{K_M}\beta_1 + \frac{k_2 E^*}{K_M}\beta_2 + \beta_1\beta_2\right)$.

All seven eigenvalues are always negative. Therefore the interior equilibrium $E_1^*$ is locally asymptotically stable.

## 4.3 Optimal Control: Theoretic Approach

Optimal control is a well-established mathematical tool that deals with systems that can be controlled. By optimizing a particular performance, one may usually solve these types of problems by finding the time-dependent values of the control parameters (Fleming and Rishel, 1975; Grigorieva et al., 2013, 2014). In the formulated ODE model (4.2.2), it is described that the viral protein Tat ($T$) plays a dominating role in HIV-1 transcription by making Tat-TAR complex ($TP_1$) which yields an elongating complex ($P_2$) that finally transforms into messenger RNA ($P_4$). Hence, to control the

transcription process, one needs to minimize the production of messenger RNA ($P_4$), and therefore, it is required to suppress the biochemical reaction between the viral protein Tat ($T$) and the TAR ($P_1$) element. In this section, the formulated model is analyzed with an additional control parameter, denoted by $u(t)$ which is the effect of Tat inhibitor. Treatment with Tat inhibitor has a significant effect on disrupting the Tat/TAR interaction by directly binding to Tat and hence reduces the production of the elongation complex ($P_2$). Therefore, the Tat inhibitor indirectly helps to suppress the formation of messenger RNA ($P_4$). Thus the same control profile $u(t)$ is considered with the messenger RNA synthesis term. One may consider the set $\Omega$ of admissible controls consists of all Lebesgue measurable functions $u(t)$, which for almost all values of $t$ from the fixed time interval $[t_0, t_f]$ satisfy the following inequality:

$$0 \leq u(t) \leq 1.$$

For the set $\Omega$, the objective function is defined as

$$J(u) = \int_{t_0}^{t_f} \left[Au^2(t) + B{P_4}^2(t)\right] dt. \tag{4.3.1}$$

The objective function (4.3.1) expresses the present goal to minimize the cost for Tat inhibitor while minimizing the messenger RNA ($P_4$). The parameter $A$ represents a weight constant related to the cost associated with Tat inhibitor treatment, while $B$ is the penalty multiplier. Therefore, for (4.3.1) one may seek an optimal control $u^*$ such that

$$\min_{u(.)\in\Omega} J(u) = J(u^*). \tag{4.3.2}$$

Taking into account the above assumptions, one can consider a control problem (4.3.2) together with the mathematical model (4.2.2) such that:

$$\begin{array}{rcl}
\frac{dS}{dt} &=& \alpha_1 - k_2\frac{E.S}{K_M} - \beta_1 S, \\
\frac{dE}{dt} &=& -k_2\frac{E.S}{K_M} + k_5 P_2 - \beta_2 E, \\
\frac{dP_1}{dt} &=& k_2\frac{E.S}{K_M} - \beta_3 P_1, \\
\frac{dT}{dt} &=& \alpha_2 - \beta_4 T, \\
\frac{dP_2}{dt} &=& k_4(1-u)\frac{P_{1_{Tot}}.T}{K_3+T} - k_5 P_2 - \beta_5 P_2, \\
\frac{dP_3}{dt} &=& k_5 P_2 - k_6 P_3 - \beta_6 P_3, \\
\frac{dP_4}{dt} &=& k_6(1-u)P_3 - \beta_7 P_4,
\end{array} \tag{4.3.3}$$

with known initial values for $S(t)$, $E(t)$, $P_1(t)$, $T(t)$, $P_2(t)$, $P_3(t)$ and $P_4(t)$ at $t_0$.

Here Pontryagin Minimum Principle (Bonnans and Hermant, 2009; Pontryagin, 1987) is used to obtain $u^*(t)$. One can construct a control Hamiltonian function $H(.,.,.)$ by adjoining the state equation to the integrand $L$ using the Lagrange multipliers, $\lambda(t)$, as follows:

$$H(x(t), u(t), \lambda(t)) = L(x(t), u(t)) + \lambda^T(t) f(x(t), u(t)), \tag{4.3.4}$$

where $u(t)$ is the optimal control and $x(t)$ is the corresponding optimal state. By the Pontryagin Minimum Principle (Krik, 2004; Lee and Markus, 1967; Lenhart and Workman, 2007) it is known that there exists a continuous function $\lambda$ such that:

$$\dot{\lambda}(t) = -\Big(\frac{\partial H(x, u, \lambda)}{\partial x}\Big)^T, \tag{4.3.5}$$

along with the proper initial (or final) condition of $\lambda$. The above equation (4.3.5) is called the adjoint or costate equation and the function $\lambda$ is known as an adjoint function. According to the Pontryagin Minimum Principle, the optimal control $u(t)$ and the corresponding optimal state $x(t)$ and adjoint function $\lambda(t)$ must minimize the Hamiltonian so that

$$H(x(t), u(t), \lambda(t)) \leq H(x(t), u^*(t), \lambda(t)), \tag{4.3.6}$$

for all admissible trajectory control variables $u^*(t)$, satisfying the adjoint equation (4.3.5). Taking account of the above considerations, the necessary condition for optimality can now be defined. For an admissible control trajectory that satisfies the minimum principle, condition (4.3.6) implies that the Hamiltonian $H$ is minimum at the optimal control $u(t)$, so that

$$H_u(x(t), u(t), \lambda(t)) = 0. \tag{4.3.7}$$

The condition (4.3.7) is known as the first-order necessary condition for optimality. For the present optimal control system, the Hamiltonian is defined as (following equation (4.3.4) where integrand $L$ is given by equation (4.3.1) and the state equation is

represented by the model (4.3.3)) :

$$\begin{aligned} H &= Au^2 + B{P_4}^2 + \xi_1\Big(\alpha_1 - \tfrac{k_2E.S}{K_M} - \beta_1 S\Big) + \xi_2\Big( - \tfrac{k_2E.S}{K_M} + k_5P_2 - \beta_2 E\Big) \\ &\quad +\xi_3\Big(\tfrac{k_2E.S}{K_M} - \beta_3 P_1\Big) + \xi_4\Big(\alpha_2 - \beta_4 T\Big) \\ &\quad +\xi_5\Big(k_4(1-u)\tfrac{P_{1_{Tot}}T}{K_3+T} - k_5P_2 - \beta_5P_2\Big) + \xi_6\Big(k_5P_2 - (k_6+\beta_6)P_3\Big) \\ &\quad +\xi_7\Big(k_6(1-u)P_3 - \beta_7P_4\Big), \end{aligned} \tag{4.3.8}$$

where $\xi_1, \xi_2, ..., \xi_7$ are Lagrange multipliers. According to the Pontryagin minimum principle and the necessary optimality conditions for the present optimal control problem, one may obtain the following theorem:

**Theorem 4.3.1** *If the objective cost function $J(u)$ obtains its minimum for the optimal control $u^*$, and $(S^*, E^*, P_1^*, T^*, P_2^*, P_3^*, P_4^*)$ be the corresponding optimal state, then there exist adjoint functions $\xi_1$, $\xi_2$, $\xi_3$, $\xi_4$, $\xi_5$, $\xi_6$, $\xi_7$ satisfying the following equations:*

$$\begin{aligned} \tfrac{d\xi_1}{dt} &= \xi_1\Big(\tfrac{k_2E}{K_M} + \beta_1\Big) + \xi_2\tfrac{k_2E}{K_M} - \xi_3\tfrac{k_2E}{K_M}, \\ \tfrac{d\xi_2}{dt} &= \xi_1\tfrac{k_2S}{K_M} + \xi_2\Big(\tfrac{k_2S}{K_M} + \beta_2\Big) - \xi_3\tfrac{k_2S}{K_M}, \\ \tfrac{d\xi_3}{dt} &= \xi_3\beta_3, \\ \tfrac{d\xi_4}{dt} &= \xi_4\beta_4 - \xi_5\tfrac{K_3k_4(1-u)P_{1_{Tot}}}{(K_3+T)^2}, \\ \tfrac{d\xi_5}{dt} &= -\xi_2k_5 + \xi_5(k_5+\beta_5) - \xi_6k_5, \\ \tfrac{d\xi_6}{dt} &= \xi_6(k_6+\beta_6) - \xi_7k_6(1-u), \\ \tfrac{d\xi_7}{dt} &= \xi_7\beta_7 - 2BP_4, \end{aligned}$$

*with the transversality conditions $\xi_i(t_f) = 0$, for $i = \{1, ..., 7\}$. Moreover, the optimal control is given by*

$$u^*(t) = \max\left\{0, \min\left\{1, \frac{\xi_5k_4P_{1_{Tot}}T^* + \xi_7k_6{P_3}^*(K_3+T^*)}{2A(K_3+T^*)}\right\}\right\}.$$

**Proof.** The Pontryagin Minimum Principle affirms that the solution to the optimal control problem satisfies the adjoint equations

$$\frac{d\xi_1}{dt} = -\frac{\partial H}{\partial S}, \frac{d\xi_2}{dt} = -\frac{\partial H}{\partial E}, \frac{d\xi_3}{dt} = -\frac{\partial H}{\partial P_1}, \frac{d\xi_4}{dt} = -\frac{\partial H}{\partial T},$$
$$\frac{d\xi_5}{dt} = -\frac{\partial H}{\partial P_2}, \frac{d\xi_6}{dt} = -\frac{\partial H}{\partial P_3}, \frac{d\xi_7}{dt} = -\frac{\partial H}{\partial P_4},$$

and the transversality conditions $\xi_i(t_f) = 0$, for $i = \{1, ..., 7\}$.
Again, $H$ can be expressed as :

$$\begin{aligned} H &= Au^2 + \xi_5 \frac{k_4(1-u){P_1}_{Tot}T}{K_3+T} + \xi_7 k_6(1-u)P_3 + B{P_4}^2 \\ &+\xi_1\Big(\alpha_1 - \frac{k_2 E.S}{K_M} - \beta_1 S\Big) + \xi_2\Big(-\frac{k_2 E.S}{K_M} + k_5 P_2 - \beta_2 E\Big) \\ &+\xi_3\Big(\frac{k_2 E.S}{K_M} - \beta_3 P_1\Big) + \xi_4\Big(\alpha_2 - \beta_4 T\Big) - \xi_5\Big(k_5 + \beta_5\Big)P_2 \\ &+\xi_6\Big(k_5 P_2 - (k_6 + \beta_6)P_3\Big) - \xi_7\beta_7 P_4. \end{aligned}$$

Differentiating the above expression for $H$ with respect to $u$, one gets

$$\frac{\partial H}{\partial u} = 2Au - \xi_5 \frac{k_4 {P_1}_{Tot} T}{K_3+T} - \xi_7 k_6 P_3. \tag{4.3.9}$$

Now, according to the condition (4.3.7), the derivative of $H$ with respect to $u$ expressed by above equation (4.3.9) must be equal to zero at $u^*$. Hence, it follows

$$u^*(t) = \frac{\xi_5 k_4 {P_1}_{Tot} T^* + \xi_7 k_6 {P_3}^*(K_3 + T^*)}{2A(K_3 + T^*)}.$$

Due to the boundedness of the standard control, i.e., the fact that admissible control takes values such that $0 \leq u(t) \leq 1$, it follows from the minimality condition of Pontryagin's principle that

$$u^*(t) = \max\left\{0, \min\left\{1, \frac{\xi_5 k_4 {P_1}_{Tot} T^* + \xi_7 k_6 {P_3}^*(K_3 + T^*)}{2A(K_3 + T^*)}\right\}\right\}.$$

This completes the proof.

## 4.4 The Impulsive Model

In this section, an attempt is made to show the effectiveness of the Tat inhibitor in the treatment of HIV-1 infection using impulsive differential equations (Baınov and Simeonov, 2017; Lakshmikantham and Simeonov, 1989; Smith?, 2008). It is assumed that the inhibitor is given at independent time $t_k$ and the effect of the inhibitor is instantaneous. For $t \neq t_k$, the solution of the impulsive differential equations is continuous and satisfies the associated ordinary differential equation, while going through

an instantaneous change in state when $t = t_k$. According to impulsive theory, the characteristic of the impulse at time $t_k$ can be described as

$$\Delta x \equiv x(t_k^+) - x(t_k^-) = f_k(x(t_k^-)), \tag{4.4.1}$$

where $x(t)$ is the solution of the corresponding impulsive differential equation model; in the present paper $x$ represents $P_2$ (see equation 4.4.2).
Here one can evaluate the effect of impulse with fixed administration of Tat inhibitor to control the production of messenger RNA ($P_4$) by lowering the elongating complex ($P_2$) formation. It is assumed that during periodic treatment the concentration of elongating complex ($P_2$) is reduced by some proportion $r$, where $0 < r < 1$. Now by taking the maximum concentration of elongating complex ($P_2$), one should have the one-dimensional impulsive differential equation

$$\begin{array}{rcl} \frac{dP_2}{dt} & = & M_1 - (k_5 + \beta_5)P_2, \text{ for } t \neq t_k, \\ \Delta P_2 & = & -rP_2, \text{ for } t = t_k \text{ where } k = 1, 2, 3, ..., n, \end{array} \tag{4.4.2}$$

where, $M_1$ is defined in (4.2.3).
Note that using (4.4.1), one may get

$$P_2(t_k^+) - P_2(t_k^-) = -rP_2.$$

For a single impulsive cycle $t_k \leq t \leq t_{k+1}$, the solution is

$$P_2(t_{k+1}^-) = \frac{M_1}{(k_5 + \beta_5)}\left[1 - e^{-(k_5+\beta_5)(t_{k+1}-t_k)}\right] + P_2(t_k^+)e^{-(k_5+\beta_5)(t_{k+1}-t_k)}.$$

Here $P_2(t_k^+)$ and $P_2(t_k^-)$ are the concentration of elongating complex immediately after and before the impulse ($t_k^-$ and $t_k^+$ stand for immediately before and immediately after impulse, respectively). For simplicity of notation, one may denote $N_1 = k_5 + \beta_5$. Now, for the different successive time intervals, the elongating complex concentration satisfies

the following:

$$
\begin{aligned}
P_2(t_1^-) &= \tfrac{M_1}{N_1}, \\
P_2(t_1^+) &= (1-r)\tfrac{M_1}{N_1}, \\
P_2(t_2^-) &= (1-r)\tfrac{M_1}{N_1}e^{-N_1(t_2-t_1)} + \tfrac{M_1}{N_1}\Big[1-e^{-N_1(t_2-t_1)}\Big], \\
P_2(t_2^+) &= \tfrac{M_1}{N_1}\Big[(1-r)^2e^{-N_1(t_2-t_1)} + (1-r) - (1-r)e^{-N_1(t_2-t_1)}\Big], \\
P_2(t_3^-) &= \tfrac{M_1}{N_1}\Big[(1-r)^2e^{-N_1(t_3-t_1)} + (1-r)e^{-N_1(t_3-t_2)} + 1 - (1-r)e^{-N_1(t_3-t_1)} \\
&\quad -e^{-N_1(t_3-t_2)}\Big], \\
P_2(t_3^+) &= \tfrac{M_1}{N_1}\Big[(1-r)^3e^{-N_1(t_3-t_1)} + (1-r)^2e^{-N_1(t_3-t_2)} + (1-r) - (1-r)^2e^{-N_1(t_3-t_1)} \\
&\quad -(1-r)e^{-N_1(t_3-t_2)}\Big], \\
P_2(t_4^-) &= \tfrac{M_1}{N_1}\Big[(1-r)^3e^{-N_1(t_4-t_1)} + (1-r)^2e^{-N_1(t_4-t_2)} + (1-r)e^{-N_1(t_4-t_3)} + \\
&\quad 1-(1-r)^2e^{-N_1(t_4-t_1)} - (1-r)e^{-N_1(t_4-t_2)} - e^{-N_1(t_4-t_3)}\Big], \\
P_2(t_4^+) &= \tfrac{M_1}{N_1}\Big[(1-r)^4e^{-N_1(t_4-t_1)} + (1-r)^3e^{-N_1(t_4-t_2)} + (1-r)^2e^{-N_1(t_4-t_3)} + (1-r) \\
&\quad -(1-r)^3e^{-N_1(t_4-t_1)} - (1-r)^2e^{-N_1(t_4-t_2)} - (1-r)e^{-N_1(t_4-t_3)}\Big].
\end{aligned}
$$

Therefore, the general solution can be written as

$$
\begin{aligned}
P_2(t_n^-) &= \tfrac{M_1}{N_1}\Big[(1-r)^{(n-1)}e^{-N_1(t_n-t_1)} + (1-r)^{(n-2)}e^{-N_1(t_n-t_2)} + \ldots \\
&\quad +(1-r)e^{-N_1(t_n-t_{n-1})} + 1 - (1-r)^{(n-2)}e^{-N_1(t_n-t_1)} \\
&\quad -(1-r)^{(n-3)}e^{-N_1(t_n-t_2)} - \ldots - e^{-N_1(t_n-t_{n-1})}\Big],
\end{aligned} \tag{4.4.3}
$$

and

$$
\begin{aligned}
P_2(t_n^+) &= \tfrac{M_1}{N_1}\Big[(1-r)^ne^{-N_1(t_n-t_1)} + (1-r)^{(n-1)}e^{-N_1(t_n-t_2)} + \ldots \\
&\quad +(1-r)^2e^{-N_1(t_n-t_{n-1})} + (1-r) - (1-r)^{(n-1)}e^{-N_1(t_n-t_1)} \\
&\quad -(1-r)^{(n-2)}e^{-N_1(t_n-t_2)} - \ldots - (1-r)e^{-N_1(t_n-t_{n-1})}\Big].
\end{aligned} \tag{4.4.4}
$$

The above general solutions represented by (4.4.3) and (4.4.4) help to predict the maximum concentration of elongating complex present just before and after the $n$th number of drug doses is administered.

### 4.4.1 For fixed time interval of dosing

One may consider a fixed time interval of dosing, i.e., $t_n - t_{n-1} = \tau$ is constant. Thus one should have

$$\begin{aligned}
P_2(t_n^-) &= \tfrac{M_1}{N_1}\Big[1+(1-r)e^{-N_1\tau}+(1-r)^2e^{-2N_1\tau}+...+(1-r)^{(n-1)}e^{-(n-1)N_1\tau} \\
&\quad -e^{-N_1\tau}\Big\{1+(1-r)e^{-N_1\tau}+...+(1-r)^{(n-2)}e^{-(n-2)N_1\tau}\Big\}\Big] \\
&= \tfrac{M_1}{N_1}\Big[\tfrac{1-(1-r)^ne^{-nN_1\tau}}{1-(1-r)e^{-N_1\tau}}-e^{-N_1\tau}\Big\{\tfrac{1-(1-r)^{(n-1)}e^{-(n-1)N_1\tau}}{1-(1-r)e^{-N_1\tau}}\Big\}\Big] \\
\lim_{n\to\infty}P_2(t_n^-) &= \tfrac{M_1}{N_1}\Big[\tfrac{1}{1-(1-r)e^{-N_1\tau}}-e^{-N_1\tau}\tfrac{1}{1-(1-r)e^{-N_1\tau}}\Big] \\
&= \tfrac{M_1}{N_1}\Big[\tfrac{1-e^{-N_1\tau}}{1-(1-r)e^{-N_1\tau}}\Big].
\end{aligned}$$

This is the long-term maximum concentration of elongating complex before applying the drug. To keep this below a proper threshold $\hat{P}_2$, thus one should have

$$\tau < \tfrac{1}{N_1} ln\Big[\tfrac{M_1-(1-r)N_1\hat{P}_2}{M_1-N_1\hat{P}_2}\Big].$$

Substituting $M_1 = \frac{k_4P_{1_{Tot}}\alpha_2}{K_3\beta_4+\alpha_2}$ and $N_1 = (k_5+\beta_5)$ in the above inequality, one obtains

$$\tau < \tfrac{1}{k_5+\beta_5}\ln\Big[\tfrac{\alpha_2k_4P_{1_{Tot}}-(1-r)P_2(K_3\beta_4+\alpha_2)(k_5+\beta_5)}{\alpha_2k_4P_{1_{Tot}}-(K_3\beta_4+\alpha_2)(k_5+\beta_5)\hat{P}_2}\Big] \equiv \tau_{\max} \text{ say.} \tag{4.4.5}$$

The above equation (4.4.5) represents the maximum period between two consecutive drug doses required to keep the elongating complex concentration below $\hat{P}_2$. The threshold value $\hat{P}_2$ must satisfy

$$\hat{P}_2 < \tfrac{\alpha_2k_4P_{1_{Tot}}}{(K_3\beta_4+\alpha_2)(k_5+\beta_5)}. \tag{4.4.6}$$

Therefore, one can infer that for fixed dosing, one may obtain a maximal time gap (fixed) of dosing that will keep the concentration of elongating complex strictly below a threshold value mentioned by (4.4.6).

### 4.4.2 Corollary

**Some Basic Definitions:**

Consider the linear impulsive differential equation at fixed moments

$$\begin{aligned}
&\tfrac{dx}{dt} = A(t)x, \text{ for } t \neq t_k, \\
&\Delta x = A_kx, \text{ for } t = t_k;\ \text{k } \in \mathbb{N}.
\end{aligned} \tag{4.4.7}$$

**Definition 4.4.1** *Equation (4.4.7) is said to be stable if for any number $k, k = 1, 2, ...,$ there exists a positive constant $N_k$ such that for any solution $x \in L_k$ (the linear space of the solutions $x(t)$ of equation (4.4.7)) defined in the interval $[t_k + 0, +\infty)$ the following inequality should hold:*

$$|x(t)| \leq N_k |x(t_k + 0)| \quad for \quad t \geq t_k + 0.$$

**Definition 4.4.2** *Equation (4.4.7) is said to be uniformly stable if there exists a positive constant $N$ such that for any number $k, k = 1, 2, ...,$ and for any solution $x \in L_k$ the following inequality should hold:*

$$|x(t)| \leq N|x(s)| \quad \forall \quad t \geq s \geq t_k + 0.$$

The interested reader can have a look at (Milev and Bainov, 1990) for more details on the stability of linear impulsive differential equations.

Using the transformation $\bar{P}_2 = P_2 - \frac{M_1}{k_5+\beta_5}$, the model (4.4.2) can be converted to the below-mentioned linear homogeneous impulsive differential equation:

$$\begin{aligned} \frac{d\bar{P}_2}{dt} &= -(k_5 + \beta_5)\bar{P}_2, \text{ for } t \neq t_k, \\ \Delta\bar{P}_2 &= -r\Big(\bar{P}_2 + \frac{M_1}{k_5 + \beta_5}\Big), \text{ for } t = t_k \text{ where } k = 1, 2, 3, ..., n. \end{aligned}$$

For $t$ satisfying $t_k < t \leq t_{k+1}$, one may have

$$\bar{P}_2(t) = \bar{P}_2(t_k^+)e^{-(k_5+\beta_5)(t-t_k)}.$$

Considering $\tau = t_n - t_{n-1}$ be the fixed time interval of dosing of the Tat inhibitor and denoting $N_1 = k_5 + \beta_5$, one should have a recursion relation at the moments of impulse, represented by

$$\bar{P}_2(t_n^+) - \bar{P}_2(t_n^-) = -r\bar{P}_2 - r\frac{M_1}{N_1}.$$

Thus

$$\bar{P}_2(t_n^+) = -r\frac{M_1}{N_1}\left[\frac{1 - (1-r)^n e^{-nN_1\tau}}{1 - (1-r)e^{-N_1\tau}}\right] \longrightarrow -r\frac{M_1}{N_1}\left[\frac{1}{1 - (1-r)e^{-N_1\tau}}\right]$$

as $n \longrightarrow \infty$.

However, if $\bar{P}_2(t_n^+) = -r\frac{M_1}{N_1}\left[\frac{1}{1-(1-r)e^{-N_1\tau}}\right]$, then $\bar{P}_2(t_{n+1}^-) = -r\frac{M_1}{N_1}\left[\frac{1}{1-(1-r)e^{-N_1\tau}}\right]e^{-N_1\tau}$ and so

$$\begin{aligned}\bar{P}_2(t_{n+1}^+) &= -r\frac{M_1}{N_1}\left[\frac{1}{1-(1-r)e^{-N_1\tau}}\right]e^{-N_1\tau} + r^2\frac{M_1}{N_1}\left[\frac{1}{1-(1-r)e^{-N_1\tau}}\right]e^{-N_1\tau} - r\frac{M_1}{N_1}\\ &= -r\frac{M_1}{N_1}\left[\frac{1}{1-(1-r)e^{-N_1\tau}}\right].\end{aligned}$$

Moreover, it is worth noting that

$$\bar{P}_2(t_n^+) - \left[-r\frac{M_1}{N_1}\left[\frac{1}{1-(1-r)e^{-N_1\tau}}\right]\right] = r\frac{M_1}{N_1}\left[\frac{(1-r)^n e^{-nN_1\tau}}{1-(1-r)e^{-N_1\tau}}\right].$$

It follows that the impulse points $r\frac{M_1}{N_1}\left[\frac{1}{1-(1-r)e^{-N_1\tau}}\right]$ and $r\frac{M_1}{N_1}\left[\frac{1}{1-(1-r)e^{-N_1\tau}}\right]e^{-N_1\tau}$ define the ends of a positive impulsive periodic orbit (generally, impulsive models do not display steady state, but rather impulsive periodic orbits) in the elongating complex concentration, to which the endpoints of each cycle monotonically increase and the monotonicity of the impulsive trajectory imply that

$$\bar{P}_2(t) < r\frac{M_1}{N_1}\left[\frac{1}{1-(1-r)e^{-N_1\tau}}\right].$$

Therefore according to the definition of stability of linear impulsive differential equations, the impulsive elongating complex orbit is stable.

**Note:** One can establish results similar to Theorem 1 (i.e., non-negativity and boundedness) for the impulsive system (4.4.2) (one can have a look at (Bainov et al., 1995) for details). The proofs are quite obvious and, hence, omitted from the text.

## 4.5 Numerical Simulations

The behaviour of the present models (4.2.2) and (4.3.3), is illustrated through numerical simulations, utilizing a set of parameter values provided in Table 4.1. A portion of these values is derived from the existing literature (Carlotti et al., 2000; Kim and Yin, 2005;

Likhoshvai et al, 2014; Mohammadi et al., 2013; Reddy and Yin, 1999; Robert-Guroff et al., 1990; Shcherbatova et al., 2020; Slice et al., 1992), while some parameter values are presumed hypothetically. The resulting simulations are depicted graphically in Figs. 4.4-4.6. The execution of the present numerical study was carried out using MATLAB 2016A.

Table 4.1: List of parameters, their descriptions, and range of values for models (4.2.2) and (4.3.3).

| Parameter | Parameter description | Value (Unit) |
|---|---|---|
| $k_2$ | The rate of the forward reaction from $ES$ to $P_1$ | $(1.4 - 4.5)\ hr^{-1}$ |
| $K_3$ | Reaction dissociation constant between $P_1$ and $T$ | $(0.01 - 2.05)\ \mu M$ |
| $K_M$ | Michaelis constant for $S$ | $(1.0 - 2.8)\ \mu M$ |
| $k_4$ | The rate of forward reaction from $TP_1$ to $P_2$ | $(0.8 - 3.8)\ hr^{-1}$ |
| $k_5$ | The rate of forward reaction from $P_2$ to $P_3$ | $(0.2 - 3.0)\ hr^{-1}$ |
| $k_6$ | The rate of forward reaction from $P_3$ to $P_4$ | $(1.2 - 4.6)\ hr^{-1}$ |
| $\alpha_1$ | Accumulation rate of $S$ | $(1.0 - 2.5)\ hr^{-1}$ |
| $\alpha_2$ | Synthesis rate of $T$ | $(0.5 - 2.0)\ hr^{-1}$ |
| $\beta_1$ | Degradation rate of $S$ | $(0.001 - 0.65)\ hr^{-1}$ |
| $\beta_2$ | Degradation rate of $E$ | $(0.01 - 0.7)\ hr^{-1}$ |
| $\beta_3$ | Degradation rate of $P_1$ | $(0.02 - 0.5)\ hr^{-1}$ |
| $\beta_4$ | Degradation rate of $T$ | $(0.04 - 0.45)\ hr^{-1}$ |
| $\beta_5$ | Degradation rate of $P_2$ | $(0.001 - 0.12)\ hr^{-1}$ |
| $\beta_6$ | Degradation rate of $P_3$ | $(0.02 - 0.2)\ hr^{-1}$ |
| $\beta_7$ | Degradation rate of $P_4$ | $(0.03 - 0.65)\ hr^{-1}$ |

Figure 4.4 displays phase portraits of model (4.2.2) for varying initial values of model compartments. In Figure 4.4(A), it is demonstrated that the trajectories of TAR ($S(t)$), enzyme RNA polymerase II ($E(t)$), and DNA unit RNA polymerase II elongation complex ($P_2(t)$) converge towards the unique positive equilibrium densities $S^*$, $E^*$, and $P_2^*$, respectively. Similarly, in Figure 4.4(B), the trajectories of DNA unit RNA polymerase II _elongation complex ($P_2(t)$), immature 9kb RNA ($P_3(t)$), and mature 9kb messenger RNA ($P_4(t)$) also converge towards the unique positive equilibrium densities $P_2^*$, $P_3^*$, and $P_4^*$, respectively. This demonstrates the stability of the singular positive equilibrium $E_1^*$. Each of these observations is discernible from the graphical depictions.

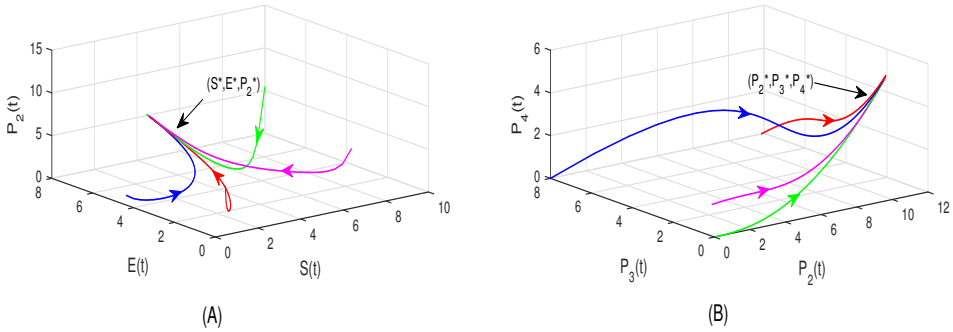


Figure 4.4: Stability of the unique interior equilibrium $E_1^*$ concerning different initial conditions: (A) considering three components TAR, RNA polymerase II, DNA unit_RNA polymerase II_elongation complex; (B) considering three components DNA unit_RNA polymerase II_elongation complex, immature 9kb RNA, mature 9kb messenger RNA. Here we use $S(0) = 4.5\mu M$, $E(0) = 4.2\mu M$, $P_1(0) = 3.8\mu M$, $T(0) = 2\mu M$ as initial values and the parameter values are taken from Table 4.1.

Figure 4.5 depicts the temporal evolution of reactant concentrations over time, both with and without the implementation of the control approach. The introduction of control input $u(t)$ to regulate the concentrations of the elongating complex $P_2$ and messenger RNA ($P_4$) results in a notable deceleration of their progress curves compared to the uncontrolled reaction. The application of control input leads to a reduction in the formation rate of the elongating complex ($P_2(t)$), subsequently influencing the

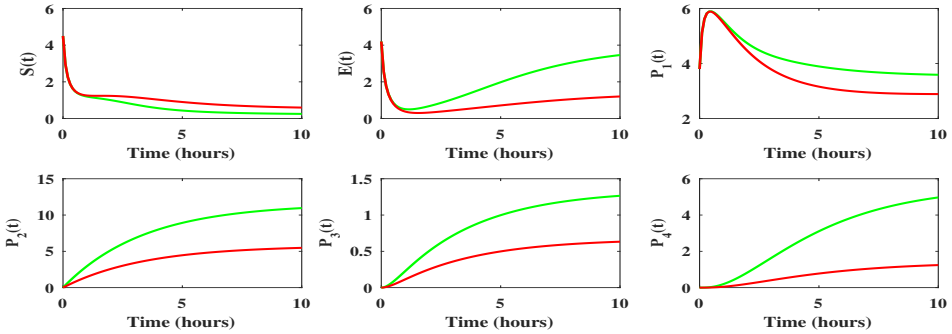


Figure 4.5: The nature of the curves of reactants with and without control, using $S(0) = 4.5\mu M$, $E(0) = 4.2\mu M$, $P_1(0) = 3.8\mu M$, $T(0) = 2\mu M$ as initial concentrations. Here, the parameter values are taken from the range in Table 4.1.

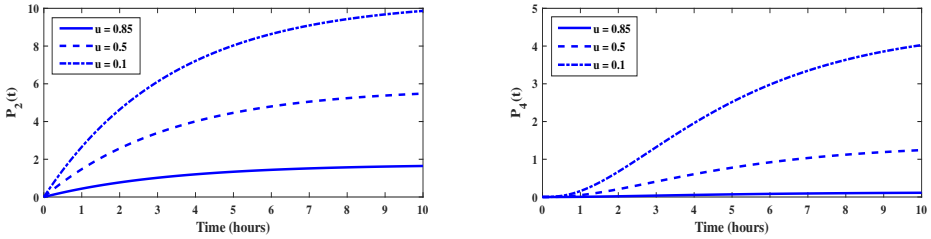


Figure 4.6: Qualitative behavior of the components DNA unit_RNA polymerase II elongation complex and messenger RNA using three different values of $u$, considering model (4.3.3). The parameter values are the same as in Table 4.1.

progress curves of immature 9kb RNA ($P_3(t)$) and enzyme RNA polymerase II ($E(t)$) in a similar downward trend. Conversely, the concentration of TAR ($S(t)$) exhibits an increment over time. The consequences of the more pronounced decrease in enzyme concentration ($E(t)$) and the concurrent increase in substrate concentration ($S(t)$) reverberate across the $P_1$ complex, a key participant in HIV-1 transcription. This figure supports the conclusion that the Tat inhibitor significantly suppresses HIV-1 transcription by prominently reducing the synthesis of mature 9kb messenger RNA (mRNA), offering substantial advantages for HIV-1-infected patients.

Figure 4.6 portrays the qualitative patterns of concentration curves for the DNA unit RNA polymerase II_ elongation complex ($P_2(t)$) and messenger RNA ($P_4(t)$) in model (4.3.3), utilizing three distinct fixed values of the control function $u$ ($u = 0.1,\ 0.5$, and $0.85$). The illustration clearly demonstrates the potent efficacy of the Tat inhibitor in governing messenger RNA formation, thereby hindering the progression of HIV-1 infection toward AIDS. It is noteworthy that the synthesis of messenger RNA ($P_4(t)$) diminishes with escalating values of the control function $u$, reaffirming the therapeutic efficacy of the Tat inhibitor against HIV-1 replication.

In Figure 4.7, a comparison can be made between the progress curves of the components (($P_1$), ($P_2$), ($P$), and ($P_4$)) that are involved in the HIV-1 transcription process for both continuous dosing (optimal drug dose) and impulsive dosing

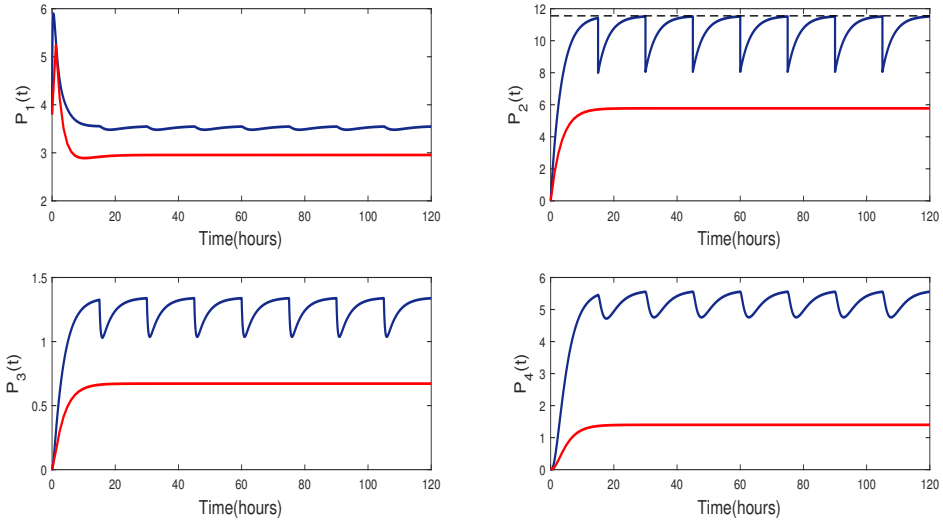


Figure 4.7: Pattern of the curves of reactants with continuous therapy (red line) and with impulse therapy (blue line) using Tat inhibitor. Here we have taken $S(0) = 4.5\mu M$, $E(0) = 4.2\mu M$, $P_1(0) = 3.8\mu M$, $T(0) = 2\mu M$ as initial values and the parameter values are chosen from the range given in Table 4.1. The black line represents the upper threshold level of $P_2$ obtained from equation (4.4.6).

(drug efficacy $r = 0.3$, dosing interval $\tau = 15$ hours) of the Tat inhibitor. The upper threshold level of the elongating complex $P_2$ is determined as 11.552 $\mu M$ by equation (4.4.6) from the present analytical study. It can be observed from this figure that, in the case of impulsive dosing, the concentration of elongating complex $P_2$ is situated just below the threshold value and exhibits oscillations with a fixed amplitude. In contrast, in the continuous dosing method, the concentration of complex $P_2$ remains significantly lower than the threshold level, thereby creating a more favourable condition for combating HIV-1 transcription. Additionally, more favourable outcomes are recorded for the concentrations of $P_3$ and $P_4$ with continuous dosing in comparison to impulsive therapy. Another noteworthy observation from this figure is the sharp decline in the peak point of the TAR-RNA Polymerase II_elongation complex ($P_1$) progress curve upon the application of an optimal dose of the Tat inhibitor. Following this peak point, the concentration of elongation complex $P_1$ diminishes over time at a slower rate through impulse therapy, which is advantageous for an overall reduction in messenger RNA synthesis ($P_4$) from the elongating

complex $P_1$. Therefore, to achieve an overall decline in the HIV-1 transcription process and extend patients' compliance, enhancing the impulse dosing strategy is desired.

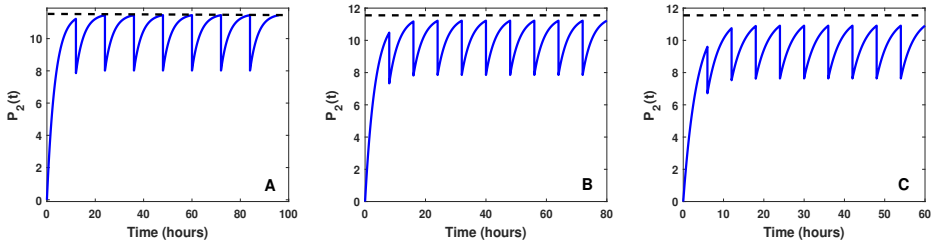


Figure 4.8: Nature of the curves for the component $P_2$ with impulsive dosing time interval $\tau$: (A) $\tau = 12$h (B) $\tau = 8$h (C) $\tau = 6$h. The black line represents the upper threshold level of $P_2$ (11.552 $\mu M$) obtained from equation (4.4.6).

To determine the ideal and safe dosing regimen for administering the Tat inhibitor impulsively, Figure 4.8 is employed. By utilizing the same values as in Figure 4.7, the maximum time gap between consecutive dosing instances is calculated as $\tau_{max} = 34.693$ hours (using equation (4.4.5)). As a result, the time interval $\tau$ between two consecutive doses should be $\tau < 34.693$ hours. By considering the fixed drug efficacy $r = 0.3$ and varying the dosing interval $\tau$ (= 12h, 8h, 6h), changes in the nature of the elongating complex $P_2$'s progress curve can be observed in each corresponding figure. It is evident from Figure 4.8(A) that a dosing interval of $\tau = 12$h hours (twice a day) is too extensive for the considered drug efficacy to effectively control HIV-1 transcription. This is due to the fact that the concentration of elongating complex $P_2$ decreases immediately after the initial application of the Tat inhibitor, then rises again, participating in the reaction mechanism until the second dose of the Tat inhibitor is administered. Conversely, in Figures 4.8(B) and 4.8(C), the elongating complex $P_2$ has less opportunity to contribute to HIV-1 transcription, indicating better outcomes for dosing intervals of 8 hours (thrice a day) and 6 hours (four times a day), respectively. Furthermore, in Figure 4.8(C), the peak point of the $P_2$ progress curve remains notably below its upper threshold value, creating a more favourable condition for the dosing interval $\tau = 6$ hours. Consequently, it can be concluded from

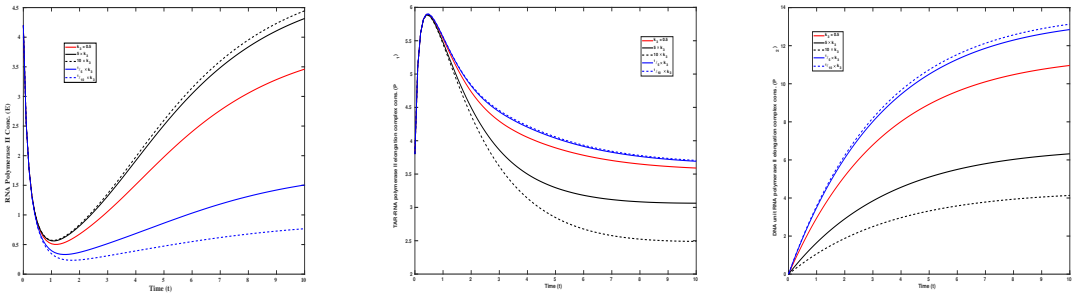

Figure 4.9: The nature of the curves of $E$, $P_1$, and $P_2$ for different values of $K_3$, using $S(0) = 4.5\mu M$, $E(0) = 4.2\mu M$, $P_1(0) = 3.8\mu M$, $T(0) = 2\mu M$ as initial values and keeping the other parameters fixed as in Table 4.1.

this figure that, for impulsive dosing of the Tat inhibitor (with drug efficacy $r = 0.3$), a dosing interval of $\tau = 6$ hours, corresponding to four times a day dosing, is more suitable for HIV-1 infected patients.

## 4.6 Variation of Parameters

In this section, sensitized parameter variation is performed to get a clearer perception regarding parameter sensitivity so that one may take care while choosing different parameter values.

Figure 4.9 depicts the qualitative characteristics of the progress curves pertaining to the enzyme RNA Polymerase II ($E$), the TAR-RNA polymerase II_ elongation complex ($P_1$), and the DNA unit RNA polymerase II _elongation complex ($P_2$), under varying conditions of the parameter $K_3$. The remaining parameter values remain constant, as outlined in Table 4.1. Notably, when $K_3$ is augmented by a factor of five from its baseline value, a precipitous reduction in the concentration of complex $P_2$ becomes evident. This corresponding trend is also observable in the concentration profile of complex $P_1$. The rationale behind the pronounced reduction in $P_2$ complex concentration can be elucidated from the conceptual model (4.2.2). Considering that $K_3$ is defined as the ratio of the reverse rate constant $k_{-3}$ to the forward rate constant $k_3$, an elevation

in $K_3$ implies an increase in the reverse rate constant $k_{-3}$. Consequently, a higher $K_3$ value leads to a notable diminution in the concentration of complex $P_2$. Given that a heightened $K_3$ results in decreased $P_2$ complex concentration, a similar effect is observed on the concentration of enzyme $E$. The concentration of the elongating complex $P_1$ is similarly affected due to the same underlying mechanism. A comprehensive explanation is omitted here to maintain brevity.

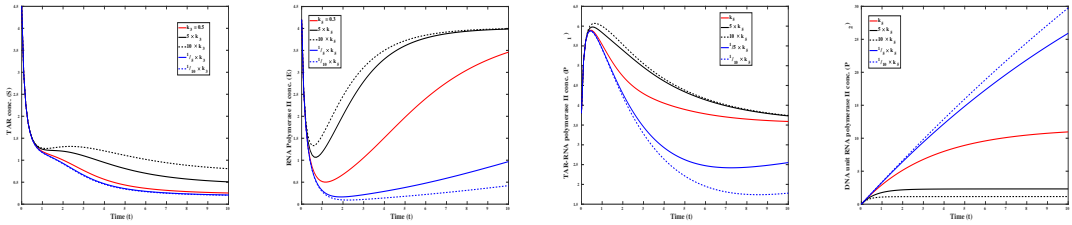

Figure 4.10: Concentration-time curves of the model (4.2.2) for compartments $S$, $E$, $P_1$, and $P_2$ for different values of $k_5$. Here the initial conditions and the remaining parameters are fixed as those in Figure 4.9.

Figure 4.10 portrays the graphical representation of curves denoted as $S$, $E$, $P_1$, and $P_2$, corresponding to distinct values of the rate constant $k_5$. Notably, an increase in $k_5$ magnitudes leads to a conspicuous decline in the concentration of $P_2$. This reduction is characterized by a rate of decrease surpassing the rate of $k_5$ augmentation. This trend is attributable to the fact that the elongating complex $P_2$ undergoes conversion into immature 9kb RNA, represented as $P_3$, under the influence of the $k_5$ rate constant, as prescribed by the conceptual model (4.2.2). As the concentration of $P_2$ complex diminishes at a pace exceeding the rate of $k_5$ escalation, a commensurate increase in the concentration of enzyme RNA Polymerase II ($E$) ensues. Consequently, this heightened enzyme concentration contributes to a depletion in substrate ($S$) levels. It is pertinent to highlight that the escalation in enzyme ($E$) concentration outpaces the reduction rate in substrate ($S$) concentration, thereby resulting in an elevation of the TAR-RNA polymerase II_ elongation complex ($P_1$) concentration for elevated $k_5$ values. The depicted observations from this figure substantiate the alignment between the current numerical findings and the corresponding analytical results.

Figure 4.11 offers a comprehensive overview of the transformative shifts in the

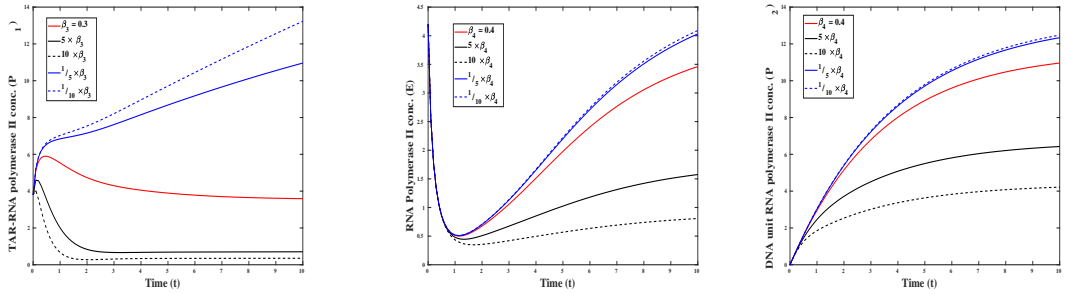


Figure 4.11: Nature of the curves $P_1$ (for different values of $\beta_3$), $E$ and $P_2$ (for different values of $\beta_4$) while keeping the other parameters fixed as in Table 4.1. The initial conditions are the same as the figure 4.9.

concentrations of $P_1$, $E$, and $P_2$ complexes, under varying conditions of $\beta_3$ and $\beta_4$. It becomes evident upon examination of the figure that an escalation in the $\beta_3$ rate yields a corresponding decrease in the concentration of complex $P_1$, a phenomenon that can be rigorously substantiated through analytical evaluation of model ((4.2.2)). Upon closer inspection of the model (4.2.2), it becomes apparent that the concentration of HIV-1 protein Tat ($T$) exhibits a decline proportional to the increasing rate of $\beta_4$. This diminishment in Tat protein ($T$) concentration subsequently reverberates onto the concentration of the DNA unit RNA polymerase II_ elongation complex ($P_2$). Clearly discernible is the reduction in $P_2$ concentration for elevated values of $\beta_4$, which in turn contributes to the decline in the concentration of enzyme RNA Polymerase II ($E$). This sequence of events aligns with the tenets of the corresponding analytical counterparts. In summation, the coherent findings derived from Figures 4.9, 4.10 and 4.11 collectively affirm the robustness of the devised mathematical model, thus underlining its empirical validity.

## 4.7 Conclusion

The existing literature lacks comprehensive mathematical models addressing HIV-1 replication within infected cells, particularly concerning Tat-mediated transcription through enzyme kinetics. Few theoretical studies have explored the inhibitory effects of Tat inhibitors on HIV-1 transcription but haven't integrated them into mathematical

models. Addressing this gap, this study contributes in several significant aspects:

1. Describes HIV-1 Tat-mediated transcription using nonlinear differential equations.

2. Introduces quasi-steady-state approximations (QSSA) for substrate-catalyst complex concentrations.

3. Utilizes Tat inhibitor as a control parameter $u(t)$ to reduce messenger RNA (mRNA) production.

4. Proposes a one-dimensional impulsive differential equation model to optimize Tat inhibitor dosing.

The study demonstrates the bounded and non-negative nature of the model solutions and establishes the local stability of the endemic equilibrium point. The Pontryagin minimum principle is applied to an optimal control problem. Numerical results indicate that continuous therapeutic administration stabilizes mRNA synthesis after 10 hours. An impulsive model yields an upper threshold for DNA unit_ RNA Polymerase II _elongation complex ($P_2$) and a maximum time gap between doses ($\tau_{max} = 34.693$).

Comparative analysis of continuous and impulse dosing of Tat inhibitor shows that a 6-hour interval effectively controls HIV-1 transcription, with a maximum dosing interval of 34.693 hours. Notably, the study indicates that impulsive administration of Tat inhibitor is safer and more effective than continuous treatment, ensuring patient compliance and comfort.

In conclusion, applying Tat inhibitor through a 6-hour impulse dosing regimen offers long-term benefits for HIV-1 treatment, with a maximum dosing interval of 34.693 hours. This approach is safer and more effective than continuous treatment, offering a systematic approach to combat AIDS with reduced side effects. The study's mathematical model and findings provide valuable guidance for developing therapeutic strategies in the scientific community.

# Chapter 5

# A control-based mathematical study on HIV-1 transcription by introducing Tat and Rev inhibitor

## 5.1 Introduction

The global issue of Acquired Immune Deficiency Syndrome (AIDS) continues to be an ongoing crisis. According to current data, approximately 39.9 million individuals are living with HIV-1, with 1.3 million new infections reported in 2023 (unaids, 2023). Given the significant threat these new cases pose to global health, urgent attention must be given to addressing this issue. In order to effectively combat HIV-1, it is essential to have a thorough understanding of the biological, physical, and chemical processes involved.

The initiation of viral infections occurs when the envelope glycoprotein binds to the CD4 receptor and a co-receptor on the surface of immune cells. This results in the fusion of the membranes of the host cell and the virion, allowing HIV-1 to enter the host cell and release its viral core, which contains the single-stranded RNA genome, reverse transcriptase (RT), integrase (IN), and other viral components into the host

cell cytoplasm (Das and Arnold, 2013; Friedrich et al., 2011; Hu and Hughes, 2012; Sarafianos et al., 2009). After that the enzyme reverse transcriptase (RT) copies the single-stranded viral RNA genome into double-stranded DNA which is subsequently transported to the cell nucleus and integrated into the host cell chromosome by another enzyme integrase (IN) (Engelman et al., 1991; Sarafianos et al., 2009). Upon integration into the host DNA, HIV-1 initiates the transcription of the integrated proviral DNA into full-length unspliced 9kb messenger RNA by means of host enzyme RNA polymerase II (Pol II) (Likhoshvai et al, 2014; Ott et al., 2011). The RNA polymerase II binds to the Transactivation Responsive (TAR) element on HIV-1 proviral DNA LTR promoter region yielding TAR – RNA polymerase II elongation complex (Likhoshvai et al, 2014; Ott et al., 2011). The HIV-1 transcription process is further positively regulated by an essential auxiliary protein called the transcriptional transactivator Tat. Tat binds directly to the Transactivation Responsive (TAR) element on TAR-RNA polymerase II elongation generating Tat-TAR complex that eventually transforms into DNA unit RNA Pol II elongation complex from which full length unspliced 9kb messenger RNA is produced inside the nucleus of the host cell (Likhoshvai et al, 2014; Mousseau et al., 2015; Reddy and Yin, 1999). After that the 9kb messenger RNA is either transported intact to the cell cytoplasm or spliced to form 4kb singly spliced messenger RNA and then transported to cytoplasm (Likhoshvai et al, 2014; Reddy and Yin, 1999). The same procedure happens with the 4kb singly spliced messenger RNA, i.e., the 4kbs mRNA is either transported intact to the cytoplasm or undergoes splicing to generate doubly spliced 2kb messenger RNA before being transported to the cell cytoplasm (Likhoshvai et al, 2014; Reddy and Yin, 1999). However, to produce new virus particles, transport of both the full-length unspliced 9 kb RNA and 4kb singly spliced mRNA from the nucleus to the cytoplasm are necessary. Towards the later phase of HIV-1 life cycle, the translation of the 9kb and 4kb mRNAs in the cytoplasm produces specific proteins which eventually generate a new virion after undergoing several modifications. The cytoplasmic transport of the 9kb and 4kb mRNAs is carried out by a viral protein called Rev. The Rev protein is produced from the doubly spliced 2kb viral mRNA, which is transported from the nucleus to the cytoplasm through internal cellular processes. Research has shown that

Rev serves as a traffic signal in the nucleus, guiding viral mRNAs away from splicing to create singly spliced and doubly spliced viral mRNA (Cao et al., 2009; Likhoshvai et al, 2014; Prado et al., 2018; Reddy and Yin, 1999), which is crucial for transporting the 9 kb and 4 kb types of HIV-1 messenger RNA to the cytoplasm. This leads to a decrease in the production of doubly spliced 2kb mRNA, resulting in a reduced synthesis of the Rev protein overall (Cao et al., 2009; Prado et al., 2018). Without Rev function, the 9kb and 4kb messenger RNA are trapped in the nucleus, and only the 2kb class RNA is transported to the cytoplasm as the transport of doubly spliced 2kb mRNA is Rev-independent. Therefore, Rev generates a negative feedback loop causing a reduction in the production of viral spliced messages, which is very important for maintaining a balance in the products of viral gene expressions. This control over viral gene expression ultimately leads to higher levels of virion production.

It is now intended to delve deep in the search of possible remedy for AIDS yielding patient compliance. Since the discovery of AIDS, significant progress has been achieved for diagnosis and treatment of HIV-1 infection. The implementation of highly active anti-retroviral therapy (HAART) has greatly reduced morbidity and mortality among patients with HIV-1, extending the lifespan of those infected individuals. Unfortunately, the virus still persists in latently infected CD4+T cells as a latent integrated provirus and therefore, patients should remain on antiretroviral therapy (ART) for an indefinite period of time (Mousseau et al., 2015). If the treatment is discontinued, the latent integrated provirus may get activated leading to viral replication thereby rapidly weakening the immune system of an individual (Arlen et al., 2006; Mousseau et al., 2015). Since currently available anti-HIV drugs do not hinder the transcription process, it is important to focus on permanently inhibiting this process. Because of the important functions of the two viral essential proteins Tat and Rev in HIV-1 transcription, both Tat and Rev have become appealing targets for the advancement of AIDS treatment. Various approaches have been used to target the Tat/TAR interaction in order to control the synthesis of full length 9kb unspliced messenger RNA, which is essential for new virion production (Cecchetti et al. 2000; Wan and Chen 2014; Mousseau et al. 2012, 2015). Besides, several

strategies have been made use of towards targeting the Rev mediated nuclear export of viral 9kb and 4kb messenger RNA in order to suppress HIV-1 replication (Cao et al., 2009; Prado et al., 2018). According to current clinical research, finding and creating a drug that focuses on one or more stages of HIV-1 RNA development can provide new chances for treatment to effectively manage viral reproduction and potentially solve the issue of resistance to antiretroviral therapies (Chowdhury and Roy, 2016; Mousseau et al., 2012, 2015). Although quite a good number of clinical and experimental investigations have been carried out on the efficacy of Tat/Rev inhibitor, yet a mathematical model-based analysis is not widely explored. To address this gap, the current focus is on developing a mathematical model that covers the mechanics of the entire Tat-Rev regulation of HIV-1 replication. This proposed model is expected to provide a foundational framework for better understanding the infection transmission dynamics and offering strategic guidance for effectively managing the infection, signifying the innovative essence of our study.

Quite a few mathematical models have been developed to describe the dynamics of viral replication during HIV-1 infection (Covert and Kirschner, 2000; Nowak and May, 2000; Perelson, 2002), supplemented by various treatment strategies and the effects of different drug therapies as well (Nowak and May, 2000; Perelson, 2002; Wahl and Nowak, 2000). The effect of perfect adherence to antiretroviral therapy has been carried out by means of impulsive differential equations (Lou and Smith, 2011; Smith, 2006). Using the method mentioned above, the dosing period and the threshold values of dosage can be precisely estimated. Recently, S. Mondal (Mondal et al., 2023) has carried out an enzyme kinetics model on Tat regulation of HIV-1 replication with the incorporation of Tat inhibitor, aiming to investigate the impact of Tat inhibitor on suppressing the transcriptional activity of HIV-1. Moreover, several theoretical studies established facts regarding the inhibitory effect of Rev inhibitor on HIV-1 post-transcriptional processing of viral mRNA and its ability to reduce Rev function (Cao et al., 2009; Prado et al., 2018). The present chapter takes into account the formulation of an enzyme kinetics model in order to observe the effect of both the viral proteins: Tat and Rev on HIV-1 replication. Also, the impact and effectiveness of a combined

therapy (administering Tat and Rev inhibitor) is examined by employing an optimal control problem. By using the Pontryagin maximum principle, the optimal control problem of minimizing the cost of therapy while simultaneously optimizing the effect of this therapy on Tat-Rev regulation of HIV-1 replication has been studied. It is believed that the outcomes of the model system will be of some help for both the theoretical modellers and clinicians.

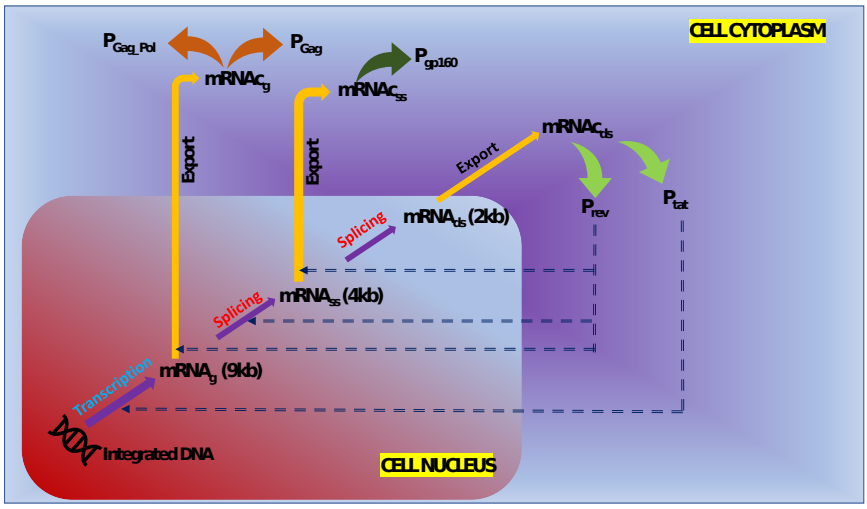


Figure 5.1: A schematic representation of HIV-1 life-cycle.

## 5.2 Preliminaries

### 5.2.1 The Model

Let $T$ denote the concentration of HIV-1 Tat protein and $P_1$ denote the concentration of TAR-RNA polymerase II elongation complex. During HIV-1 transcription, viral Tat ($T$) protein binds to TAR (Trans Activation Response) element at the TAR-RNA polymerase II_elongation ($P_1$) and forms Tat-TAR complex ($TP_1$). This complex then converts into the DNA unit_RNA polymerase II_elongation complex ($P_2$) through a series of reactions with forward and backward rate constants, labeled as $k_1$, $k_2$, $k_{-1}$, and $k_{-2}$ respectively. Subsequently, the elongation complex is transformed into 9kb unspliced messenger RNA ($P_{3\_nuc}$) inside the host cell nucleus, with the help of the

rate constant $k_3$. The 9kb messenger RNA is further converted into 4kb singly spliced messenger RNA ($P_{4\_nuc}$), which undergoes a transformation into 2kb doubly spliced messenger RNA ($P_{5\_nuc}$), facilitated by the rate constants $k_5$ and $k_7$ respectively. Moreover, the process of HIV-1 replication is aided by the viral protein Rev ($R$), which promotes the nuclear export of unspliced and singly spliced RNA transcripts to the cytoplasm. The Rev protein binds to the Rev Recognition Element (RRE) in the virus RNA and positively regulates the transportation of 9kb ($P_{3\_nuc}$) and 4kb ($P_{4\_nuc}$) messenger RNAs from nucleus to the cell cytoplasm. The rate constants for the afore-mentioned Rev-dependent reaction pathway are $k_4$ and $k_6$ respectively. The doubly spliced 2kb messenger RNA ($P_{5\_nuc}$) is transported to the cell cytoplasm through normal mRNA export pathway with the help of the rate constant $k_8$. Furthermore, Rev generates a negative feedback loop to inhibit the splicing of 9kb and 4kb messenger RNA respectively. Here $\gamma$ is represented as the inhibitory effect of Rev on the splicing rates of 9kb ($P_{3\_nuc}$) and 4kb ($P_{4\_nuc}$) messenger RNA; whereas, $k_5$, $k_7$ are the rate of splicing for 9kb and 4kb mRNA respectively. The schematic diagram in Figure (5.2) illustrates the process of HIV-1 Tat/Rev mediated transcription.

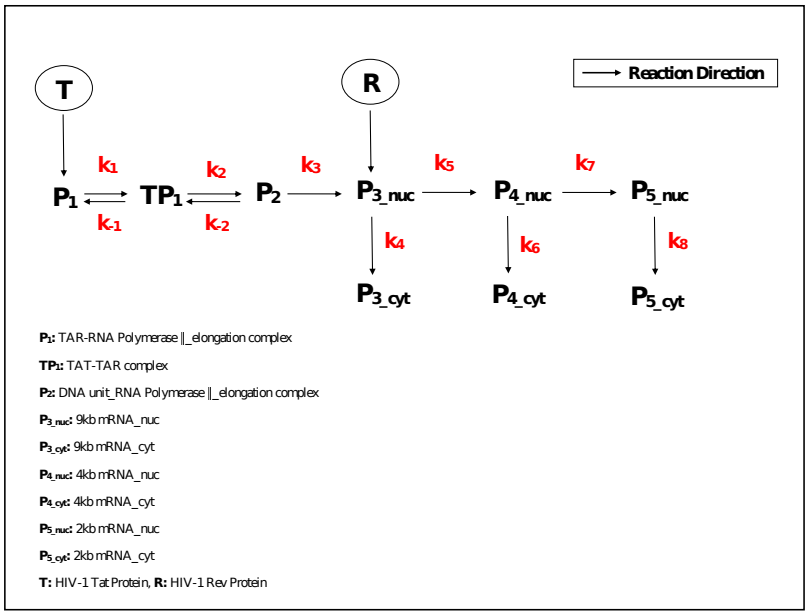


Figure 5.2: The schematic diagram of Tat/Rev mediated reactions.

Furthermore, complying with the Law of Mass Action, the set of nonlinear differential equations describing the above enzymatic reactions is as follows:

$$\begin{aligned}
\tfrac{dP_1}{dt} &= \alpha_1 - k_1 T.P_1 + k_{-1} TP_1 - \beta_1 P_1,\\
\tfrac{dT}{dt} &= \alpha_2 - k_1 T.P_1 + k_{-1} TP_1 - \beta_2 T,\\
\tfrac{dTP_1}{dt} &= k_1 T.P_1 - k_{-1} TP_1 - k_2 TP_1 + k_{-2} P_2,\\
\tfrac{dP_2}{dt} &= k_2 TP_1 - k_{-2} P_2 - k_3 P_2 - \beta_3 P_2,\\
\tfrac{dR}{dt} &= \alpha_3 - k_5 R P_{3_nuc} - \beta_4 R,\\
\tfrac{dP_{3_nuc}}{dt} &= k_3 P_2 - k_5\Big(1 - \tfrac{\gamma R}{K+R}\Big) P_{3_nuc} - k_4 \tfrac{R}{K+R} P_{3_nuc} - \beta_5 P_{3_nuc},\\
\tfrac{dP_{3_cyt}}{dt} &= k_4 \tfrac{R}{K+R} P_{3_nuc} - \beta_6 P_{3_cyt},\\
\tfrac{dP_{4_nuc}}{dt} &= k_5\Big(1 - \tfrac{\gamma R}{K+R}\Big) P_{3_nuc} - k_7\Big(1 - \tfrac{\gamma R}{K+R}\Big) P_{4_nuc} - k_6 \tfrac{R}{K+R} P_{4_nuc} - \beta_7 P_{4_nuc},\\
\tfrac{dP_{4_cyt}}{dt} &= k_6 \tfrac{R}{K+R} P_{4_nuc} - \beta_8 P_{4_cyt},\\
\tfrac{dP_{5_nuc}}{dt} &= k_7\Big(1 - \tfrac{\gamma R}{K+R}\Big) P_{4_nuc} - k_8 P_{5_nuc} - \beta_9 P_{5_nuc},\\
\tfrac{dP_{5_cyt}}{dt} &= k_8 P_{5_nuc} - \beta_{10} P_{5_cyt},
\end{aligned} \tag{5.2.1}$$

where $\alpha_i$, $i = \{1, 2, 3\}$ are the rates of production of $P_1, T, R$ and $\beta_j$, $j = \{1, 2, ..., 10\}$ are the natural degradation rates of $P_1, T, P_2, R, P_{3\_nuc}, P_{3\_cyt}, P_{4\_nuc}, P_{4\_cyt}, P_{5\_nuc}$ and $P_{5\_cyt}$ respectively. $K$ is the threshold for half-maximal boosting of the export of 9kb and 4kb mRNA from nucleus to cytoplasm by Rev.

The initial conditions are $P_1(0) = P_{10}, T(0) = T_0, TP_1(0) = TP_{10}, P_2(0) = P_{20}, R(0) = R_0, P_{3\_nuc}(0) = 0, P_{3\_cyt}(0) = 0, P_{4\_nuc}(0) = 0, P_{4\_cyt}(0) = 0, P_{5\_nuc}(0) = 0$, and $P_{5\_cyt}(0) = 0$.

### 5.2.2 Model Properties

#### Non-negativity

In this section, the non-negativity of the solutions of the system (5.2.1) is studied using the following theorem.

**Theorem 5.2.1** *Each solution of the system (5.2.1) with initial conditions, remains non-negative for all* $t \geqslant 0$.

**Proof.** From the first equation of system (5.2.1), one can write,

$$\begin{aligned} \frac{dP_1}{dt} &= \alpha_1 - k_1 T.P_1 + k_{-1} T P_1 - \beta_1 P_1 \\ &> -(k_1 T + \beta_1) P_1 \quad \forall \quad t \in [0, t_1]. \end{aligned} \tag{5.2.2}$$

Hence,

$$P_1(t) > P_1(0) e^{-\int_0^t (k_1 T(T) + \beta_1) dT}, \tag{5.2.3}$$

as $t \in [0, t_1]$ and as long as

$$\int_0^t T(T) dT < +\infty. \tag{5.2.4}$$

Again, from the second equation of system (5.2.1), one can write

$$\begin{aligned} \frac{dT}{dt} &= \alpha_2 - k_1 T.P_1 + k_{-1} T P_1 - \beta_2 T \\ &> -(k_1 P_1 + \beta_2) T \quad \forall \quad t \in [0, t_1]. \end{aligned} \tag{5.2.5}$$

Which implies,

$$T(t) > T(0) e^{-\int_0^t (k_1 P_1(T) + \beta_2) dT}, \tag{5.2.6}$$

as $t \in [0, t_1]$ and as long as

$$\int_0^t P_1(T) dT < +\infty. \tag{5.2.7}$$

In the similar way, one may show that the components $TP_1(t), P_2(t)$, and $R(t)$ of the formulated model are positive for all $t \geqslant 0$. Again from the sixth equation of (5.2.1), one gets

$$\begin{aligned} \frac{dP_{3\_nuc}}{dt} &= k_3 P_2 - k_5 (1 - \frac{\gamma R}{K + R}) P_{3\_nuc} - k_4 \frac{R}{K + R} P_{3\_nuc} - \beta_5 P_{3\_nuc}, \\ &> -(k_5 + k_4 \frac{R}{K + R} + \beta_5) P_{3\_nuc}. \end{aligned} \tag{5.2.8}$$

But the initial value of $P_{3\_nuc}$ is zero. So, one can write,

$$\frac{dP_{3\_nuc}}{dt} \geqslant 0, \tag{5.2.9}$$

which implies,

$$P_{3\_nuc} \geqslant 0. \tag{5.2.10}$$

Similarly, one can show that $P_{3\_cyt}(t), P_{4\_nuc}(t), P_{4\_cyt}(t), P_{5\_nuc}(t), P_{5\_cyt}(t) > 0, \forall t \geqslant 0$. Thus, the non-negativity of the solutions of the system (5.2.1) with the initial conditions is established.

**Boundedness**

In this section, it is shown that the solutions of the system (5.2.1) are bounded, using the following theorem.

**Theorem 5.2.2** *Every solution of the system (5.2.1) with initial conditions, starts in $R_+^{11}$, is uniformly bounded.*

**Proof.** First, we consider that $W_1(t) = P_1(t) + TP_1(t) + P_2(t)$. Then we add the first, third and fourth equations of system (5.2.1), and thus, we get

$$\begin{aligned} \frac{dW_1}{dt} &= \alpha_1 - \beta_1 P_1 - k_3 P_2 - \beta_3 P_2, \\ &> -\beta_1 P_1 - (k_3 + \beta_3) P_2 \\ &> -\delta(P_1 + TP_1 + P_2) \\ &= -\delta W_1. \end{aligned} \tag{5.2.11}$$

This implies that

$$-\delta W_1 < \frac{dW_1}{dt} < 0, \tag{5.2.12}$$

and after integration, one may have

$$(P_{10} + TP_{10} + P_{20})e^{-\delta t} < W_1(t) < (P_{10} + TP_{10} + P_{20}). \tag{5.2.13}$$

From second equation of system (5.2.1), one gets

$$\frac{dT}{dt} = \alpha_2 + k_{-1}TP_1 - k_1T.P_1 - \beta_2T. \tag{5.2.14}$$

Since, $P_1, TP_1$ and $P_2$ are bounded, equation (5.2.14) can be written as

$$\frac{dT}{dt} \leqslant m - nT, \tag{5.2.15}$$

where $m$ and $n$ depend on the bounds of $P_1, TP_1$ and $P_2$.

The Gronwall Lemma guarantees that

$$T(t) \leq \frac{m}{n}(1 - e^{-nt}) + T_0e^{-nt}.$$

Thus, for sufficiently large $t$, one obtains

$$\limsup_{t\to+\infty} T(t) \leqslant \frac{m}{n}.$$

Similarly, from fifth equation of (5.2.1), one can determine

$$\limsup_{t\to+\infty} R(t) = \frac{\alpha_3}{\beta_4}.$$

Now we consider that $W_2(t) = P_{3\_nuc} + P_{3\_cyt} + P_{4\_nuc} + P_{4\_cyt} + P_{5\_nuc} + P_{5\_cyt}$. Then we add the last six equations of system (5.2.1), and obtain the following inequality:

$$\frac{dW_2}{dt} \leq k_3\bar{P}_2 - \beta W_2, \quad \text{where } \beta = min\{\beta_5, \beta_6, \beta_7, \beta_8, \beta_9, \beta_{10}\}.$$

By the Gronwall Lemma, one gets

$$W_2(t) \leq \frac{k_3\bar{P}_2}{\beta}(1 - e^{-\beta t}) + W_2(0)e^{-\beta t}.$$

Solving the above inequality (5.2.16) for sufficiently large $t$, one can get the following result,

$$\limsup_{t\to+\infty} W_2(t) \leq \frac{k_3\bar{P}_2}{\beta}. \tag{5.2.16}$$

Thus, $W_2(t)$ is bounded for all $t$. Therefore, all solutions of the system (5.2.1) are bounded.

### 5.2.3 Equilibrium analysis

The system (5.2.1) has a unique interior equilibrium position $E^*({P_1}^*, T^*, {TP_1}^*, {P_2}^*, R^*, {P_{3\_nuc}}^*, {P_{3\_cyt}}^*, {P_{4\_nuc}}^*, {P_{4\_cyt}}^*, {P_{5\_nuc}}^*, {P_{5\_cyt}}^*)$, which satisfies

$$\begin{aligned}
{P_1}^* &= \tfrac{\alpha_1-(k_3+\beta_3){P_2}^*}{\beta_1},\\
T^* &= \tfrac{\alpha_2-(k_3+\beta_3){P_2}^*}{\beta_2},\\
{TP_1}^* &= \tfrac{(k_{-2}+k_3+\beta_3){P_2}^*}{k_2},\\
R^* &= \tfrac{\alpha_3}{k_5{P_{3_nuc}}^*+\beta_4},\\
{P_{3_cyt}}^* &= \tfrac{k_4 f(R^*)}{\beta_6}{P_{3_nuc}}^*,\\
{P_{5_nuc}}^* &= \tfrac{k_7(1-\gamma f(R^*))}{k_8+\beta_9}{P_{4_nuc}}^*,\\
{P_{5_cyt}}^* &= \tfrac{k_7k_8(1-\gamma f(R^*))}{\beta_{10}(k_8+\beta_9)}{P_{4_nuc}}^*,\\
{P_{4_nuc}}^* &= \tfrac{k_5(1-\gamma f(R^*))}{k_7(1-\gamma f(R^*))+k_6 f(R^*)+\beta_7}{P_{3_nuc}}^*,\\
{P_{4_cyt}}^* &= \tfrac{k_6 f(R^*)}{\beta_8}{P_{4_nuc}}^*,
\end{aligned}$$

where $f(R^*) = \frac{R^*}{K+R^*}$. Here ${P_2}^*$, ${P_{3\_nuc}}^*$ satisfy the following quadratic equations respectively:

$${P_2}^{*2} - \left\{\frac{\alpha_1+\alpha_2}{k_3+\beta_3} + \frac{\beta_1\beta_2k_{-1}k_{-2}}{k_1k_2(k_3+\beta_3)^2} + \frac{\beta_1\beta_2(k_{-1}+k_2)}{k_1k_2(k_3+\beta_3)}\right\}{P_2}^* + \frac{\alpha_1\alpha_2}{(k_3+\beta_3)^2} = 0,$$

and

$$Kk_5(k_5+\beta_5){P_{3\_nuc}}^{*2} + (Z - Kk_3k_5{P_2}^*){P_{3\_nuc}}^* - (K\beta_4+\alpha_3)k_3{P_2}^* = 0,$$

where $Z = K(k_5+\beta_5)\beta_4 + \alpha_3\{(k_5+\beta_5) + k_4 - \gamma k_5\}$. The above quadratic equations always have a unique positive real root.

The Jacobin matrix at the unique interior equilibrium $E^*$ is

$$J = \begin{bmatrix} J_1 & 0 \\ J_2 & J_3 \end{bmatrix},$$

where

$$J_1 = \begin{bmatrix} A_{11} & 0 \\ B_{11} & C_{11} \end{bmatrix},$$

$$J_2 = \begin{bmatrix} 0 & 0 & 0 & 0 & \frac{Kk_4{P_{3\_nuc}}^*}{(K+R^*)^2} & \frac{k_4R^*}{K+R^*} \\ 0 & 0 & 0 & 0 & \left({P_{4\_nuc}}^*(k_7\gamma - k_6) - k_5\gamma {P_{3\_nuc}}^*\right)\frac{K}{(K+R^*)^2} & k_5\left(1 - \frac{\gamma R^*}{K+R^*}\right) \\ 0 & 0 & 0 & 0 & \frac{Kk_6{P_{4\_nuc}}^*}{(K+R^*)^2} & 0 \\ 0 & 0 & 0 & 0 & -\frac{Kk_7\gamma {P_{4\_nuc}}^*}{(K+R^*)^2} & 0 \\ 0 & 0 & 0 & 0 & 0 & 0 \end{bmatrix},$$

and

$$J_3 = \begin{bmatrix} -\beta_6 & 0 & 0 & 0 & 0 \\ 0 & \frac{(k_7\gamma - k_6)R^*}{K+R^*} - (k_7 + \beta_7) & 0 & 0 & 0 \\ 0 & \frac{k_6R^*}{K+R^*} & -\beta_8 & 0 & 0 \\ 0 & k_7\left(1 - \frac{\gamma R^*}{K+R^*}\right) & 0 & -(k_8 + \beta_9) & 0 \\ 0 & 0 & 0 & k_8 & -\beta_{10} \end{bmatrix}.$$

Therefore, we get a block diagonal matrix $J_1$, where

$$A_{11} = \begin{bmatrix} -k_1T^* - \beta_1 & -k_1{P_1}^* & k_{-1} & 0 \\ -k_1T^* & -k_1{P_1}^* - \beta_2 & k_{-1} & 0 \\ k_1T^* & k_1{P_1}^* & -k_{-1} - k_2 & k_{-2} \\ 0 & 0 & k_2 & -(k_{-2} + k_3 + \beta_3) \end{bmatrix},$$

$$B_{11} = \begin{bmatrix} 0 & 0 & 0 & 0 \\ 0 & 0 & 0 & k_3 \end{bmatrix},$$

and

$$C_{11} = \begin{bmatrix} -k_5{P_{3\_nuc}}^* - \beta_4 & -k_5R^* \\ \frac{K{P_{3\_nuc}}^*(k_5\gamma - k_4)}{(K+R^*)^2} & \frac{R^*(k_5\gamma - k_4)}{K+R^*} - (k_5 + \beta_5) \end{bmatrix}.$$

From these block diagonal matrices, it is evident that all the eigenvalues of the Jacobian matrix are either negative or possess a negative real part. Therefore the interior equilibrium $E^*$ is locally asymptotically stable.

## 5.3 Optimal Control Theoretic Approach

Optimal control is a well-established mathematical tool which deals with systems that can be controlled. By optimizing a particular performance, one may usually solve these types of problems through finding the time dependent values of the control parameter (Fleming and Rishel, 1975; Grigorieva et al., 2013, 2014). In the formulated mathematical model (5.2.1), it is described that the viral protein Tat ($T$) plays a dominating role in HIV-1 transcription by making Tat-TAR complex ($TP_1$) which yields an elongating complex ($P_2$) that finally transforms into 9kb messenger RNA ($P_{3\_nuc}$) in the nucleus. Besides, Rev dependent nuclear export of 9kb and 4kb messenger RNA is an essential part of HIV-1 life-cycle. Hence, to control the transcription process, one needs to minimize the production of messenger RNA ($P_{3\_nuc}$) as well as to reduce the transportation of 9kb and 4kb mRNA from nucleus to cytoplasm by Rev. Therefore, it is required to suppress the biochemical reaction between the viral protein Tat ($T$) and the TAR ($P_1$) element and to control the Rev-mediated nuclear export of 9kb, 4kb mRNA. In this section, the formulated model is analysed with two additional control parameters, denoted by $u_1(t)$ and $u_2(t)$, one of which is the effect of Tat inhibitor and another one is Rev inhibitor. Treatment with Tat inhibitor has a significant effect on disrupting the Tat/TAR interaction by directly binding to Tat and hence reduces the production of elongation complex ($P_2$). Therefore, the Tat inhibitor indirectly helps to suppress the formation of 9kb messenger RNA ($P_{3\_nuc}$). Thus the same control profile ($u_1(t)$) is considered with the messenger RNA synthesis term. On the other hand, Rev inhibitor disrupts the reaction pathway for transportation of 9kb, 4kb mRNA from nucleus to cytoplasm by Rev, thereby reducing the concentration of 9kb, 4kb mRNA in the cell cytoplasm. One may consider the set $\Omega$ of admissible controls consists of all Lebesgue measurable functions $(u_1(t), u_2(t))$, which for almost all values of $t$ from the fixed time interval $[t_0, t_f]$ satisfy the following inequality:

$$0 \leq u_1(t) \leq u_1^{max} < 1, \quad 0 \leq u_2(t) \leq u_2^{max} < 1. \tag{5.3.1}$$

For the set $\Omega$, the objective function is defined as

$$J(u_1(.), u_2(.)) = \int_{t_0}^{t_f} [A_1 P_{3\_nuc}(t) + A_2 P_{3\_cyt}(t) + A_3 P_{4\_cyt}(t) + \{B_1 u_1^2(t) + B_2 u_2^2(t)\}]dt, \tag{5.3.2}$$

where, $A_2 P_{3\_cyt}(t) + A_3 P_{4\_cyt}(t)$ represents the number of transported 9kb and 4kb messenger RNAs from cell nucleus to cell cytoplasm by Rev during treatment. The objective function (5.3.2) expresses the present goal to minimize the cost for combined biologic therapy in continuous way while minimizing the production of 9kb messenger RNA ($P_{3\_nuc}$) in the cell nucleus and reducing the nuclear export of 9kb, 4kb messenger RNA to the cytoplasm. The parameters $A_1$, $A_2$, $A_3$ represent weight constants of the 9kb mRNA ($P_{3\_nuc}$)in nucleus, 9kb mRNA ($P_{3\_cyt}$), and 4kb mRNA ($P_{4\_cyt}$) in cytoplasm respectively. $B_1 \geq 0$, $B_2 \geq 0$ are weight constants for Tat inhibitor and Rev inhibitor, respectively. Therefore, for (5.3.2) one may seek a pair of optimal controls $u_1^*(t)$ and $u_2^*(t)$ such that

$$\min_{u(.)\in\Omega} J(u_1(.), u_2(.)) = J(u_1^*, u_2^*). \tag{5.3.3}$$

Taking into account the above assumptions, one can consider a control problem (5.3.3) together with mathematical model (5.2.1) such that:

$$\begin{aligned}
\tfrac{dP_1}{dt} &= \alpha_1 - k_1 T.P_1 + k_{-1} TP_1 - \beta_1 P_1,\\
\tfrac{dT}{dt} &= \alpha_2 - k_1 T.P_1 + k_{-1} TP_1 - \beta_2 T,\\
\tfrac{dTP_1}{dt} &= k_1 T.P_1 - k_{-1} TP_1 - k_2 TP_1 + k_{-2} P_2,\\
\tfrac{dP_2}{dt} &= k_2(1-u_1)TP_1 - k_{-2} P_2 - k_3 P_2 - \beta_3 P_2,\\
\tfrac{dR}{dt} &= \alpha_3 - k_5 R P_{3_nuc} - \beta_4 R,\\
\tfrac{dP_{3_nuc}}{dt} &= k_3(1-u_1)P_2 - k_5\Big(1 - \tfrac{\gamma R}{K+R}\Big)P_{3_nuc} - k_4 \tfrac{R}{K+R} P_{3_nuc} - \beta_5 P_{3_nuc},\\
\tfrac{dP_{3_cyt}}{dt} &= k_4(1-u_2)\tfrac{R}{K+R} P_{3_nuc} - \beta_6 P_{3_cyt},\\
\tfrac{dP_{4_nuc}}{dt} &= k_5\Big(1 - \tfrac{\gamma R}{K+R}\Big)P_{3_nuc} - k_7\Big(1 - \tfrac{\gamma R}{K+R}\Big)P_{4_nuc} - k_6 \tfrac{R}{K+R} P_{4_nuc} - \beta_7 P_{4_nuc},\\
\tfrac{dP_{4_cyt}}{dt} &= k_6(1-u_2)\tfrac{R}{K+R} P_{4_nuc} - \beta_8 P_{4_cyt},\\
\tfrac{dP_{5_nuc}}{dt} &= k_7\Big(1 - \tfrac{\gamma R}{K+R}\Big)P_{4_nuc} - k_8 P_{5_nuc} - \beta_9 P_{5_nuc},\\
\tfrac{dP_{5_cyt}}{dt} &= k_8 P_{5_nuc} - \beta_{10} P_{5_cyt},
\end{aligned}$$

with known initial values for $P_1(t), T(t), TP_1(t), P_2(t), R(t), P_{3\_nuc}(t), P_{3\_cyt}(t)$, $P_{4\_nuc}(t), P_{4\_cyt}(t), P_{5\_nuc}(t)$, and $P_{5\_cyt}(t)$ at $t_0$.

### 5.3.1 Dynamics of the Optimal System

Here Pontryagin Maximum Principle (Bonnans and Hermant, 2009; Pontryagin, 1987) is used to obtain $u_1^*(t)$, $u_2^*(t)$. For the present optimal control system, we define the Hamiltonian as follows:

$$\begin{aligned} H &= -\{A_1 P_3\_nuc + A_2 P_3\_cyt + A_3 P_4\_cyt + B_1 u_1^2 + B_2 u_2^2\} \\ &\quad +\xi_1(\alpha_1 - k_1 T.P_1 + K_{-1} T P_1 - \beta_1 P_1) + \xi_2(\alpha_2 - k_1 T.P_1 + k_{-1} T P_1 - \beta_2 T) \\ &\quad +\xi_3(k_1 T.P_1 - k_{-1} T P_1 - k_2 T P_1 + k_{-2} P_2) \\ &\quad +\xi_4\Big(k_2(1-u_1) T P_1 - (k_{-2} + k_3 + \beta_3) P_2\Big) \\ &\quad +\xi_5(\alpha_3 - k_5 R P_3\_nuc - \beta_4 R) \\ &\quad +\xi_6\Big(k_3(1-u_1) P_2 - k_5(1 - \tfrac{\gamma R}{K+R}) P_3\_nuc - (k_4 \tfrac{R}{K+R} + \beta_5) P_3\_nuc\Big) \\ &\quad +\xi_7\Big(k_4(1-u_2)\tfrac{R}{K+R} P_3\_nuc - \beta_6 P_3\_cyt\Big) \\ &\quad +\xi_8\Big(k_5(1 - \tfrac{\gamma R}{K+R}) P_3\_nuc - \Big(k_7(1 - \tfrac{\gamma R}{K+R}) + k_6 \tfrac{R}{K+R} + \beta_7\Big) P_4\_nuc\Big) \\ &\quad +\xi_9\Big(k_6(1-u_2)\tfrac{R}{K+R} P_4\_nuc - \beta_8 P_4\_cyt\Big) \\ &\quad +\xi_{10}\Big(k_7(1 - \tfrac{\gamma R}{K+R}) P_4\_nuc - (k_8 + \beta_9) P_5\_nuc\Big) \\ &\quad +\xi_{11}(k_8 P_5\_nuc - \beta_{10} P_5\_cyt), \end{aligned} \tag{5.3.4}$$

where $\xi_1, \xi_2, ..., \xi_{11}$ are Lagrange multipliers. According to the Pontryagin Maximum principle and the necessary optimality conditions for the present optimal control problem, one may obtain the theorem stated below:

**Theorem 5.3.1** *If the objective cost function $J(u_1, u_2)$ obtains its minimum for the optimal control $u_1^*$, $u_2^*$ and $P_1^*, T^*, TP_1{}^*, P_2{}^*, R^*, P_3\_nuc^*, P_3\_cyt^*, P_4\_nuc^*, P_4\_cyt^*, P_5\_nuc^*, P_5\_cyt^*$ be the corresponding optimal state, then there exists adjoint functions $\xi_1, \xi_2, \xi_3, \xi_4, \xi_5, \xi_6, \xi_7$, $\xi_8, \xi_9, \xi_{10}, \xi_{11}$ satisfying the following equations:*

$$
\begin{aligned}
\tfrac{d\xi_1}{dt} &= \xi_1(k_1T+\beta_1)+\xi_2k_1T-\xi_3k_1T,\\
\tfrac{d\xi_2}{dt} &= \xi_1k_1P_1+\xi_2(k_1P_1+\beta_2)-\xi_3k_1P_1,\\
\tfrac{d\xi_3}{dt} &= -\xi_3k_{-1}-\xi_2k_{-1}+\xi_3(k_{-1}+k_2)-\xi_4(k_2(1-u_1)),\\
\tfrac{d\xi_4}{dt} &= -\xi_3k_{-2}+\xi_4(k_{-2}+k_3+\beta_3)-\xi_6(k_3(1-u_1)),\\
\tfrac{d\xi_5}{dt} &= \xi_5(k_5P_{3_{nuc}}+\beta_4)-\xi_6\Big((k_5-k_4)P_{3_{nuc}}\tfrac{K}{(K+R)^2}\Big)-\xi_7\Big(k_4(1-u_2)P_{3_{nuc}}\tfrac{k}{(K+R)^2}\Big)\\
&- \xi_8\Big((-k_5P_{3_{nuc}}+(k_7-k_6)P_{4_{nuc}})\tfrac{K}{(K+R)^2}\Big)-\xi_9\Big(k_6(1-u_2)P_{4_{nuc}}\tfrac{K}{(K+R)^2}\Big)\\
&+ \xi_{10}k_7P_{4_{nuc}}\tfrac{K}{(K+R)^2},\\
\tfrac{d\xi_6}{dt} &= A_1+\xi_5k_5R+\xi_6\Big((1-\tfrac{\gamma R}{K+R})(k_5-\xi_8k_5)+(k_4-\xi_7k_4(1-u_2))\tfrac{R}{K+R}\Big),\\
\tfrac{d\xi_7}{dt} &= A_2+\xi_7\beta_6,\\
\tfrac{d\xi_8}{dt} &= \xi_8\Big(k_7(1-\tfrac{\gamma R}{K+R})+k_6\tfrac{R}{K+R}+\beta_7\Big)-\xi_9\Big(k_6(1-u_2)\tfrac{R}{K+R}\Big)-\xi_{10}k_7\Big(1-\tfrac{\gamma R}{K+R}\Big),\\
\tfrac{d\xi_9}{dt} &= A_3+\xi_9\beta_8,\\
\tfrac{d\xi_{10}}{dt} &= \xi_{10}(k_8+\beta_9)-\xi_{11}k_8,\\
\tfrac{d\xi_{11}}{dt} &= \xi_{11}\beta_{10},
\end{aligned}
$$

*with the transversality conditions* $\xi_i(t_f)=0$, *for* $i=\{1,...,11\}$. *Moreover, the optimal controls are given by*

$$
u_1^*(t)=\begin{cases}0, & \text{if } \phi_1(t)<0,\\ \phi_1(t), & \text{if } 0\leqslant\phi_1(t)\leqslant u_1^{max},\\ u_1^{max}, & \text{if } \phi_1>u_1^{max},\end{cases}
$$

$$
u_2^*(t)=\begin{cases}0, & \text{if } \phi_2(t)<0,\\ \phi_2(t), & \text{if } 0\leqslant\phi_2(t)\leqslant u_2^{max},\\ u_2^{max}, & \text{if } \phi_2>u_2^{max}.\end{cases}
$$

**Proof.** The Pontryagin Maxiimum Principle affirms that the solution to the optimal

control problem satisfies the adjoint equations

$$\frac{d\xi_1}{dt} = -\frac{\partial H}{\partial P_1}, \frac{d\xi_2}{dt} = -\frac{\partial H}{\partial T}, \frac{d\xi_3}{dt} = -\frac{\partial H}{\partial TP_1}, \frac{d\xi_4}{dt} = -\frac{\partial H}{\partial P_2}, \frac{d\xi_5}{dt} = -\frac{\partial H}{\partial R}, \frac{d\xi_6}{dt} = -\frac{\partial H}{\partial P_3\_nuc},$$
$$\frac{d\xi_7}{dt} = -\frac{\partial H}{\partial P_3\_cyt}, \frac{d\xi_8}{dt} = -\frac{\partial H}{\partial P_4\_nuc}, \frac{d\xi_9}{dt} = -\frac{\partial H}{\partial P_4\_cyt}, \frac{d\xi_{10}}{dt} = -\frac{\partial H}{\partial P_5\_nuc}, \frac{d\xi_{11}}{dt} = -\frac{\partial H}{\partial P_5\_cyt},$$

and the transversality conditions $\xi_i(t_f) = 0$, for $i = \{1, ..., 11\}$.

Besides, according to the Pontryagin Maximum Principal, the Hamiltonian $H$ is maximized with respect to $u_1$ and $u_2$ at the optimal value $u_1^*$, $u_2^*$ respectively. Therefore, the derivative of $H$ with respect to $u_1$, $u_2$ must be equal to zero at $u_1^*$, $u_2^*$.
Again, $H$ can be expressed as:

$$\begin{aligned}
H &= -B_1u_1^2 - B_2u_2^2 + \xi_4k_2(1-u_1)TP_1 + \xi_6k_3(1-u_1)P_2 + \xi_7k_4(1-u_2)\frac{R}{K+R}P_3_nuc \\
&+\xi_9\Big(k_6(1-u_2)\frac{R}{K+R}P_4_nuc\Big) + \xi_1(\alpha_1 - k_1T.P_1 + k_{-1}TP_1 - \beta_1P_1) \\
&+\xi_2(\alpha_2 - k_1T.P_1 + k_{-1}TP_1 - \beta_2T) + \xi_3(k_1T.P_1 - k_{-1}TP_1 - k_2TP_1 + k_{-2}P_2) \\
&-\xi_4(k_{-2} + k_3 + \beta_3)P_2 + \xi_5(\alpha_3 - k_5RP_3_nuc - \beta_4R) \\
&-\xi_6\Big(k_5(1 - \frac{\gamma R}{K+R}) + k_4\frac{R}{K+R} + \beta_5\Big)P_3_nuc - \xi_7\beta_6P_3_cyt \\
&+\xi_8\Big(k_5(1 - \frac{\gamma R}{K+R})P_3_nuc - \Big(k_7(1 - \frac{\gamma R}{K+R}) + k_6\frac{R}{K+R} + \beta_7\Big)P_4_nuc\Big) \\
&-\xi_9\beta_8P_4_cyt + \xi_{10}\Big(k_7(1 - \frac{\gamma R}{K+R})P_4_nuc - (k_8 + \beta_9)P_5_nuc\Big) \\
&+\xi_{11}(k_8P_5_nuc - \beta_{10}P_5_cyt) - A_1P_3_nuc - A_2P_3_cyt - A_3P_4_cyt.
\end{aligned}$$

Now, taking partial differentiation of the above expression for $H$ with respect to $u_1$ and $u_2$ respectively, one gets

$$\frac{\partial H}{\partial u_1} = -2B_1u_1 - \xi_4k_2TP_1 - \xi_6k_3P_2, \tag{5.3.5}$$
$$\frac{\partial H}{\partial u_2} = -2B_2u_2 - \xi_7k_4\frac{R}{K+R}P_3\_nuc - \xi_9k_6\frac{R}{K+R}P_4\_nuc. \tag{5.3.6}$$

Now, according to the first-order necessary condition for optimality, the derivatives of $H$ with respect to $u_1$ and $u_2$ expressed by above equations must be equal to zero at $u_1^*$,

$u_2^*$. Hence, the following relationships hold:

$$u_1^*(t) = \begin{cases} 0, & \text{if } \phi_1(t) < 0, \\ \phi_1(t), & \text{if } 0 \leqslant \phi_1(t) \leqslant u_1^{max}, \\ u_1^{max}, & \text{if } \phi_1 > u_1^{max}, \end{cases}$$

and

$$u_2^*(t) = \begin{cases} 0, & \text{if } \phi_2(t) < 0, \\ \phi_2(t), & \text{if } 0 \leqslant \phi_2(t) \leqslant u_2^{max}, \\ u_2^{max}, & \text{if } \phi_2 > u_2^{max}. \end{cases}$$

Here the functions $\phi_1(t)$, $\phi_2(t)$ are the indicator functions. The functions are as follows:

$$\begin{aligned} \phi_1(t) &= -\frac{1}{2B_1}\Big(\xi_4 k_2 T {P_1}^* + \xi_6 k_3 {P_2}^*\Big), \\ \phi_2(t) &= -\frac{1}{2B_2}\Big((\xi_7 k_4 + \xi_9 k_6)\frac{R^*}{K + R^*} P_{3\_}nuc^*\Big). \end{aligned}$$

This completes the proof.

## 5.4 Results and Discussion

To illustrate the behaviour of the present models (5.2.1) and (5.3.4), numerical simulations are performed with the set of parameter values in Table 5.1. Some of these values are estimated from (Carlotti et al., 2000; Kim and Yin, 2005; Likhoshvai et al, 2014; Mohammadi et al., 2013; Reddy and Yin, 1999; Robert-Guroff et al., 1990; Shcherbatova et al., 2020; Siliciano et al., 2003; Slice et al., 1992), while some parameter values are partially assumed. The current numerical study was conducted using MATLAB 2016A.

In Figure (5.3), we plot the phase portraits of model (5.2.1) for different initial values of model compartments. Figure (5.3)(A) illustrates that for different initial values of TAR-RNA Polymerase II elongation complex ($P_1(t)$), Tat-TAR complex ($TP_1(t)$), and 9kb mRNA in nucleus ($P_{3\_}nuc(t)$), the trajectories converge to a unique point ($P_1^*$, $P_2^*$, $P_{3\_}nuc^*$). Similarly, in Figure (5.3)(B), we see that the trajectories of DNA

Table 5.1: List of parameters for models (5.2.1) and (5.3.4).

| Parameter | Parameter description | Value (Unit) |
|---|---|---|
| $k_1$ | The rate of forward reaction from $P_1$ to $TP_1$ | $(0.8 - 4.2)\ hr^{-1}$ |
| $k_{-1}$ | The rate of backward reaction from $TP_1$ to $P_1$ | $(0.01 - 0.3)\ hr^{-1}$ |
| $k_2$ | The rate of forward reaction from $TP_1$ to $P_2$ | $(0.8 - 3.8)\ hr^{-1}$ |
| $k_{-2}$ | The rate of backward reaction from $P_2$ to $TP_1$ | $(0.01 - 0.4)\ hr^{-1}$ |
| $k_3$ | The rate of forward reaction from $P_2$ to $P_{3\_nuc}$ | $(0.2 - 5.0)\ hr^{-1}$ |
| $k_4$ | The rate of forward reaction from $P_{3\_nuc}$ to $P_{3\_cyt}$ | $(1.5 - 4.8)\ hr^{-1}$ |
| $k_5$ | The rate of forward reaction from $P_{3\_nuc}$ to $P_{4\_nuc}$ | $(2.0 - 5.0)\ hr^{-1}$ |
| $k_6$ | The rate of forward reaction from $P_{4\_nuc}$ to $P_{4\_cyt}$ | $(1.5 - 4.8)\ hr^{-1}$ |
| $k_7$ | The rate of forward reaction from $P_{4\_nuc}$ to $P_{5\_nuc}$ | $(2.0 - 5.0)\ hr^{-1}$ |
| $k_8$ | The rate of forward reaction from $P_{5\_nuc}$ to $P_{5\_cyt}$ | $(2.5 - 6.0)\ hr^{-1}$ |
| $K$ | Threshold for half-maximal boosting of the export of $P_{3\_nuc}$ and $P_{4\_nuc}$ | $(0.05 - 3.0)\ \mu M$ |
| $\gamma$ | Inhibitory effect of Rev | $(0.5 - 1.5)$ |
| $\alpha_1$ | Accumulation rate of $P_1$ | $(1.0 - 4.5)\ hr^{-1}$ |
| $\alpha_2$ | Synthesis rate of $T$ | $(0.5 - 2.0)\ hr^{-1}$ |
| $\alpha_3$ | Synthesis rate of $R$ | $(0.3 - 3.5)\ hr^{-1}$ |
| $\beta_1$ | Degradation rate of $P_1$ | $(0.02 - 0.5)\ hr^{-1}$ |
| $\beta_2$ | Degradation rate of $T$ | $(0.01 - 0.4)\ hr^{-1}$ |
| $\beta_3$ | Degradation rate of $P_2$ | $(0.001 - 0.2)\ hr^{-1}$ |
| $\beta_4$ | Degradation rate of $R$ | $(0.04 - 0.45)\ hr^{-1}$ |
| $\beta_5$ | Degradation rate of $P_{3\_nuc}$ | $(0.01 - 0.65)\ hr^{-1}$ |
| $\beta_6$ | Degradation rate of $P_{3\_cyt}$ | $(0.02 - 0.7)\ hr^{-1}$ |
| $\beta_7$ | Degradation rate of $P_{4\_nuc}$ | $(0.07 - 0.65)\ hr^{-1}$ |
| $\beta_8$ | Degradation rate of $P_{4\_cyt}$ | $(0.04 - 0.6)\ hr^{-1}$ |
| $\beta_9$ | Degradation rate of $P_{5\_nuc}$ | $(0.07 - 0.25)\ hr^{-1}$ |
| $\beta_{10}$ | Degradation rate of $P_{5\_cyt}$ | $(0.05 - 0.25)\ hr^{-1}$ |

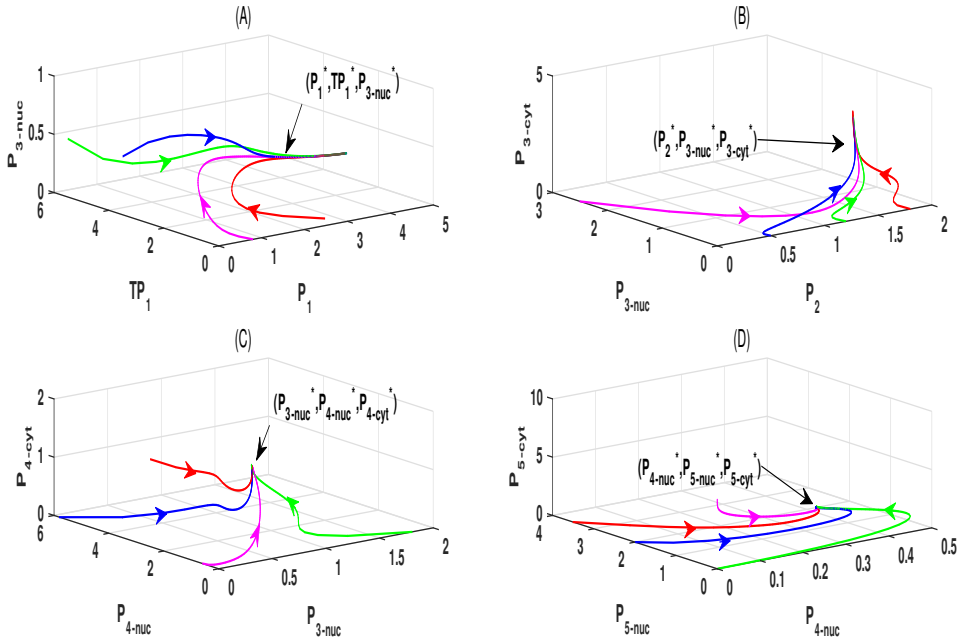


Figure 5.3: Stability analysis using different reaction compartments and finding the interior equilibrium $E^*$ of system dynamics: (A) considering three components TAR-RNA polymerase II elongation complex, Tat-TAR complex, 9kb mRNA in nucleus; (B) considering three components DNA unit_RNA polymerase II_elongation complex, 9kb mRNA in nucleus, 9kb RNA in cytoplasm; (C) considering three compartments 9kb mRNA in nucleus, 4kb mRNA in nucleus, 4kb mRNA in cytoplasm; (D) considering three reactants 4kb mRNA in nucleus, 2kb mRNA in nucleus, 2kb mRNA in cytoplasm. Here We use $P_1(0) = 3.8\mu M$, $T(0) = 2\mu M$, $TP_1(0) = 1.2\mu M$, $P_2(0) = 1.2\mu M$, $R(0) = 2\mu M$ as initial values. The model parameter values are taken from Table 5.1.

unit_RNA polymerase II_elongation complex ($P_2(t)$), 9kb mRNA ($P_3\_nuc(t)$) in nucleus and 9kb mRNA ($P_3\_cyt(t)$) in cytoplasm also converge to a unique point ($P_2^*$, $P_3\_nuc^*$, $P_3\_cyt^*$). Also in figure (5.3)(C), the trajectories of 9kb mRNA ($P_3\_nuc(t)$) in nucleus , 4kb mRNA ($P_4\_nuc(t)$) in nucleus, 4kb mRNA ($P_4\_cyt(t)$) in cytoplasm converge towards the unique positive equilibrium densities $P_3\_nuc^*$, $P_4\_nuc^*$, $P_4\_cyt^*$ respectively. Similarly, in figure (5.3)(D), we can notice that the trajectories of 4kb mRNA ($P_4\_nuc(t)$) in nucleus, 2kb mRNA ($P_5\_nuc(t)$) in nucleus, and 2kb mRNA ($P_5\_cyt(t)$) in cytoplasm converge towards the unique positive equilibrium densities $P_4\_nuc^*$, $P_5\_nuc^*$, $P_5\_cyt^*$ respectively. This shows the existence of nonlinear stability of $E^*$.

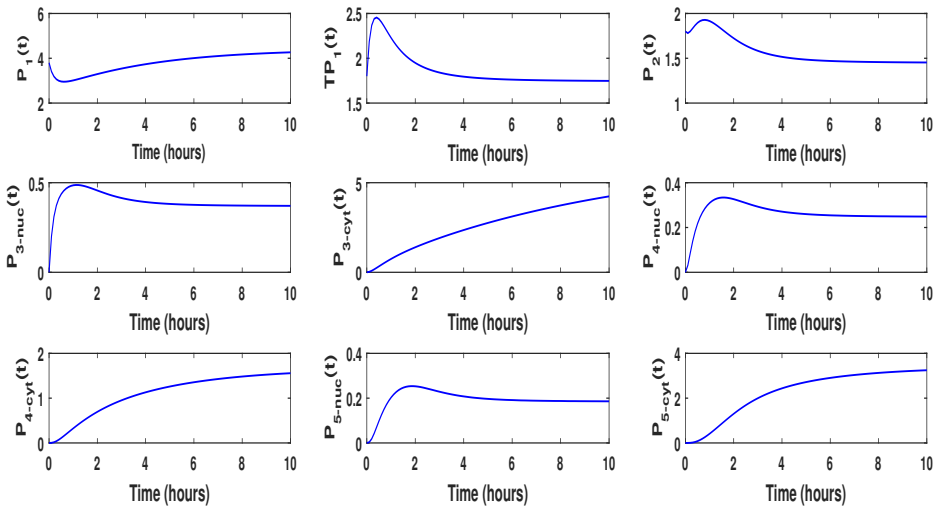


Figure 5.4: The nature of the curves of reactants during HIV-1 transcription, using $P_1(0) = 3.8\mu M$, $T(0) = 2\mu M$, $TP_1(0) = 1.2\mu M$, $P_2(0) = 1.2\mu M$, $R(0) = 2\mu M$, as initial values. The model parameter values are taken from Table 5.1.

Figure (5.4) illustrates the dynamics of the HIV-1 Tat and Rev-mediated transcription process in patients infected with HIV-1. During the transcription of HIV-1, the viral Tat protein binds to the TAR element at the TAR-RNA polymerase II elongation stage ($P_1$), resulting in the formation of the Tat-TAR complex ($TP_1$). As a result, the concentration of the $P_1$ complex decreases while the concentration of the Tat-TAR complex ($TP_1$) increases over time at a specific rate. Subsequently, the Tat-TAR complex ($TP_1$) is converted into the DNA unit RNA polymerase II elongation complex ($P_2$), with a small fraction of the Tat-TAR complex reverting back to the $P_1$ complex. Consequently, the concentration of complex $P_1$ begins to rise, while the concentration of the Tat-TAR complex ($TP_1$) declines. Additionally, the DNA unit RNA polymerase II elongation complex ($P_2$) converts into 9kb unspliced messenger RNA ($P_{3\_nuc}$) within the nucleus of the host cell. A small fraction of the elongating complex $P_2$ reverts to the Tat-TAR complex $TP_1$, resulting in a concentration curve for $P_2$ that mirrors that of $TP_1$. The unspliced 9kb messenger RNA ($P_{3\_nuc}$) is subsequently processed into 4kb singly-spliced messenger RNA ($P_{3\_nuc}$), which is then transformed into 2kb

doubly-spliced messenger RNA ($P_{5\_nuc}$) within the host cell nucleus. Furthermore, both the unspliced 9kb messenger RNA ($P_{3\_nuc}$) and the 4kb singly-spliced messenger RNA ($P_{4\_nuc}$) are transported to the cell cytoplasm with the assistance of the HIV-1 protein Rev. Consequently, the concentrations of $P_{3\_nuc}$ and $P_{4\_nuc}$ begin to decline over time. As the viral Rev protein inhibits the splicing of both the 9kb and 4kb messenger RNAs, the rate of decrease in the concentrations of $P_{3\_nuc}$ and $P_{4\_nuc}$ slows, leading to similar trends in both compartments. In the case of $P_{3\_cyt}$, $P_{4\_cyt}$, and $P_{5\_cyt}$, one may observe analogous nature of the components ($P_{3\_cyt}$; $P_{4\_cyt}$; $P_{5\_cyt}$) participating in HIV-1 transcription.

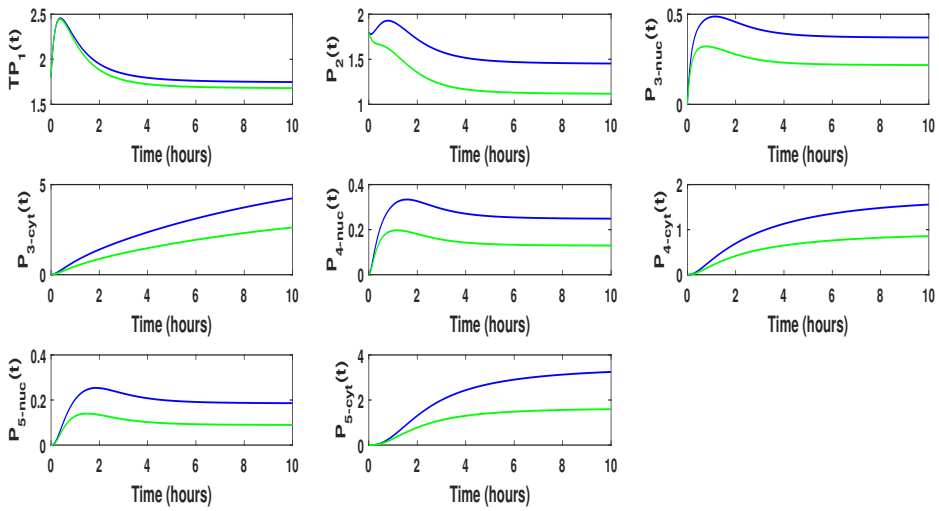


Figure 5.5: The nature of the curves of reactants with and without control, using $P_1(0) = 3.8\mu M$, $T(0) = 2\mu M$, $TP_1(0) = 1.2\mu M$, $P_2(0) = 1.2\mu M$, $R(0) = 2\mu M$, as initial values. The model parameter values are taken from Table 5.1.

Figure (5.5) represents the changes in reactant concentrations over time ($t$) for both controlled and uncontrolled scenarios. It is evident that upon the introduction of the control input ($u_1(t)$), the progress curves for the elongating complex $P_2$ and the 9kb unspliced messenger RNA ($P_{3\_nuc}$) exhibit a slower rate of increase compared to the uncontrolled reaction. The application of control therapy leads to a decrease in the formation of the elongating complex ($P_2(t)$), which in turn results in a similar decline in

the progress curves for the 9kb RNA ($P_{3\_nuc}(t)$), as well as the 4kb singly-spliced RNA ($P_{4\_nuc}(t)$) and the 2kb doubly-spliced messenger RNA ($P_{5\_nuc}(t)$). Additionally, Figure (5.5) shows that the concentrations of unspliced 9kb messenger RNA and 4kb singly-spliced messenger RNA in the cell cytoplasm decrease following the application of the control input ($u_2(t)$). This figure indicates that the Tat inhibitor is crucial in suppressing HIV-1 transcription by decreasing the production of mature 9kb messenger RNA ($P_{3\_nuc}(t)$). In contrast, the Rev inhibitor effectively blocks the cytoplasmic transport of both 9kb and 4kb mRNA, which is highly beneficial for patients infected with HIV-1.

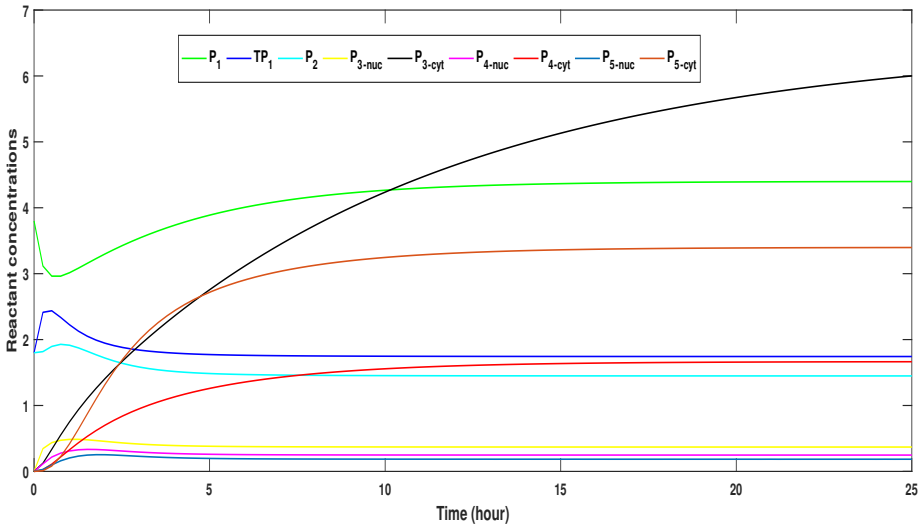


Figure 5.6: Persistence of the system (5.2.1). The initial conditions and parameter values are same as Fig. 5.5.

Figure 5.6 depicts the changes in reactant concentrations over time in a single illustration, showing that the reactants do not reach extinction, which confirms the persistence of system (5.2.1).

Figure 5.7 illustrates the qualitative patterns of concentration curves for the Tat-TAR complex ($TP_1(t)$), DNA unit_RNA polymerase II_elongation complex ($P_2(t)$), 9kb mRNA ($P_3\_nuc(t)$) in nucleus, 9kb mRNA ($P_3\_cyt(t)$) in cytoplasm, 4kb mRNA ($P_4\_nuc(t)$) in nucleus, 4kb mRNA ($P_3\_cyt(t)$) in cytoplasm, 2kb mRNA

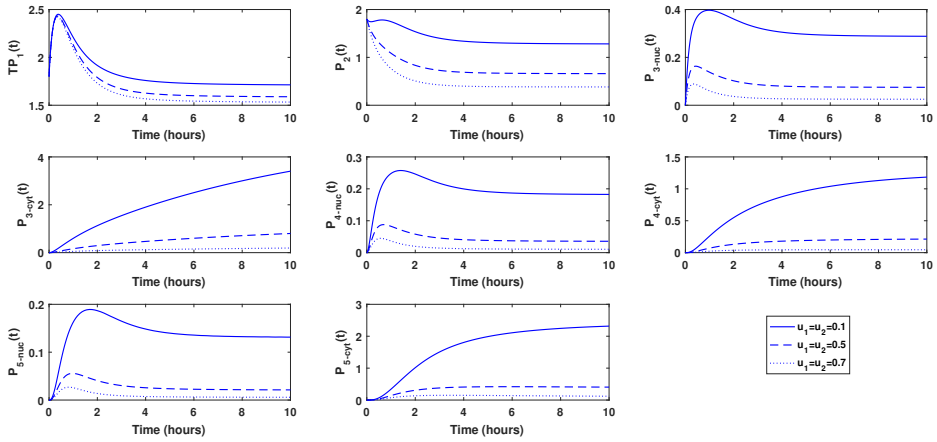


Figure 5.7: Qualitative behavior of the components Tat-TAR complex, DNA unit_RNA polymerase II_ elongation complex, 9kb mRNA in nucleus, 9kb mRNA in cytoplasm, 4kb mRNA in nucleus, 4kb mRNA in cytoplasm, 2kb mRNA in nucleus and 2kb mRNA in cytoplasm using three different values of $u_1$ and $u_2$ respectively, considering model (5.3.4). The parameter values are the same as in Table 5.1.

($P_5\_nuc(t)$) in nucleus and 2kb mRNA ($P_5\_cyt(t)$) in cytoplasm in model (5.3.4), using three different fixed values of the control function $u_1$ ($u = 0.1,\ 0.5$, and 0.85) and $u_2$ ($u = 0.1,\ 0.5$, and 0.85) respectively. The graphic clearly highlights the strong effectiveness of the Tat inhibitor as well as Rev inhibitor in regulating HIV-1 transcription, thereby impeding the advancement of HIV-1 infection towards AIDS. It is important to note that the synthesis of 9kb messenger RNA ($P_3\_nuc(t)$) decreases as the values of the control function $u_1$ increase, further confirming the therapeutic potential of the Tat inhibitor against HIV-1 replication. Additionally, the figure indicates that the transport of 9kb mRNA ($P_3\_nuc(t)$) and 4kb mRNA ($P_4\_nuc(t)$) from the cell nucleus to the cytoplasm declines with rising values of $u_2$, reinforcing the therapeutic effectiveness of the Rev inhibitor against HIV-1 replication.

## 5.5 Conclusion

HIV-1 infection is a chronic, incurable condition that arises when the virus damages the body's immune system. Researchers have previously investigated the biochemical processes involved in the replication cycle of HIV-1 within activated target cells using mathematical analysis. Notably, S. Mondal et al. (Mondal et al., 2023) have demonstrated the positive regulatory influence of the viral Tat protein on HIV-1 transcription. They have also proposed potential treatment strategies and drug regimens aimed at controlling HIV-1 transcription through a one-dimensional impulsive differential equation model that incorporates a Tat inhibitor. However, the role of the viral Rev protein in the HIV-1 life cycle has not yet been examined in these studies. Recent biological literature indicates that the viral Rev protein enhances the nuclear transport of unspliced 9kb and singly-spliced 4kb messenger RNAs to the cytoplasm, while simultaneously inhibiting the splicing of these 9kb and 4kb messenger RNAs. This dual action helps to maintain a balance in the expression products of viral genes. In this context, we have examined the dynamics of HIV-1 by analyzing the roles of two viral key proteins, Tat and Rev, from a mathematical perspective to gain a clearer understanding of Tat and Rev-mediated transcription. Additionally, we have focused on exploring pathways to identify optimal therapeutic strategies by introducing inhibitors for both Tat and Rev.

Due to the absence of adequate primary data, we have selected our parameter values to ensure that our formulated model is biologically plausible. Our suggested treatment regimen, which incorporates a Tat inhibitor and a Rev inhibitor, relies on hypothetical values for the model parameters. However, the outcomes can inform future clinical trials by taking clinical results into account. Additionally, these analytical and numerical methods can be employed to identify the optimal therapy schedule for other medications.

The research illustrates that the model solutions are both bounded and non-negative, while also confirming the local stability of the endemic equilibrium point.

The Pontryagin maximum principle is utilized in addressing an optimal control problem. Numerical findings suggest that continuous therapeutic administration stabilizes mRNA synthesis after 8 hours. The mathematical model and results of the study offer important insights for the development of therapeutic strategies within the scientific community.

# Chapter 6

# Conclusion and future direction

## 6.1 Concluding remark

In this thesis, we have done mathematical modelling on enzyme catalysed reactions, describing different biochemical systems for HIV-1 replication. In the treatment of HIV-1 infection, the existing anti-HIV drugs do not permanently cure the disease and HIV-1 remains latent within the infected cells. In this context, it is essential to focus on creating new and improved medications that target various independent stages of the HIV-1 replication cycle. Here we have developed quantitative mathematical models that describe the biochemical reactions involved in the replication of HIV-1 within target cells.

In our first project, which is in *Chapter (2)*, we examined the effect of alcohol consumption in HIV-1 infected patients through an enzyme kinetic model that describes the enzymatic activity of Cytochrome P3A4 (CYP3A4) toward protease inhibitors. It is seen that alcohol consumption increases the metabolism rate of protease inhibitors by CYP3A4 enzyme and hence, may increase the viral load in alcoholic HIV-1 infected individuals.

In our second project, we concentrated on deriving fully analytical solutions for a two-compartment model that demonstrates nonlinear Michaelis–Menten elimination kinetics in *Chapter (3)*. Additionally, we aimed to provide foundational insights into

developing an effective dosing regimen for applying a dual inhibitor of HIV-1 reverse transcriptase and integrase in the treatment of HIV-1 infection.

In the third problem, we have outlined the transcription process mediated by HIV-1 Tat by developing a mathematical framework based on non-linear differential equations in *Chapter (4)*. This study aims to explore the effects of a Tat inhibitor on the reduction of HIV-1 transcriptional activity, approached from the perspective of an optimal control problem. Additionally, we incorporate a one-dimensional impulsive model to evaluate the effectiveness of the Tat inhibitor in treating HIV-1 infection, which reveals a maximum interval of 34.693 hours between doses. Our numerical findings suggest that continuous therapeutic administration stabilizes mRNA synthesis after 10 hours. Our research indicates that administering the Tat inhibitor through a 6-hour impulse dosing schedule provides long-term advantages for HIV-1 treatment, with a maximum dosing interval of 34.693 hours.

In the fourth problem presented in *Chapter (5)*, we have explored the dynamics of HIV-1 by mathematically analyzing the functions of two crucial viral proteins, Tat and Rev. We have investigated the effectiveness of combined drug therapy, specifically the administration of inhibitors for both Tat and Rev, through the framework of an optimal control problem. Utilizing the Pontryagin maximum principle, we have examined the optimal control problem focused on minimizing therapy costs while maximizing its impact on the regulation of HIV-1 replication by Tat and Rev. Our findings indicate that continuous therapeutic administration stabilizes HIV-1 mRNA synthesis after a duration of 8 hours.

We expect that our research and the proposed mathematical models will help broaden the treatment options available for HIV-1 infected patients undergoing complex HAART therapy.

## 6.2 Future research: An outline

The biochemical processes in the human body related to HIV-1 infection have been examined through enzyme kinetics modeling in the preceding chapters. Various mathematical tools have been employed to provide a clearer analysis of the biochemical

system. This thesis primarily focuses on the strategies of impulsive drug dosing and optimal control therapy to address the selected issues. In the near future, I aim to explore the following potential areas:

- Enzyme kinetics model including delay differential equation as it is considered a relevant mathematical approach for this research work.

- Formulation of stochastic mathematical models for HIV-1 infection to predict the efficiency of different antiviral drugs against HIV-1 replication.

- Mathematical model consisting of fractional differential equations to describe the population dynamics of various chronic diseases like HIV-1 infection, COVID-19, etc.

# Bibliography


Abdulla, F.A. (2011). Using fractional differential equations to model the Michaelis-Menten reaction in a 2-d region containing obstacles. environments, 10, p.11.

Acosta, E.P. (2002). Pharmacokinetic enhancement of protease inhibitors. Journal of acquired immune deficiency syndromes, 29, pp.S11-8.

Alawneh, A. (2013). Application of the Multistep Generalized Differential Transform Method to Solve a Time-Fractional Enzyme Kinetics. Discrete Dynamics in Nature and Society, 2013(1), p.592938.

Albornoz, J.M., Parravano, A. (2007). Modeling a simple enzyme reaction with delay and discretization. arXiv preprint arXiv: 0712.0391.

Althaus, I.W., Chou, J.J., Gonzales, A.J., Deibel, M.R., Chou, K.C., Kezdy, F.J., Romero, D.L., Aristoff, P.A., Tarpley, W.G., Reusser, F. (1993) Steady-state kinetic studies with the non-nucleoside HIV-1 reverse transcriptase inhibitor U-87201E. Journal of Biological Chemistry, 268(9): 6119-6124.

Anstett, K., Brenner, B., Mesplede, T., Wainberg, M.A. (2017). HIV drug resistance against strand transfer integrase inhibitors. Retrovirology, 14(1): 1-16.

Arisi, I., Cattaneo, A., Rosato, V. (2006). Parameter estimate of signal transduction pathways. BMC neuroscience, 7, pp.1-19.

Arlen, P.A., Brooks, D.G., Gao, L.Y., Vatakis, D., Brown, H.J., Zack, J.A. (2006). Rapid expression of human immunodeficiency virus following activation of latently infected cells. Journal of Virology, 80(3):1599-1603.

Baınov, D. & Simeonov, P.S. (1993). Impulsive differential equations: periodic solutions and applications.

Bainov, D., Dishliev, A. & Hfustova, S. (1995) Lyapunov's functions and boundedness of the solutions of impulsive differential equations. Applicable Analysis, 59(1-4), 257-269.

Bainov, D.D. and Simeonov, P. (1995). Impulsive differential equations: asymptotic properties of the solutions (Vol. 28). World Scientific.

Baınov, D. and Simeonov, P. (2017). Impulsive differential equations: periodic solutions and applications. Routledge.

Balbaa, M., EI Ashry, E.S. (2012). Enzyme inhibitors as therapeutic tools. Biochem Physiol, 1(2):1000103.

Barry, D.A., Parlange, J.Y., Li, L., Prommer, H., Cunningham, C.J., Stagnitti, F. (2000). Analytical approximations for real values of the Lambert W-function. Mathematics and Computers in Simulation, 53: 95-103.

BARMAN, D., KUMAR, V., ROY, S., MANDAL, S.C. and their application.

Bhagavan, N.V., Ha, C.E. (2015). Essentials of medical biochemistry. With Clinical Cases, Second edition Academic Press, London, UK.

Biswas, D., Datta, A., Roy, P.K. (2016). Combating Leishmaniasis through awareness campaigning: a mathematical study on media efficiency. International Journal of Mathematical, Engineering and Management Sciences, 1(3), pp.139-149.

Boyer, R.F. (2002). Concepts in biochemistry. Pacific Grove, CA: Brooks/Cole.

Bonnans, J.F., Hermant, A. (2009). Revisiting the analysis of optimal control problems with several state constraints. Control Cybern, 38(4A):1021-1052.

Briggs, G.E., Haldane, J.B.S. (1925). A note on the kinetics of enzyme action. Biochem 19(2): 338-339.

Brussel, A., Sonigo. P. (2004). Evidence for gene expression by unintegrated human immunodeficiency virus type 1 DNA species. Journal of Virology, 78(20): 11263-11271.

Butler, S.L., Hansen, M.S., Bushman, F.D. (2001). A quantitative assay for HIV DNA integration in vivo. Nature Medicine, 7(5): 631-634.

Cai, J., Zuo, H.F. and Wang, H.W. (2007). Optimal inspection model using delay-time concept. Journal of Applied Sciences, 25(4), pp.26-31.

Cao, Y., Liu, X. and De Clercq, E. (2009). Cessation of HIV-1 transcription by inhibiting regulatory protein Rev-mediated RNA transport. Current HIV Research, 7(1), pp.101-108.

Carlotti, F., Dower, S.K., Qwarnstrom, E.E. (2000). Dynamic shuttling of nuclear factor kappa B between the nucleus and cytoplasm as a consequence of inhibitor dissociation. Journal of Biological Chemistry, 275(52):41028-41034.

Cecchetti, V., Parolin, C., Moro, S., Pecere, T., Filipponi, E., Calistri, A., Tabarrini, O., Gatto, B., Palumbo, M., Fravolini, A., Giorgio, P. (2000). 6-Aminoquinolones as new potential anti-HIV agents. Journal of Medicinal Chemistry, 43(20):3799-3802.

Centennial, J.B. (2006). Centennial 1905–2005 100 Years of Biochemistry and Molecular Biology. The Development of Two-dimensional Electrophoresis by Patrick H. O'Farrell. The Journal of Biological Chemistry. Aug;281(32):e26.

Chander, G., Lau, B. and Moore, R.D., (2006). Hazardous alcohol use: a risk factor for non-adherence and lack of suppression in HIV infection. Journal of acquired immune deficiency syndromes, 43(4), p.411.

Chander, G., Himelhoch, S., Fleishman, J.A. Hellinger, J., Gaist, P., Moore, R.D., Gebo, K.A. (2009). HAART receipt and viral suppression among HIV-infected patients with co-occurring mental illness and illicit drug use. AIDS care, 21(5), pp.655-663.

Chander, G. (2011). Addressing alcohol use in HIV-infected persons. Topics in antiviral medicine, 19(4), p.143.

Chatterjee, A.N., Roy, P.K. (2012). Anti-viral drug treatment along with immune activator IL-2: a control-based mathematical approach for HIV infection. International Journal of Control, 85(2), pp.220-237.

Chen, W.W., Niepel, M., Sorger, P.K. (2010). Classic and contemporary approaches to modeling biochemical reactions. Genes & development, 24(17), pp.1861-1875.

Chowdhury, S., Roy, P.K. (2016). Mathematical modelling of enfuvirtide and protease inhibitors as combination therapy for HIV. International Journal of Nonlinear Sciences and Numerical Simulation, 17(6), pp.259-275.

Coddington, E.A., Levinson, N. (1955). Theory of ordinary differential equations (Vol. 158). New York: McGraw-Hill.

Copeland, R.A. (2004). Enzymes: a practical introduction to structure, mechanism, and data analysis. John Wiley & Sons.

Copeland, R.A, Harpel, M.R., Tummino, P.J. (2007). Targeting enzyme inhibitors in drug discovery. Expert opinion on therapeutic targets, Jul 1;11(7):967-78.

Copeland, R.A. (2013). Evaluation of enzyme inhibitors in drug discovery: a guide for medicinal chemists and pharmacologists. John Wiley & Sons.

Corless, R.M., Gonnet, G.H., Hare, D.E., Jeffrey, D.J., Knuth, D.E. (1996). On the LambertW function. Advances in Computational Mathematics, 5(1), 329-359.

Cornish-Bowden, A. (2013). Fundamentals of enzyme kinetics. John Wiley & Sons.

Covert, D., Kirschner, D.E. (2000). Revisiting early models of the host-pathogen interactions in HIV infection.

Craigie, R., Bushman, F.D. (2012). HIV DNA integration. Cold Spring Harb, 2(7): a006890.

Culshaw, R.V. and Ruan, S. (2000). A delay-differential equation model of HIV infection of CD4+ T-cells. Mathematical biosciences, 165(1), pp.27-39.

Das, K., Arnold, E. (2013). HIV-1 reverse transcriptase and antiviral drug resistance. Part 1. Current opinion in virology, 3(2):111-118.

DANCIS, J.(1972). Mattenheimer's Clinical Enzymology: Principles and Applications. American Journal of Diseases of Children, Mar 1;123(3):267-267.

Das, K., Arnold, E. (2013). HIV-1 reverse transcriptase and antiviral drug resistance. Part 2. Current opinion in virology, 3(2): 119-128.

Dawood, A., Abdul Basit, S., Jayaraj, M., Gish, R.G. (2017). Drugs in development for hepatitis B. Drugs, Aug;77:1263-80.

de Castro, S., Camarasa, M.J. (2018). Polypharmacology in HIV inhibition: can a drug with simultaneous action against two relevant targets be an alternative to combination therapy? European Journal of Medicinal Chemistry, 150:206-227.

Eisenhammer, T., Hübler, A., Packard, N. and Kelso, J.S. (1991). Modeling experimental time series with ordinary differential equations. Biological cybernetics, 65, pp.107-112.

Engelman, A., Mizuuchi, K., Craigie, R. (1991). HIV-1 DNA integration: mechanism of viral DNA cleavage and DNA strand transfer. Cell 67(6):1211-1221.

Érdi, P., Tóth, J. (1989). Mathematical models of chemical reactions: theory and applications of deterministic and stochastic models. Manchester University Press.

Ferrari, L.F., Levine, J.D. (2010). Alcohol consumption enhances antiretroviral painful peripheral neuropathy by mitochondrial mechanisms. European Journal of Neuroscience, 32(5), pp.811-818.

Finkel, R., Clark, M.A., Cubeddu, L.X.eds. (2009). Pharmacology. Lippincott Williams & Wilkins.

Finn, N.A., Findley, H.W. and Kemp, M.L., (2011). A switching mechanism in doxorubicin bioactivation can be exploited to control doxorubicin toxicity. PLoS computational biology, 7(9), p.e1002151.

Fishbone, L.G. and Abilock, H., (1981). Markal, a linear-programming model for energy systems analysis: Technical description of the bnl version. International journal of Energy research, 5(4), pp.353-375.

Fleming, W.H. and Rishel, R.W. (1975). Deterministic and Stochastic Optimal Control Springer Verlag Berlin. DANIEL AKUME, BERND LUDERER AND RALF WUNDERLICH, pp.156-167.

Flexner, C.W., Cargill, V.A., Sinclair, J., Kresina, T.F. and Cheever, L. (2001). Alcohol use can result in enhanced drug metabolism in HIV pharmacotherapy. AIDS patient care and STDs, 15(2), pp.57-58.

Friedrich, B.M, Dziuba, N., Li, G., Endsley, M.A., Murray, J.L., Ferguson, M.R. (2011). Host factors mediating HIV-1 replication. Virus Research, 161(2):101-114.

Galluzzi, L. (2020). Tumor Immunology and Immunotherapy-Cellular Methods. Academic Press.

Garcia, B.A (2019). Post-translational modifications that modulate enzyme activity. Academic Press.

Gass, S.I. (2003). Linear programming: methods and applications. Courier Corporation.

Ghosh, P., Peters, J.F. (2020). Impulsive differential equation model in methanol poisoning detoxification. Journal of Mathematical Chemistry, 58(1): 126-145.

Ghosh, P., Roy, P.K. (2018). Mathematical modelling of methanol poisoning with impulsive dosing of antidote therapeutics to prevent toxicity. Mathematical Methods in the Applied Sciences, 41(18), pp.9176-9190.

Ghosh, P., Cao, X., Pal, J., Chowdhury, S., Saha, S., Nandi, S., Roy, P.K. (2018). Mathematical Modeling for the Prevention of Methanol Poisoning Through Ethanol by Impulsive Way. Differential Equations and Dynamical Systems, pp.1-18.

Giordano, G., Blanchini, F., Bruno, R., Colaneri, P., Di Filippo, A., Di Matteo, A., Colaneri, M. (2020). Modelling the COVID-19 epidemic and implementation of population-wide interventions in Italy. Nature medicine, 26(6):855-60.

Glenner, G.G., Page, D., Isersky, C., Harada, M., Cuatrecasas, P., Eanes, E.D., DeLellis, R.A., Bladen, H.A., Keiser, H.R. (1971). Murine amyloid fibril protein: isolation, purification and characterization. Journal of Histochemistry & Cytochemistry, 19(1), pp.16-28.

Global status report on AIDS. *Tech. rep.*, WHO 2021. https://www.unaids.org/en

Global status report on AIDS. *Tech. rep.*, WHO 2023. https://www.unaids.org/en

Gonzalez, A., Barinas, J., O'Cleirigh, C. (2011). Substance use: impact on adherence and HIV medical treatment. Current HIV/AIDS Reports, 8(4), p.223.

Gonze, D., Kaufman, M. (2016). Chemical and enzyme kinetics (Doctoral dissertation, Master's thesis).

Goudar, C.T., Sonnad, J.R., Duggleby, R.G., (1999). Parameter estimation using a direct solution of the integrated Michaelis-Menten equation. Biochimica et Biophysica Acta (BBA)-Protein Structure and Molecular Enzymology, 1429(2), pp.377-383.

Grigorieva, E.V., Khailov, E.N., Korobeinikov, A. (2013). An optimal control problem in HIV treatment. Discrete and Continuous Dynamical Systems-Series S.

Grigorieva, E.V., Khailov, E.N., Bondarenko, N.V., Korobeinikov, A. (2014). Modeling and optimal control for antiretroviral therapy. J. Biol. Syst. 22(02):199-217.

Gu, S.X., Xue, P., Ju, X.L., Zhu, Y.Y. (2016). Advances in rationally designed dual inhibitors of HIV-1 reverse transcriptase and integrase. Bioorganic & medicinal chemistry, 24(21):5007-5016.

Haag, N.L., Velk, K.K., Wu, C. (2012). Potential antibacterial targets in bacterial central metabolism. International journal on advances in life sciences, 4(1-2), p.21.

He, J.H. (1999). Variational iteration method–a kind of non-linear analytical technique: some examples. International journal of non-linear mechanics, 34(4), pp.699-708.

Hendershot, C.S., Stoner, S.A., Pantalone, D.W., Simoni, J.M. (2009). Alcohol use and antiretroviral adherence: review and meta-analysis. Journal of acquired immune deficiency syndromes, 52(2), p.180.

Hirsch, M.S., Günthard, H.F., Schapiro, J.M., Vézinet, F.B., Clotet, B., Hammer, S.M., Johnson, V.A., Kuritzkes, D.R., Mellors, J.W., Pillay, D. and Yeni, P.G. (2008). Antiretroviral drug resistance testing in adult HIV-1 infection: 2008 recommendations of an International AIDS Society-USA panel. Clinical Infectious Diseases, 47(2), pp.266-285.

Hu, W.S, Hughes, S.H. (2012). HIV-1 reverse transcription. Cold Spring Harbor Perspectives in Medicine, 2(10): a006882.

Huang, S.A., Lie, J.D. (2013), Phosphodiesterase-5 (PDE5) inhibitors in the management of erectile dysfunction. Pharmacy and therapeutics.38(7):407.

Ianiro, G., Pecere, S., Giorgio, V., Gasbarrini, A., Cammarota, G. (2016). Digestive enzyme supplementation in gastrointestinal diseases. Current drug metabolism, 17(2):187-93.

Jeltsch, A. (2006). On the enzymatic properties of Dnmt1: specificity, processivity, mechanism of linear diffusion and allosteric regulation of the enzyme. Epigenetics, 1(2), pp.63-66.

Jencks, W.P. (1987). Catalysis in chemistry and enzymology. Courier Corporation.

Ji, Z., Su, J., Liu, C., Wang, H., Huang, D., Zhou, X. (2014). Integrating genomics and proteomics data to predict drug effects using binary linear programming. PloS one, 9(7), p.e102798.

Jose, S.A., Raja, R., Zhu, Q., Alzabut, J., Niezabitowski, M. and Balas, V.E. (2022). An Integrated Eco-Epidemiological Plant Pest Natural Enemy Differential Equation Model with Various Impulsive Strategies. Mathematical Problems in Engineering, 2022(1), p.4780680.

Kalman, T.I. (1981). Enzyme inhibition as a source of new drugs. Drug Development Research, 1(4):311-28.

Kapoor, G., Saigal, S., Elongavan, A. (2017). Action and resistance mechanisms of antibiotics: A guide for clinicians. Journal of Anaesthesiology Clinical Pharmacology, 33(3):300-5.

Karp, G. (2009). Cell and molecular biology: concepts and experiments. John Wiley & Sons.

Kendrew, J.C., Bodo, G., Dintzis, H.M., Parrish, R.G., Wyckoff, H., Phillips, D.C. (1958). A three-dimensional model of the myoglobin molecule obtained by x-ray analysis. Nature, 181(4610):662-6.

Kim, H., Yin, J. (2005). Robust growth of human immunodeficiency virus type 1 (HIV-1). Biophysical journal, 89(4):2210-2221.

Kirschner, D., Lenhart, S., Serbin, S. (1997). Optimal control of the chemotherapy of HIV. Journal of mathematical biology, 35(7):775-792.

Knowlton, J.L., Graham, C.H. (2010). Using behavioral landscape ecology to predict species' responses to land-use and climate change. Biological Conservation, 143(6), pp.1342-1354.

Koh, G. and Lee, D.Y. (2011). Mathematical modeling and sensitivity analysis of the integrated TNF$\alpha$-mediated apoptotic pathway for identifying key regulators. Computers in biology and medicine, 41(7), pp.512-528.

Kostyuchenko, Y.V. (2018). On the Methodology of Satellite Data Utilization in Multi-Modeling Approach for Socio-Ecological Risks Assessment Tasks: A Problem Formulation. International Journal of Mathematical, Engineering and Management Sciences, 3(1), pp.1-8.

Kirk, D.E. (2004). Optimal control theory: an introduction. Courier Corporation.

Kumar, N., Hendriks, B.S., Janes, K.A., de Graaf, D., Lauffenburger, D.A. (2006). Applying computational modeling to drug discovery and development. Drug discovery today, 11(17-18), pp.806-811.

Kumar, S., Kumar, A. (2011). Differential effects of ethanol on spectral binding and inhibition of cytochrome P450 3A4 with eight protease inhibitors antiretroviral drugs. Alcoholism: Clinical and Experimental Research, 35(12), pp.2121-2127.

Kumar, S., Jin, M., Ande, A., Sinha, N., Silverstein, P.S., Kumar, A. (2012). Alcohol consumption effect on antiretroviral therapy and HIV-1 pathogenesis: role of cytochrome P450 isozymes. Expert opinion on drug metabolism & toxicology, 8(11), pp.1363-1375.

Kustikova, O.S., Wahlers, A., Kuhlcke, K., Stahle, B., Zander, A.R., Baum, C., Fehse, B. (2003). Dose finding with retroviral vectors: correlation of retroviral vector copy numbers in single cells with gene transfer efficiency in a cell population. Blood, 102(12): 3934-3937.

Lakshmikantham, V., Lakshmikantham, P.S. (1989). Theory of impulsive differential equations (Vol. 6). World scientific.

Lakshmikantham, V., Simeonov, P.S. (1989). Theory of impulsive differential equations, Vol.6, World Scientific.

Lander, E.S., Linton, L.M., Birren, B., Nusbaum, C., Zody, M.C., Baldwin, J., Devon, K., Dewar, K., Doyle, M., Fitzhugh, W., Funke, R. (2001). Erratum: Initial sequencing and analysis of the human genome: international human genome sequencing consortium. Nature, 409, pp.860-921).

Lee, E.B., Markus, L. (1967). Foundation of optimal control theory. new york-london-sydney: John wiley & sons. Inc.

Leggett, R.M., Ramirez-Gonzalez, R.H., Clavijo, B.J., Waite, D., Davey R.P. (2013). Sequencing quality assessment tools to enable data-driven informatics for high throughput genomics. Frontiers in genetics, 4, p.288.

Lenhart, S., Workman, J.T. (2007). Optimal control applied to biological models. CRC press.

Lewars, E.G. (2011). Computational chemistry. Introduction to the theory and applications of molecular and quantum mechanics, 318.

Li, A., Li, J., Johnson, K.A., (2016). HIV-1 reverse transcriptase polymerase and RNase H (ribonuclease H) active sites work simultaneously and independently. Journal of Biological Chemistry, 291(51): 26566-26585.

Likhoshvai, V.A., Khlebodarova, T.M., Bazhan, S.I., Gainova, I.A., Chereshnev, V.A., Bocharov, G.A. (2014). Mathematical model of the Tat-Rev regulation of HIV-1 replication in an activated cell predicts the existence of oscillatory dynamics in the synthesis of viral components. BMC Genom. 15(12):1-18.

Liu. Y., Li, R., Xiao, X., Wang, Z. (2018). Molecules that inhibit bacterial resistance enzymes. Molecules. 24(1):43.

Lopez-Sendon, J., Swedberg, K., McMurray, J., Tamargo, J., Maggioni, A.P., Dargie, H., Tendera, M., Waagstein, F., Kjekshus, J., Lechat, P., Pedersen, C.T. (2004). Expert consensus document on angiotensin converting enzyme inhibitors in cardiovascular disease: The Task Force on ACE-inhibitors of the European Society of Cardiology. European heart journal, 25(16):1454-70.

Lopina, O.D. (2017). Enzyme inhibitors and activators. InEnzyme inhibitors and activators. IntechOpen.

Lou, J., Smith, R.J. (2011). Modelling the effects of adherence to the HIV fusion inhibitor enfuvirtide. J. Theor. Biol. 268(1):1-13.

Majumder, M., Tiwari, P.K., Pal, S. (2022). Impact of saturated treatments on HIV-TB dual epidemic as a consequence of COVID-19: optimal control with awareness and treatment, Nonlinear Dyn. 109(1): 143-176.

Majumder, M., Tiwari, P.K., Pal, S. (2023). Impact of nonlinear infection rate on HIV/AIDS considering prevalence-dependent awareness. Mathematical Methods in the Applied Sciences, 46(4):3821-48.

Mao, T.Q., He, Q.Q, Wan, Z.Y., Chen, W.X., Chen, F.E., Tang, G.F., De Clercq, E., Daelemans, D., Pannecouque, C. (2015). Anti-HIV diarylpyrimidine–quinolone hybrids and their mode of action. Bioorganic & Medicinal Chemistry, 23(13): 3860-3868.

Marshall, W.J., Lapsley, M., Day, A., Ayling, R. (2014). Clinical biochemistry: metabolic and clinical aspects. Elsevier Health Sciences.

Meister, A. (2009). Advances in enzymology and related areas of molecular biology. John Wiley & Sons.

Michaelis, L., Menten, M.L. (1913). Die kinetik der invertinwirkung, Biochem Z 49: 333–369.

Midde, N.M., Rahman, M.A., Rathi, C., Li, J., Meibohm, B., Li, W., Kumar, S. (2016). Effect of ethanol on the metabolic characteristics of HIV-1 integrase inhibitor elvitegravir and elvitegravir/cobicistat with CYP3A: an analysis using a newly developed LC-MS/MS method. PloS one, 11(2), p.e0149225.

Miguez, M.J., SHOR-POSNER, G.A.I.L., Morales, G., Rodriguez, A. and Burbano, X. (2003). HIV treatment in drug abusers: impact of alcohol use. Addiction biology, 8(1), pp.33-37.

Milev, N.V., Bainov, D.D. (1990). Stability of linear impulsive differential equations. International journal of systems science, 21(11):2217-2224.

Miller, G.T., Spoolman, S. (2012), Environmental science. Cengage Learning.

Miron, R.E., Smith, R.J. (2014). Resistance to protease inhibitors in a model of HIV-1 infection with impulsive drug effects. Bulletin of mathematical biology, 76, pp.59-97.

Mislak, A.C, Frey, K.M., Bollini, M., Jorgensen, W.L., Anderson, K.S. (2014). A mechanistic and structural investigation of modified derivatives of the diaryltriazine class of NNRTIs targeting HIV-1 reverse transcriptase. Biochim. Biophys. Acta, 1840(7): 2203-2211.

Mohammadi, P., Desfarges, S., Bartha, I., Joos, B., Zangger, N., Munoz, M., Günthard, H.F., Beerenwinkel, N., Telenti, A., Ciuffi, A. (2013). 24 hours in the life of HIV-1 in a T cell line. PLoS Pathogens, 9(1): e1003161, 2013.

Mondal, S., Murmu, T., Chakravarty, K., Sarkar, A.K., Sasmal, S.K. (2023). Mathematical modelling of HIV-1 transcription inhibition: a comparative study between optimal control and impulsive approach. Computational and Applied Mathematics, 42(8), p.340.

Mousseau, G., Clementz, M.A., Bakeman, W.N., Nagarsheth, N., Cameron, M., Shi, J., Baran, P., Fromentin, R., Chomont, N., Valente, S.T. (2012). An analog of the natural steroidal alkaloid cortistatin A potently suppresses Tat-dependent HIV transcription. Cell Host & Microbe 12(1):97-108.

Mousseau, G., Mediouni, S., Valente, S.T. (2015). Targeting HIV transcription: the quest for a functional cure. The Future of HIV-1 Therapeutics, 121-145.

Murata, T. (1989). Petri nets: Properties, analysis and applications. Proceedings of the IEEE, 77(4), pp.541-580.

Murray, J.M., McBride, K., Boesecke, C., Bailey, M., Amin, J., Suzuki, K., Baker, D., Zaunders, J.J., Emery, S., Cooper, D.A., Koelsch, K.K. (2012). Integrated HIV DNA accumulates prior to treatment while episomal HIV DNA records ongoing transmission afterward. Aids, 26(5): 543-550.

Norman, L.R., Kumar, A. (2006). Neuropscyhological Complications of HIV Disease and Substances of Abuse. American journal of infectious diseases, 2(2), p.67.

Nowak, M., May, R.M. (2000). Virus dynamics: mathematical principles of immunology and virology: mathematical principles of immunology and virology. Oxford University Press, UK.

Oliveira, S.C., Pereira, F.M., Ferraz, A., Silva, F.T. and Goncalves, A.R. (2000). Mathematical modeling of controlled-release systems of herbicides using lignins as matrices: A Review. In Twenty-First Symposium on Biotechnology for Fuels and Chemicals: Proceedings of the Twenty-First Symposium on Biotechnology for Fuels and Chemicals Held May 2–6, 1999, in Fort Collins, Colorado (pp. 595-615). Humana Press.

Omidiniya, P., Alipour M. (2019). Modified variational iteration method to solve a model for HIV infection of CD4T-cells. In 1st Annual National Conference on Biomathematics, p. 95.

Ott, M., Geyer, M., Zhou, Q. (2011). The control of HIV transcription: keeping RNA polymerase II on track. Cell Host & Microbe 10(5):426-435.

Page, C.P. (2015), Phosphodiesterase inhibitors for the treatment of asthma and chronic obstructive pulmonary disease. International archives of allergy and immunology, 165(3):152-64.

Pal, D., Mitra, A.K. (2006). MDR-and CYP3A4-mediated drug–drug interactions. Journal of Neuroimmune Pharmacology, 1(3), pp.323-339.

Papin, J.A., Hunter, T., Palsson, B.O. and Subramaniam, S. (2005). Reconstruction of cellular signalling networks and analysis of their properties. Nature reviews Molecular cell biology, 6(2), pp.99-111.

Peng, H., Wen, J., Li, H., Chang, J. and Zhou, X. (2011). Drug inhibition profile prediction for NF$\kappa$B pathway in multiple myeloma. PloS one, 6(3), p.e14750.

Peng, H., Wen, J., Zhang, L., Li, H., Chang, C.C., Zu, Y. and Zhou, X. (2012). A systematic modeling study on the pathogenic role of p38 MAPK activation in myelodysplastic syndromes. Molecular BioSystems, 8(4), pp.1366-1374.

Peng, H., Peng, T., Wen, J., Engler, D.A., Matsunami, R.K., Su, J., Zhang, L., Chang, C.C. and Zhou, X. (2014). Characterization of p38 MAPK isoforms for drug resistance study using systems biology approach. Bioinformatics, 30(13), pp.1899-1907.

Perelson, A.S. (20002). Modelling viral and immune system dynamics, Nat. Rev. Immunol. 2(1):28-36.

Pirmohamed, M., Breckenridge, A.M., Kitteringham, N.R., Park, B.K. (1998). Adverse drug reactions. Bmj. 316(7140):1295-8.

Pohanka, M. (2019). Antidotes against methanol poisoning: A review. Mini Reviews in Medicinal Chemistry, 19(14):1126-33.

Pontryagin, L.S. (1987). Mathematical theory of optimal processes. CRC press.

Prado, S., Beltrán, M., Moreno, Á., Bedoya, L.M., Alcamí , J. and Gallego, J. (2018). A small-molecule inhibitor of HIV-1 Rev function detected by a diversity screen based on RRE-Rev interference. Biochemical Pharmacology, 156, pp.68-77.

Price, N.C., Frey, P.A. (2001). Fundamentals of enzymology. Biochemistry and Molecular Biology Education, 1(29):34-5.

Purohit, V., Rapaka, R., Shurtleff, D. (2011). Drugs of abuse, dopamine, and HIV-associated neurocognitive disorders/HIV-associated dementia. Molecular neurobiology, 44(1), pp.102-110.

Qian, H. (2008). Cooperativity and specificity in enzyme kinetics: a single-molecule time-based perspective. Biophysical journal, 95(1), pp.10-17.

Rahal Jr, J.J., Meyers, B.R., Weinstein, L. (1968). Treatment of bacterial endocarditis with cephalothin. New England Journal of Medicine, 279(24), pp.1305-1309.

Rattanakul, C. and Chaiya, I. (2024). A mathematical model for predicting and controlling COVID-19 transmission with impulsive vaccination. AIMS Mathematics, 9(3), pp.6281-6304.

Reddy, B., Yin, J. (1999). Quantitative intracellular kinetics of HIV type 1. AIDS Res. Hum. Retrovir. 15(3):273-283.

Rich, D.H. (2005). Evaluation of Enzyme Inhibitors in Drug Discovery: A Guide for Medicinal Chemists and Pharmacologists. Robert A. Copeland. Hoboken, NJ: John Wiley & Sons, Inc., 2005, 271 pp., $84.95, hardcover. ISBN 0-471-68696-4.(Book web site http://www. chipsbooks. com/evalenz. htm). Clinical Chemistry, 51(11): 2219-2220.

Robert-Guroff, M., Popovic, M., Gartner, S., Markham, P., Gallo, R.C., Reitz, M.S. (1990). Structure and expression of tat-, rev-, and nef-specific transcripts of human immunodeficiency virus type 1 in infected lymphocytes and macrophages. J. Virol. 64(7):3391-3398.

Ross, B. (1977). The development of fractional calculus 1695–1900. Historia mathematica, 4(1), pp.75-89.

Roy, P.K., Saha, S. and Al Basir, F. (2015). Effect of awareness programs in controlling the disease HIV/AIDS: an optimal control theoretic approach. Advances in Difference Equations, 2015(1), p.217.

Santos, L.H., Ferreira, R.S., Caffarena, E.R. (2015). Computational drug design strategies applied to the modelling of human immunodeficiency virus-1 reverse transcriptase inhibitors. Memórias do Instituto Oswaldo Cruz, 110(7):847-64.

Sarafianos, S.G., Marchand, B., Das, K., Himmel, D.M., Parniak, M.A., Hughes, S.H., Arnold, E. (2009). Structure and function of HIV-1 reverse transcriptase: molecular mechanisms of polymerization and inhibition, J. Mol. Biol. 385(3): 693-713.

Schauer, G.D., Huber, K.D., Leuba, S.H., Sluis-Cremer, N. (2014). Mechanism of allosteric inhibition of HIV-1 reverse transcriptase revealed by single-molecule and ensemble fluorescence, Nucleic Acids Research. 42(18): 11687-11696.

Schmid, A. and Blank, L.M. (2010). Hypothesis-driven omics integration. Nature chemical biology, 6(7), pp.485-487.

Schmidt, E.M., Zhang, J., Zhou, W., Chen, J., Mohlke, K.L., Chen, Y.E., Willer, C.J. (2015). GREGOR: evaluating global enrichment of trait-associated variants in epigenomic features using a systematic, data-driven approach. Bioinformatics, 31(16), pp.2601-2606.

Schnell, S., Mendoza, C. (1997). Closed form solution for time-dependent enzyme kinetics. Journal of Theoretical Biology, 187(2): 207-212.

Schulz, A.R. (1994). Enzyme kinetics: from diastase to multi-enzyme systems. Cambridge University Press.

Segel, I.H. (1975). Enzyme kinetics: behavior and analysis of rapid equilibrium and steady-state enzyme systems. Vol. 115, New York: Wiley.

Segel, L.A. (1984). Modeling dynamic phenomena in molecular and cellular biology. Cambridge University Press.

Shao, H., Peng, T., Ji, Z., Su, J. and Zhou, X. (2013). Systematically studying kinase inhibitor induced signaling network signatures by integrating both therapeutic and side effects. PLoS One, 8(12), p.e80832.

Shcherbatova, O., Grebennikov, D., Sazonov, I., Meyerhans, A., Bocharov, G. (2020). Modeling of the HIV-1 life cycle in productively infected cells to predict novel therapeutic targets. Pathogens, 9(4): 255.

Shen, Z.H., Chu, Y.M., Khan, M.A., Muhammad, S., Al-Hartomy O.A. and Higazy M. (2021). Mathematical modeling and optimal control of the COVID-19 dynamics. Results in Physics, 31, p.105028.

Shmulevich, I., Dougherty, E.R., Kim, S. and Zhang, W. (2002). Probabilistic Boolean networks: a rule-based uncertainty model for gene regulatory networks. Bioinformatics, 18(2), pp.261-274.

Sierra, S., Walter, H. (2012). Targets for inhibition of HIV replication: entry, enzyme action, release and maturation. Intervirology, 55(2):84-97.

Siliciano, J.D., Kajdas, J., Finzi, D., Quinn, T.C. (2003). Chadwick K, Margolick JB, Kovacs C, Gange SJ, Siliciano RF, Long-term follow-up studies confirm the stability of the latent reservoir for HIV-1 in resting CD4+ T cells, Nature medicine, 9(6): 727-8.

Slabaugh, M.R. (2004). Organic and Biochemistry for Today. Brooks/Cole Publishing Company.

Slice, L.W., Codner, E., Antelman, D., Holly, M., Wegrzynski, B., Wang, J., Toome, V., Hsu, M.C., Nalin, C.M. (1992). Characterization of recombinant HIV-1 Tat and its interaction with TAR RNA. Biochemistry 31(48):12062-12068.

Smith, R.J., Aggarwala, B.D. (2009). Can the viral reservoir of latently infected CD4+ T cells be eradicated with antiretroviral HIV drugs? Journal of Mathematical Biology, 59(5): 697-715.

Smith, R.J. and Wahl, L.M. (2004). Distinct effects of protease and reverse transcriptase inhibition in an immunological model of HIV-1 infection with impulsive drug effects. Bulletin of Mathematical Biology, 66, pp.1259-1283.

Smith, R.J., Wahl, L.M. (2005). Drug resistance in an immunological model of HIV-1 infection with impulsive drug effects. Bulletin of Mathematical Biology, 67(4), pp.783-813.

Smith, R.J. (2006). Adherence to antiretroviral HIV drugs: how many doses can you miss before resistance emerges? Proc. R. Soc. B: Biol. Sci. 273(1586):617-624.

Smith? R.J. (2008). Explicitly accounting for antiretroviral drug uptake in theoretical HIV models predicts long-term failure of protease-only therapy. Journal of theoretical biology, 251(2), pp.227-237.

Song, B.J., Lou, J., Wen, Q.Z. (2011). Modelling two different therapy strategies for drug T-20 on HIV-1 patients. Applied Mathematics and Mechanics, 32(4), pp.419-436.

Soares, G.M.S., Figueiredo, L.C., Faveri, M., Cortelli, S.C., Duarte, P.M. Feres, M. (2012). Mechanisms of action of systemic antibiotics used in periodontal treatment and mechanisms of bacterial resistance to these drugs. Journal of applied oral science, 20, pp.295-309.

Srivastava, T., Chosdol, K. (2008). Clinical enzymology and its applications.

Strelow, J., Dewe, W., Iversen, P.W., Brooks, H.B., Radding, J.A., McGee, J., Weidner, J. (2012). Mechanism of action assays for enzymes. Assay Guidance Manual [Internet].

Sun, M., Tan, Y., Chen, L. (2008). Dynamical behaviors of the brusselator system with impulsive input. Journal of mathematical chemistry, 44, pp.637-649.

Sun, X., Bao, J., Nelson, K.C., Li, K.C., Kulik, G. and Zhou, X. (2013). Systems modeling of anti-apoptotic pathways in prostate cancer: psychological stress triggers a synergism pattern switch in drug combination therapy. PLoS computational biology, 9(12), p.e1003358.

Swan, G.W. (1981). Optimal control applications in biomedical engineering—a survey. Optimal Control Applications and Methods, 2(4), pp.311-334.

Tang, S., Xiao, Y. (2007). One-compartment model with Michaelis-Menten elimination kinetics and therapeutic window: an analytical approach. Journal of Pharmacokinetics and Pharmacodynamics, 34(6): 807-827.

Temesgen, Z., Siraj, D.S. (2008). Raltegravir: first in class HIV integrase inhibitor. Therapeutics and Clinical Risk Management, 4(2): 493, 2008.

Thomson, J.R. (1959). A Biologist Views the Antimetabolites. Bios, pp.195-201.

Tian, Y.P., Liu, C.L. (2009). Robust consensus of multi-agent systems with diverse input delays and asymmetric interconnection perturbations. Automatica, 45(5), pp.1347-1353.

Usach, I., Melis, V., Peris, J.E. (2013). Non-nucleoside reverse transcriptase inhibitors: a review on pharmacokinetics, pharmacodynamics, safety and tolerability. J. Int. AIDS Soc. 16(1): 18567.

Vandegraaff, N., Kumar, R., Burrell, C.J., Li, P. (2012). Kinetics of human immunodeficiency virus type 1 (HIV) DNA integration in acutely infected cells as determined using a novel assay for detection of integrated HIV DNA. Journal of Virology, 75(22): 11253-11260.

van GUNSTEREN, W.F., Mark, A.E. (1992). On the interpretation of biochemical data by molecular dynamics computer simulation. European journal of biochemistry, 204(3), pp.947-961.

Wahl, L.M., Nowak, M.A. (2000). Adherence and drug resistance: predictions for therapy outcome. Proc. R. Soc. B: Biol. Sci. 267(1445):835-843.

Waisbren, B.A. (1957). The treatment of bacterial infections with the combination of antibiotics and gamma globulin.

Walpole, C.S.J., Wrigglesworth, R. (1989). Enzyme inhibitors in medicine. Natural Product Reports, 6(4), pp.311-346.

Walters, C.J., Holling, C.S. (1990). Large-scale management experiments and learning by doing. Ecology, 71(6), pp.2060-2068.

Walubo, A. (2007). The role of cytochrome P450 in antiretroviral drug interactions. Expert opinion on drug metabolism & toxicology, 3(4), pp.583-598.

Wan, Z., Chen, X. (2014). Triptolide inhibits human immunodeficiency virus type 1 replication by promoting proteasomal degradation of Tat protein. Retrovirology 11(1):1-13.

Wang, T., Chen, L. (2009). Dynamic complexity of microbial pesticide model. Nonlinear Dynamics, 58(3), pp.539-552.

Wang, Z., Vince, R. (2008). Design and synthesis of dual inhibitors of HIV reverse transcriptase and integrase: introducing a diketoacid functionality into delavirdine. Bioorganic & Medicinal Chemistry, 16(7): 3587-3595.

Wang, Z., Bennett, E.M., Wilson, D.J., Salomon, C., Vince, R. (2007). Rationally designed dual inhibitors of HIV reverse transcriptase and integrase. Journal of Medicinal Chemistry, 50(15): 3416-3419.

Wang, Z., Tang, J., Salomon, C.E., Dreis, C.D., Vince, R. (2010). Pharmacophore and structure–activity relationships of integrase inhibition within a dual inhibitor scaffold of HIV reverse transcriptase and integrase. Bioorganic & Medicinal Chemistry, 18(12): 4202-4211.

Wang, R.S., Saadatpour, A., Albert, R. (2012). Boolean modeling in systems biology: an overview of methodology and applications. Physical biology, 9(5), p.055001.

Watson, J.D., Crick, F.H. (1953). Molecular structure of nucleic acids: a structure for deoxyribose nucleic acid. Nature, 171(4356):737-8.

Wazwaz, A.M., Rach, R. and Duan, J.S. (2016). Variational iteration method for solving oxygen and carbon substrate concentrations in microbial floc particles. MATCH Commun. Math. Comput. Chem, 76, pp.511-523.

Wijaya, K.P., Chávez, J.P. and Götz, T. (2021). A dengue epidemic model highlighting vertical–sexual transmission and impulsive control strategies. Applied Mathematical Modelling, 95, pp.279-296.

Witteveen, E., van Ameijden, E.J. (2002). Drug users and HIV-combination therapy (HAART): factors which impede or facilitate adherence. Substance use & misuse, 37(14), pp.1905-1925.

Woolley, D.W. (1952), A study of antimetabolites.

Xu, L., Desai, M.C. (2009). Pharmacokinetic enhancers for HIV drugs. Current opinion in investigational drugs (London, England: 2000), 10(8), pp.775-786.

Yang, H., Lu, J., Hu, X., Jiang, J. (2013). A cellular automaton model based on empirical observations of a driver's oscillation behavior reproducing the findings from Kerner's three-phase traffic theory. Physica A: Statistical Mechanics and its Applications, 392(18), pp.4009-4018.

Yildirim, A., Askari, H., Yazdi, M.K., Khan, Y. (2012). A relationship between three analytical approaches to nonlinear problems. Applied Mathematics Letters, 25(11), pp.1729-1733.

Zarrabi, N., Mancini, E., Tay, J., Shahand, S., Sloot, P.M. (2010). Modeling HIV-1 intracellular replication: two simulation approaches. Procedia Computer Science, 1(1): 555-564.

# List of publications

- **Mondal, S.**, Ghosh, P., Biswas, D. and Roy, P.K., 2019. Effect of alcohol consumption during antiretroviral therapy on HIV-1 replication: role of Cytochrome P3A4 enzyme. ***International Journal of Mathematical, Engineering and Management Sciences***, 4(4), p.922.

- **Mondal, S.**, Murmu, T., Chakravarty, K., Sarkar, A.K. and Sasmal, S.K., 2023. Mathematical modelling of HIV-1 transcription inhibition: a comparative study between optimal control and impulsive approach. ***Computational and Applied Mathematics***, 42(8), p.340.

- **Mondal, S.**, Peters, J.F., Ghosh, P., Sarkar, A.K. and Sasmal, S.K., 2024. Impulsive differential equation model in HIV-1 inhibition: advances in dual inhibitors of HIV-1 RT and IN for the prevention of HIV-1 replication. ***Journal of Biological Systems***, 32(02), pp.371-405.

- **Mondal, S.**, Murmu, T. and Sarkar, A.K., 2024. A control-based mathematical study on HIV-1 transcription by introducing Tat and Rev inhibitor. ***Advances in Applied Mathematics (Under Review)***

International Journal of Mathematical, Engineering and Management Sciences
Vol. 4, No. 4, 922–935, 2019
https://dx.doi.org/10.33889/IJMEMS.2019.4.4-073

# Effect of Alcohol Consumption during Antiretroviral Therapy on HIV-1 Replication: Role of Cytochrome P3A4 Enzyme

**Srijita Mondal**
Centre for Mathematical Biology and Ecology
Department of Mathematics
Jadavpur University, Kolkata - 700032, India

**Priyanka Ghosh**
Centre for Mathematical Biology and Ecology
Department of Mathematics
Jadavpur University, Kolkata - 700032, India

**Dibyendu Biswas**
Department of Mathematics
City College of Commerce and Business Administration
13, Surya Sen Street, Kolkata-700012, India

**Priti Kumar Roy**
Centre for Mathematical Biology and Ecology
Department of Mathematics
Jadavpur University, Kolkata - 700032, India
*Corresponding author*: pritiju@gmail.com

(Received July 18, 2018; Accepted April 19, 2019)

**Abstract**
Alcohol consumption is prevalent in HIV/AIDS infected patients. It possesses serious effects on protease inhibitors (PIs), which are used as an antiviral drug. While taking PIs, the secretion of Cytochrome P3A4 (CYP3A4) enzymes occurs from the liver and it metabolizes the drug to CYP3A4-PI complex. Alcohol consumption increases the rate of metabolism of PIs. In this research article, we have formulated a set of nonlinear differential equations based on the enzymatic activity of CYP3A4 for alcoholic HIV infected patients. Here, we have analytically compared the dynamics of PIs metabolism between alcoholic and non-alcoholic HIV infected patients and also investigated how the infection is being accelerated by enhancing viral load due to alcohol consumption. Finally, our analytical results are verified by numerical findings.

**Keywords-** HIV/AIDS, Viral load, Alcohol consumption, CYP3A4 enzyme, Protease inhibitor.

## 1. Introduction

HIV-1 infection is a global problem with 36.9 million people affected in the world at the end of 2017. The African region remains most severely affected with accounting for nearly two-thirds of the people living with HIV worldwide (Kumar et al., 2012). There were approximately 1.8 million people becoming newly infected in 2017 globally. People with HIV infection have to take a combination of anti-AIDS drugs on a daily basis to stay healthy.

There are about 26 FDA approved anti-AIDS drugs currently available acting on different stages of the HIV life-cycle (Das and Arnold, 2013); most fall into 4 classes: (i) Entry/Fusion Inhibitors

Computational and Applied Mathematics (2023) 42:340
https://doi.org/10.1007/s40314-023-02473-w

# Mathematical modelling of HIV-1 transcription inhibition: a comparative study between optimal control and impulsive approach

**Srijita Mondal[1] · Tanushree Murmu[2] · Koyel Chakravarty[3] · Ashis Kumar Sarkar[1] · Sourav Kumar Sasmal[4]**

Received: 6 April 2023 / Revised: 28 August 2023 / Accepted: 28 August 2023


**Abstract**
Through the utilization of a proactive approach, interaction with human immunodeficiency virus type I (HIV-1) is facilitated, enabling the sequential stages of its fusion mechanism to be navigated successfully. As a result, the efficient infiltration of a target $CD4^+T$ helper cell within the host organism by the virus is achieved. The onset of the virus's replication cycle is initiated through this infiltration. As a retrovirus, the orchestration of the conversion of its single-stranded viral RNA genome into a more stable double-stranded DNA structure by HIV-1 is observed. Integration of this newly formed DNA with the host cell's genetic material occurs. This pivotal transformation of the integrated pro-viral DNA into fully functional messenger RNA (mRNA) is facilitated by the host enzyme RNA polymerase II (Pol II). The central focus of the present ongoing research involves the construction of a meticulous mathematical framework consisting of a system of nonlinear differential equations. The investigation of the impact of a Tat inhibitor on the suppression of the transcriptional activity of HIV-1 is

✉ Srijita Mondal
mondal.srijita17@gmail.com

Tanushree Murmu
murmutanushree@gmail.com

Koyel Chakravarty
koyelchakravarty@gmail.com

Ashis Kumar Sarkar
aksarkar.jumath@gmail.com

Sourav Kumar Sasmal
sourav.sasmal@amsc.iitr.ac.in

1 Centre for Mathematical Biology and Ecology, Department of Mathematics, Jadavpur University, Kolkata 700032, India

2 Department of Mathematics, Rammohan College, Kolkata 700009, India

3 Department of Mathematics, School of Engineering and Applied Sciences, SRM University AP, Amaravati, Andhra Pradesh 522240, India

4 Department of Applied Mathematics and Scientific Computing, IIT Roorkee, Roorkee, Uttarakhand 247667, India

Published online: 24 October 2023

Journal of Biological Systems, Vol. 32 (2024) 1–35

DOI: 10.1142/S0218339024500141

World Scientific
www.worldscientific.com

# IMPULSIVE DIFFERENTIAL EQUATION MODEL IN HIV-1 INHIBITION: ADVANCES IN DUAL INHIBITORS OF HIV-1 RT AND IN FOR THE PREVENTION OF HIV-1 REPLICATION

SRIJITA MONDAL[*,§], JAMES F. PETERS[†,‡,¶], PRIYANKA GHOSH[*,‖] and ASHIS KUMAR SARKAR[*,**]

[*]*Centre for Mathematical Biology and Ecology*
*Department of Mathematics Jadavpur University*
*Kolkata 700032, India*

[†]*Computational Intelligence Laboratory*
*University of Manitoba, WPG, MB, R3T 5V6, Canada*

[‡]*Department of Mathematics, Faculty of Arts and Sciences*
*Adiyaman University, 02040 Adiyaman, Turkey*
[§]*mondal.srijita17@gmail.com*
[¶]*James.Peters3@umanitoba.ca*
[‖]*ghosh.priyanka.ju@gmail.com*
[**]*aksarkar.jumath@gmail.com*

SOURAV KUMAR SASMAL[††]

*Department of Applied Mathematics and Scientific Computing*
*IIT Roorkee, Uttarakhand 247667, India*
*sourav.sasmal@amsc.iitr.ac.in*

Received 12 May 2023
Accepted 20 November 2023
Published 27 March 2024

Reverse transcriptase (RT) and integrase (IN) are two pivotal enzymes in HIV-1 replication. RT converts the single-stranded viral RNA genome into double-stranded DNA and IN catalyzes the integration of viral double-stranded DNA into host DNA. Currently, dual inhibitors of HIV-1 RT and IN have become a hotspot in new anti-HIV drug research and development. A dual inhibitor of HIV-1 RT/IN does the same thing as the two independent drugs would do. In this paper, we develop a mathematical model comprising a system of nonlinear differential equations describing HIV-1 RT/IN catalyzed biochemical reactions based on Michaelis–Menten enzyme kinetic reaction. In the formulated model we incorporate HIV-1 RT/IN dual inhibitor which simultaneously works as a non-nucleoside RT inhibitor and IN inhibitor. To examine the efficacy of HIV-1 RT/IN dual inhibitor in the treatment of HIV-1 infection, we have introduced a one-dimensional impulsive differential equation model and determined an effective dosing regimen for applying the inhibitor numerically. Furthermore, the exact closed form solution of the impulsive differential equation model is carried out by using the Lambert W function and the local stability of the periodic solution is also obtained analytically.

[††]Corresponding author.